THE INTERNATIONAL INTRAVAL PROJECT

Phase 2, Working Group 4 Report

THE A ES OF THE AL RIVERS NATU OGUE

AEN NEA

SKi

THE INTERNATIONAL INTRAVAL PROJECT

TO STUDY VALIDATION OF GEOSPHERE
TRANSPORT MODELS FOR PERFORMANCE ASSESSMENT
OF NUCLEAR WASTE DISPOSAL

PHASE 2, Working Group 4 Report

The Analyses of the Alligator Rivers Natural Analogue

L. Birgersson
A. Larsson
K. Skagius
Kemakta Konsult AB

The Coordinating Group of the INTRAVAL Project
Swedish Nuclear Power Inspectorate (SKI)

NUCLEAR ENERGY AGENCY
ORGANISATION FOR ECONOMIC CO-OPERATION AND DEVELOPMENT

NEA **SKi**

ORGANISATION FOR ECONOMIC CO-OPERATION AND DEVELOPMENT

Pursuant to Article 1 of the Convention signed in Paris on 14th December 1960, and which came into force on 30th September 1961, the Organisation for Economic Co-operation and Development (OECD) shall promote policies designed:

- to achieve the highest sustainable economic growth and employment and a rising standard of living in Member countries, while maintaining financial stability, and thus to contribute to the development of the world economy;
- to contribute to sound economic expansion in Member as well as non-member countries in the process of economic development; and
- to contribute to the expansion of world trade on a multilateral, non-discriminatory basis in accordance with international obligations.

The original Member countries of the OECD are Austria, Belgium,Canada, Denmark, France, Germany, Greece, Iceland, Ireland, Italy, Luxembourg, the Netherlands, Norway, Portugal, Spain, Sweden, Switzerland, Turkey, the United Kingdom and the United States. The following countries became Members subsequently through accession at the dates indicated hereafter: Japan (28th April 1964), Finland (28th January 1969), Australia (7th June 1971), New Zealand (29th May 1973), Mexico (18th May 1994) the Czech Republic (21st December 1995) and Hungary (7th May 1996). The Commission of the European Communities takes part in the work of the OECD (Article 13 of the OECD Convention).

NUCLEAR ENERGY AGENCY

The OECD Nuclear Energy Agency (NEA) was established on 1st February 1958 under the name of the OEEC European Nuclear Energy Agency. It received its present designation on 20th April 1972, when Japan became its first non-European full Member. NEA membership today consists of all European Member countries of OECD as well as Australia, Canada, Japan, Republic of Korea, Mexico and the United States. The Commission of the European Communities takes part in the work of the Agency.

The primary objective of NEA is to promote co-operation among the governments of its participating countries in furthering the development of nuclear power as a safe, environmentally acceptable and economic energy source.

This is achieved by:

- *encouraging harmonization of national regulatory policies and practices, with particular reference to the safety of nuclear installations, protection of man against ionising radiation and preservation of the environment, radioactive waste management, and nuclear third party liability and insurance;*
- *assessing the contribution of nuclear power to the overall energy supply by keeping under review the technical and economic aspects of nuclear power growth and forecasting demand and supply for the different phases of the nuclear fuel cycle;*
- *developing exchanges of scientific and technical information particularly through participation in common services;*
- *setting up international research and development programmes and joint undertakings.*

In these and related tasks, NEA works in close collaboration with the International Atomic Energy Agency in Vienna, with which it has concluded a Co-operation Agreement, as well as with other international organisations in the nuclear field.

Foreword

Radioactive waste management programmes in OECD countries cover a wide range of activities in research and development with the common purpose to get the necessary scientific basis for disposal of various types of radioactive waste. The concern for the safety of final disposal is shared among the safety authorities and the radioactive waste producers, primarily the nuclear utilities. In some countries, site selection and charac-terisation programmes for high-level waste disposal are at a relatively advanced stage and several countries already have repositories for low-level waste in operation. Due to the difficulties involved and the amount of work necessary to get the required scientific information, the problems to be resolved have a high priority in national and international co-operative programmes.

INTRAVAL was set up as an international project concerned with the use of mathematical models for predicting the potential transport of radioactive substances in the geosphere. Such models are used to help assess the long-term safety of radioactive waste disposal systems. The INTRAVAL project was established by the Swedish Nuclear Power Inspectorate to evaluate the validity of these models. Results from a set of selected laboratory and field experiments as well as studies of occurrences of radioactive substances in nature (natural analogues) were compared in a systematic way with model predictions. Discrepancies between observations and predictions were discussed and analysed.

The project ran for six years, from 1987 to 1993. It was organised in two phases. The Swedish Nuclear Power Inspectorate (SKI) was managing participant during both phases and the OECD/Nuclear Energy Agency, Her Majesty's Inspectorate of Pollution (HMIP/DOE), United Kingdom, and Kemakta Consultants, Sweden took part in the project secretariat. The project had also observers from the International Atomic Energy Agency and from the State of Nevada.

The first phase of INTRAVAL was finished in 1990. Reports of the results from the first phase were issued in 1990, 1992 and 1993. A summary report of phase one of the project was published in the beginning of 1994.

The second phase of INTRAVAL was initiated in 1990 and finished 1993. Thirty-eight organisations from thirteen OECD countries participated in the second phase. Test cases were divided among four working groups which describe their findings in four separate reports. This report is one of them. In addition a summary report will be issued as well as a report from an independent subcommittee for integration.

Abstract

The Alligator Rivers study is based on work conducted at the Koongarra uranium deposit in the Alligator Rivers Region about 200 km east of Darwin, Australia. The Alligator Rivers Analogue Project (ARAP) was set up in 1987 and was later included as a test case in both phase 1 and 2 of INTRAVAL. The objective was to develop a consistent picture of the processes that have controlled the transport in the weathered zone of the Koongarra ore deposit and the time scale over which they have operated.

Uranium mineralisation occurs at Koongarra in two distinct but related ore bodies. Primary mineralisation in the main ore body is largely confined to quartz-chlorite schists and secondary uranium minerals are present from the surface down to the base of weathering at about 25 m depth and forms a tongue-like body of ore dispersing downslope for about 80 m. The primary ore body at Koongarra is estimated to be 1000 million years old and geomorphological information indicates that weathering started a few million years ago.

The work included in INTRAVAL phase 1 was mainly concentrated to hydrogeological and geochemical modelling which produced results that in INTRAVAL phase 2 were used in modelling simulations of the uranium migration. The model concepts applied in the migration modelling were based on rather simple performance assessment models accounting for advection, dispersion and linear sorption in one or two dimensions. One 1-D model was extended to include α-recoil and transfer between solid phases. The vertical movement of the weathering front was included in the 2-D model.

Studies of the Alligator Rivers Natural Analogue has demonstrated that the system is very complex. The interaction of many geochemical and geohydrological processes occurring over long times makes it difficult to create a quantitative model of the history of groundwater flow and nuclide transport. The study has shown the importance of a joint interpretation of different types of data and an iterative procedure for data collection, data interpretation and modelling in order to get a consistent picture of the evolution of the site. Furthermore, it was shown that sorption is a major retardation mechanism, that uranium fixation in crystalline phases is a potentially important retardation mechanism in geologic media where significant alteration of the rock is expected, and that α-recoil may have an impact on the distribution of uranium isotopes in the water. Modelling simulations indicated migration times in fair agreement with independent geomorphological information. A general conclusion from the INTRAVAL study is that rather simple and robust concepts and models seem able to adequately describe the long range migration processes that have occurred.

Table of contents

1 Introduction

The uranium deposit at Koongarra in the Alligator Rivers Region of the Northern Territory in Australia has been thoroughly investigated for various purposes, initially with the intention to develop an uranium mine, but later on as a research facility with the intent to get an understanding of processes that have acted upon the original uranium ore and have resulted in the present uranium deposit. Due to the character of the deposit, it has served as a so called natural analogue in order to improve the understanding of the migration of radionuclides from the ore body over the past ages and to give a basis for better possibilities to forecast the future development of radioactive waste repositories.

Mathematical models applied for radionuclide migration calculations from a repository must be evaluated in terms of the validity and reliability of the predictions. One procedure is then to compare model predictions with experimental observations. Here, information from laboratory experiments, field experiments and natural analogue studies are needed. Laboratory and field experiments yield information on relatively short time scales. Natural analogues may be viewed as naturally occurring experiments that have continued over long time periods. They may therefore provide important information regarding the understanding of the scientific basis for the long term prediction of radionuclide migration within geological environments that are relevant to radioactive waste repositories.

The modelling work of the Alligator Rivers test case in INTRAVAL phase 1 was a joint venture between The Alligator Rivers Analogue Project (ARAP) and INTRAVAL. Both ARAP and INTRAVAL were set up under the auspices of OECD Nuclear Energy Agency. The ARAP study was completed in 1992.

The modelling work of this test case during INTRAVAL phase 1 was mainly focused on hydrology, geochemistry and geochemical processes. The main aim of the phase 1 modelling was to obtain a conceptual platform for the migration modelling in phase 2. Participants were University of Arizona (USA), RIVM (the Netherlands), AEA Technology Harwell Laboratory (United Kingdom), Johns Hopkins University (USA), CSIRO (Australia), ANSTO (Australia) and Kemakta/SKI (Sweden).

The main objective of the Alligator Rivers test case in INTRAVAL phase 2 was to develop a consistent picture of the processes that have controlled the transport in the weathered zone and the time scale over which they have operated. Another objective was to test and evaluate models and concepts used in performance assessment of radioactive waste repositories. The main contributors to the test case in INTRAVAL phase 2 were the National Institute of Public Health and Environmental Protection (RIVM) *[van de Weerd et al. 1994]* and Kemakta Konsult *[Skagius et al. 1994]*. The results of their work are summarised in this report. It should be noted that additional migration modelling has been carried out by ANSTO and other organisations within the ARAP. The ARAP work is only briefly described in this report.

2 Test Case Description

2.1 Overview

The Koongarra uranium deposit in the Alligator Rivers Region, 225 km east of Darwin in the Northern Territory of Australia, is one of four major uranium deposits discovered in the area. The deposit is located close to the prominent Koongarra Reverse Fault in a quartz-chlorite schist of the lower member of the Cahill Formation. Modelling studies of radionuclide migration at the site have indicated that the time scale of the uranium mobilisation from the primary ore is of the order of one or a few million years. Consequently, the Koongarra uranium ore zones should provide a good test case for the validation of hydrogeological, geochemical and radionuclide transport models.

The extensive investigations of the site performed within the ARAP project can be divided into four broad categories: analysis of the radionuclide distribution in rock samples and rock fractures, study of the role of groundwater and colloids in radionuclide transport, analysis of in situ production and mobility of long-lived fission products and transuranic nuclides, and development of modelling codes and evaluation of the Koongarra site for modelling studies.

The ARAP programme has resulted in a large amount of data characterising the site. Hydrogeologic data were collected from drawdown and recovery tests and water pressure tests. Geologic data are based on mineralogic and uranium assay logs of percussion holes and drill cores. Groundwater chemical data were accumulated from a large number of boreholes. Distribution of uranium, thorium and radium isotopes was determined in different mineralisation zones. Laboratory sorption experiments were performed using samples from bore cores. Distribution coefficients were measured on natural particles in Koongarra groundwater.

2.2 Geology

The natural uranium mineralisation occurs at Koongarra in two distinct but related ore bodies, separated by 100 m of barren schists, which strike and dip broadly parallel to a fault, the Koongarra Reverse Fault. The main ore body (ore body 1), which is the subject of this study, persists to 100 m depth. It has a strike length of 450 m and a width that averages 30 m at the top of the unweathered schists (Figures 2.1 and 2.2).

An overview of the data that is available from the Alligator Rivers site is found in this section. A more comprehensive compilation of available data is given in Appendix 1.

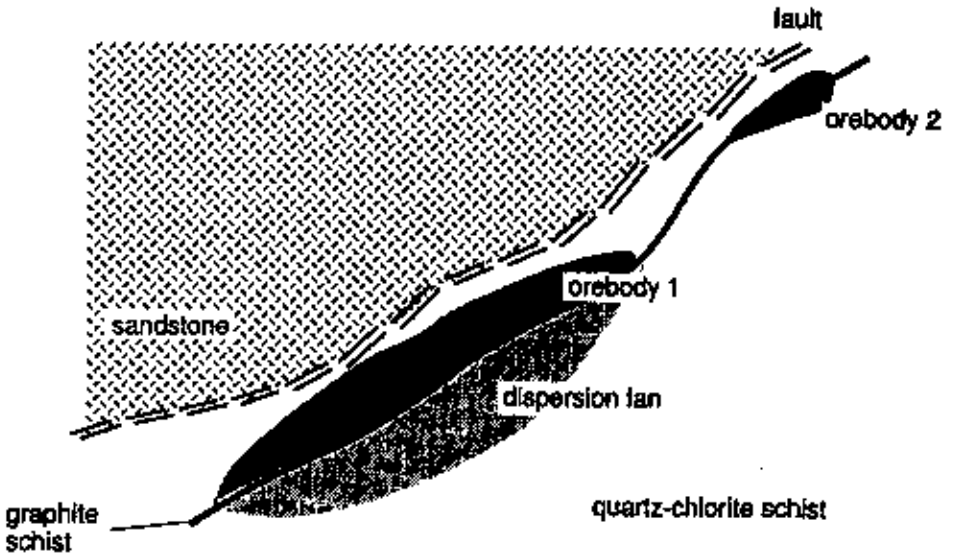

Figure 2.1 Plan view of the Koongarra ore bodies, projected to the surface.

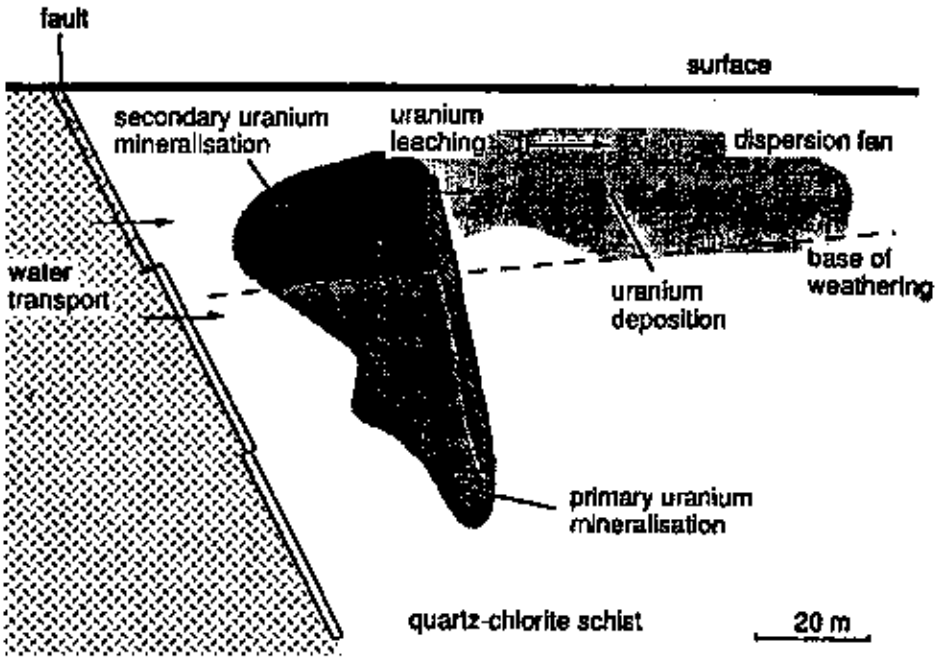

Figure 2.2 Cross-section of the Koongarra No. 1 ore body.

The primary ore consists of pitchblende or uraninite-uranium dioxide veins and veinlets which either follow or cross-cut the layering in the schist. Minor amounts of scattered sulphide minerals, primarily galena (PbS), chalcopyrite ($CuFeS_2$) and pyrite (FeS_2), are associated with the high-grade ore. The schist is weathered from the surface down to a depth of 25–30 m. In this weathered zone, another secondary uranium mineralisation, consisting of uranyl phosphates, forms a tongue-like fan. Away from the tail of the fan, uranium is dispersed in the weathered schists and adsorbed onto clays and iron oxides. The dispersion fan of ore-grade materials extends down-slope for about 80 m. The transformation of the original primary mineralisation zones into the present secondary minerals is perceived to have taken place during a period of well over one million years.

The upper extension of ore body 2 is located about 30 m below surface, which is below the base of weathering. As no weathering has occurred and no known mobilisation of uranium has taken place from ore body 2, it has not been studied further within ARAP.

2.3 Hydrology

Koongarra, in common with much of northern Australia, has a monsoonal climate with almost all rainfall occurring in the wet season between November and March. This causes a fluctuation in the water table of 5–10 m between the wet and dry seasons.

The time of the onset of the present monsoon climate in the region is not clear. Investigations indicate that periods of wetter climate than at present have occurred, but also that extreme reductions in precipitation have coincided with glacial maxima. It has been concluded from the available information that precipitation levels similar to those of today have prevailed in the area for the last 10 000 years *[Wyrwoll, 1992]*. During the last 700 000 years, the climate has probably shifted between dry glacial periods that have been lasting for about 100 000 years, and interglacial periods lasting about 10 000 years, with conditions similar to the present.

Interpretation of the present hydrology at the site suggests that recharge of groundwater to the weathered Cahill schists occurs via downflow parallel to and in close proximity to the reverse fault in the underlying Kombolgie sandstone and schists *[Duerden, 1992]*. Although the fault zone breccia was found to be practically impermeable, some water has been observed to flow from the Kombolgie sandstone into the schists via cross fractures that offset the fault. Once in the schist, the groundwater flow is towards the south and south-east, away from the sandstone cliffs behind the deposit.

The unweathered quartz-chlorite schist is a fractured crystalline rock, in which most of the water flow takes place in the fractures. As a result of weathering processes, the fracture system becomes less prominent and the flow characteristics change from being fracture dominated to being mainly matrix dominated. The weathered schist thus acts as a medium with high porosity and low permeability. The weathered zone appears to limit downward circulation of water and more of the water entering the system flows through the weathered zone than through the unweathered schist. However, the preferential groundwater discharge seems to occur in the surficial deposit of sand and gravel because of the much higher transmissivity of those materials.

The proportion of the flow that enters the deep hydrogeological units is quite small, compared to the upper units, and the flow passes mainly through the weathered zone *[Townley, 1992]*.

2.4 Hydrochemistry

The chemistry of the groundwater shows a gradual change as the water passes along the aquifer paths. The two major sources of groundwater entering the flow-system of the deposit are direct infiltration from the surface and movement across the fault. The changes in composition result from mixing, dilution, dissolution (and possibly precipitation) of minerals, adsorption/desorption, evaporation and outgassing.

During the wet season, surface waters will comprise recent rainwater, whereas in the dry season the composition will be more influenced by groundwater inflow. Measurements during the wet season have shown that the surface waters are slightly acidic with low alkalinity, conductivity, and correspondingly low levels of dissolved constituents. In the sampled dilute surface water, sodium and chloride were the only species present in significant concentrations. This is typical of rainfall that always contains some traces of dissolved sea salt originating from the evaporation of droplets of seawater *[Drever, 1988]*.

The groundwaters in the weathered zone are oxidising, as they are essentially surficial. The conditions are slightly reducing below the base of weathering which is also indicated by the presence of graphite and sulphides.

The groundwater in the mineralised zones of the Cahill formation is almost neutral with a pH close to 7. It contains uranium in concentrations of 100–500 $\mu g/dm^3$, variable phosphate concentrations up to 600 $\mu g/dm^3$ and bicarbonate concentrations above 100 mg/dm^3.

Magnesium is an important element in the groundwaters at Koongarra, since it is released by weathering of chloritised schists of mine series host rock. Magnesium is the dominant cation in the groundwater with concentrations around 25–30 mg/dm^3 at the intersection with ore body 1. Other important cations are sodium, potassium, calcium, silicon and iron. Also small amounts of manganese and copper are found.

Bicarbonate, HCO_3, is the main anion in Koongarra groundwater, being present at concentrations up to 160 mg/dm^3 near the centre of the ore body. The concentrations are lower both up-gradient and down-gradient from the ore. Other anions present in the groundwater are phosphate, chloride, fluoride and sulphate. The content of organic components in the groundwater at Koongarra is minor.

Groundwater from the boreholes at Koongarra show a very low concentration of thorium. Almost all the thorium is associated with particles above 1 μm in size, whereas most of the uranium in the groundwater is dissolved. The only significantly enriched elements in the colloidal fraction ($< 1\mu m$) are iron, thorium, actinium and uranium.

2.5 Radiochemistry

Uranium in Groundwater

Uranium levels in Koongarra groundwaters have been measured to provide an adequate basis for a general understanding of the chemistry of the system. The aim was to quantify uranium concentrations as a function of distance from a suitably defined origin.

The $^{234}U/^{238}U$ ratio has been analysed in groundwater samples using α-spectroscopy. Often this ratio was found to be below unity, with values as low as 0.65, which indicate preferential mobility of ^{238}U. This is contrary to what is commonly found in geologic systems. Particulary low values were found in the region of the dispersion fan. This agrees well with solid phase data for the readily extractable portion of core samples from this region.

Thorium in Groundwater

Since thorium is a possible chemical analogue for several components of the nuclear waste, including plutonium, an analytical programme was established to study thorium in Koongarra groundwaters. Measured levels of dissolved thorium were near to or below the detection limit of the analytical method employed, in spite of the presence of readily measurable concentrations of ^{230}Th in the solid phase. The results show that ^{230}Th is highly immobile at Koongarra. This is in agreement with the behaviour of many natural systems, except for very saline groundwaters or in the presence of organic complexants.

Uranium in Solid Phase

Ore grades up to about 30% uranium are found in some parts of the unweathered primary ore zone. Uranium concentrations greater than 200 μg/g follow the base of the weathering of the transition zone for about 80 m from the primary zone. Beyond this point the deposited uranium is concentrated at the top 3–10 m below the surficial sands.

Distribution of Uranium and Thorium in the Solid Phases

Selective extraction procedures have been used on rock samples to explain the distribution of uranium and thorium on the basis of the mineral composition of the rock *[Edghill, 1990, Yanase 1990]*. The concentration of uranium and thorium and the $^{234}U/^{238}U$, $^{230}Th/^{234}U$ and $^{226}Ra/^{230}Th$ activity ratios have been determined in amorphous and crystalline phases of the rock samples. The amorphous material was defined as a poorly ordered material, accessible to and in approximate equilibrium with the groundwater. The crystalline phase was defined as highly ordered materials (hematite, goethite, clays and quartz) which contained species inaccessible to the groundwater.

A large proportion of the uranium and thorium has been found to be associated with amorphous phases and adsorbed onto iron oxides and clay minerals. The uranium is possibly accessible to, and at near equilibrium with the groundwater. Areas upstream to the ore body show the largest leaching of uranium. The fastest accumulation of uranium seems to have occurred near the centre of the dispersion fan, close to the base of weathering at the edge of the fan. There is possibly a preferential movement and accumulation of uranium just above the base of weathering.

3 Data Examination

3.1 Kemakta

The data examination by Kemakta was primarily focused on the data required for the modelling of the selected system, such as the distribution of uranium in the bulk rock and its individual mineral phases. Radiochemical data were used to study alternative processes of radionuclide migration. Groundwater chemistry data were not employed by the Kemakta team due to the large variation in the uranium concentration in the groundwater and the uncertain Eh values that have been reported.

3.1.1 Groundwater Chemistry

The examined groundwater chemistry data originate from samplings carried out in May 1988, November 1988, March 1989, May 1989, June 1989 and October 1989. All data were distributed on floppy discs, with the exception of the data from the sampling in October 1989 *[Payne 1989]*. Additional samplings and analyses of groundwater have been carried out since Kemakta completed the data examination *[Payne et al 1992]*.

The uranium concentrations in the groundwater from different sampling occasions show large variations. No clear trend, such as an increasing or decreasing concentration with depth, can be seen. The highest concentrations of uranium were found in samples from holes located in the zone of the ore body 1 (holes W1, PH49 and W4). Maximum, minimum and mean concentrations in water samples from these holes are given in Table 3.1.

Table 3.1 Uranium concentrations in water samples taken from hole W1, PH49 and W4 at indicated depths.

Hole	Depth (m)	Uranium concentration (mg/m^3)		
		Max	Min	Mean
W1	10–30	755 (May 89)	4.3 (Oct. 89)	210
W4	10–30	577 (Oct. 89)	10.4 (Mar. 89)	292
PH49	20–30	265 (May 88)	94 (Nov. 88)	155

Eh and pH values have been reported for the samplings in May, 1988 and November, 1988. Reported Eh values range from +45 mV to +280 mV and indicate a rather oxic system with high redox potential at larger depths, a result that is somewhat doubtful. The pH values at depths larger than 20 meters range from about 5.8 to 7.3, with most of the values lying between 6.5 and 7.

Due to the large variations in the uranium concentration in the groundwater and the strange Eh values reported from the site, Kemakta decided not to use these data for comparison with results from modelling of uranium migration in the weathered zone. It should be pointed out, however, that Kemakta did not study the later data that has been reported in *[Payne et al 1992]*.

3.1.2 Uranium Concentration in Solid Materials

Uranium concentrations in solids at the Koongarra ore deposit have been collected and reported within ARAP. Most data originate from the 6110 mN transect that include holes DDH52, DDH1, DDH2, DDH3, PH55, DDH4, PH58, PH60, PH89 and PH90 (Figures 3.1 and 3.2). However, from these data it is difficult to get a detailed picture of the actual size and extension of the ore body and the dispersion fan in all directions. A large data set also exists of average uranium concentrations over 5 m drillcore sections obtained from exploratory drillings made by the mining company.

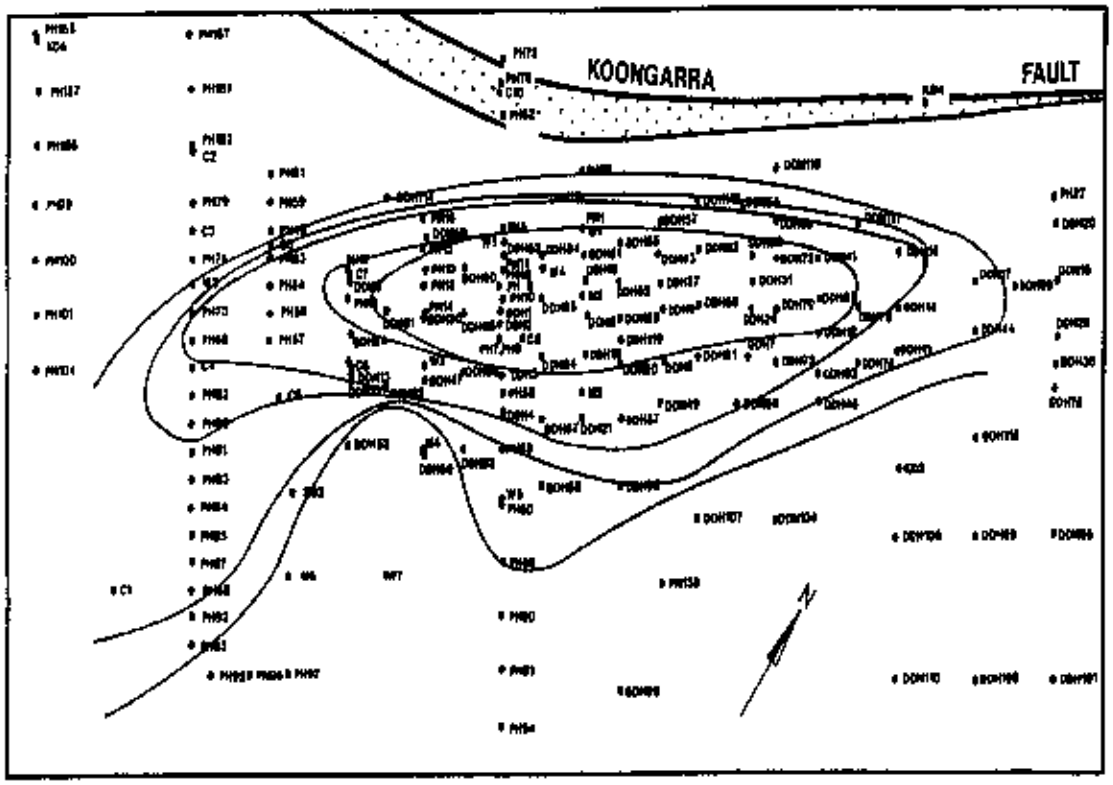

Figure 3.1. Plan view of the site showing surface projection of ore body 1 and borehole locations.

Kemakta has examined and compared the uranium concentrations in the solid phase in both small (1g) and large (5 m drillcore) samples in different directions, with the aim to investigate how representative data from the small samples are for large rock volumes. A 3-D representation of the uranium concentration in the solid phase was obtained by kriging of the 5 m drillcore data.

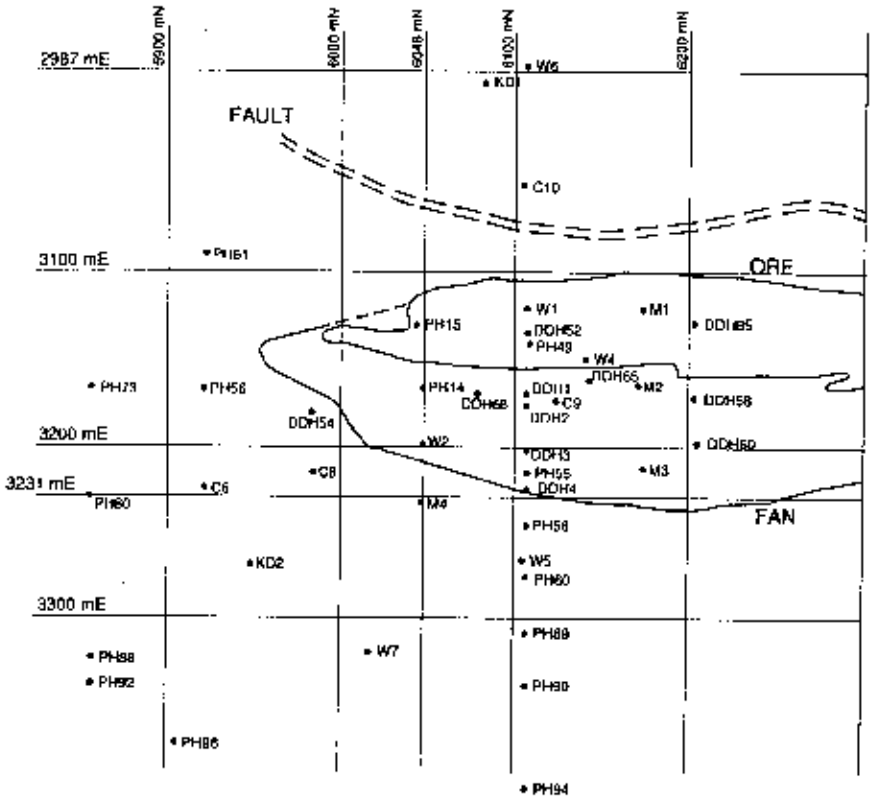

Figure 3.2. Area of transect 6110, from which most of the data used by Kemakta were collected.

Uranium Concentrations in the Solid Phase along the 6110 mN Transect

Uranium concentrations in the solid phase have been reported in several ARAP Progress Reports. The data referred to in this text are from a compilation made by different researchers *[Yanase, April 1988], [Yanase, August 1988], [Nightingale, 1988], [Sekine et al., 1988], [Edgehill, 1989].* Their data have been collected from analyses of small samples, approximately 1 g in weight. The small sample size must be considered in judging how representative these data are for the much larger system that is being studied.

Most data are from samples at the transect including the holes DDH52, DDH1, DDH2, DDH3, PH55, DDH4, PH58, PH60, PH89 and PH90 (6110 mN in Figures 3.1 and 3.2). The Kemakta team has plotted bulk uranium concentrations of samples from 10 to 20 m depth and from 20 to 30 m depth versus sample position in metres East (Figure 3.3).

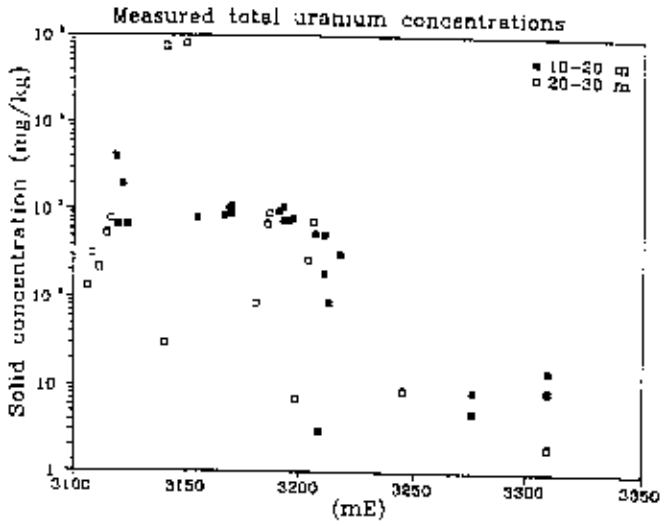

Figure 3.3. *Kemakta. Observed uranium concentrations in solid samples from 10–20 m and 20–30 m depth in the transect 6110 mN.*

At the depth interval 10–20 metres, the uranium concentrations lie within 500 to 1000 mg/kg up to about 3200 mE, where they drop to 1–10 mg/kg. A peak with concentrations up to 4000 mg/kg is found at 3120 mE, which is in the secondary mineralisation, near the outer extension towards the fault. The concentrations in the depth interval 20–30 metres are more scattered. This may be due to variations in the vertical extension of the secondary mineralisation and the dispersion fan.

All data reported in the ARAP Progress Reports were compiled in an attempt to find trends in the solid uranium concentrations at different directions of the site. The mean concentration of each hole was calculated in the depth intervals 0–10 m, 10–20 m and 20–30 m. The highest concentrations were found in holes DDH1 and DDH68 located in the dispersion fan near the interface to the secondary uranium mineralisation. Beyond that area, the concentration seems to decrease in all directions. A similar trend was found for the depth intervals 10 to 20 m and 20 to 30 m. An analysis of all the uranium data showed the highest concentrations to be located in the area around the interface of the secondary mineralisation and the dispersion fan at about 6110 mN. Beyond this area the concentration seems to decrease in all directions, as for the 0–10 m interval.

3-D View of Observed Uranium Concentrations in Solid Phase

The Kemakta team used a data set of average uranium concentrations over 5 m drillcore sections from drillings made by the mining company to get a detailed picture of the actual size and extension of the ore body and the dispersion fan in various directions. 3-D representations of observed average uranium concentrations were obtained by kriging these data. The kriging theory behind the calculations has been briefly described by Skagius et al. *[Skagius et al 1994]*. The location of the block is shown in Figure 3.4.

Figure 3.5 shows the uranium concentration in plan view at different depths. Close to the surface (Figure 3.5a), the highest uranium concentrations are found in an area around 6100–6200 mN, close to the boundary between the ore zone and the dispersion fan. High concentrations are also present in the north-east part of the ore zone at about 6300–6380 mN. The areas with high uranium concentrations in Figure 3.5 are separated by a thin violet area which normally depict very low concentrations, but may also be interpreted as areas, in which the uranium concentrations could not be predicted, due to the fact that the closest observation points were not within the calculated correlation length.

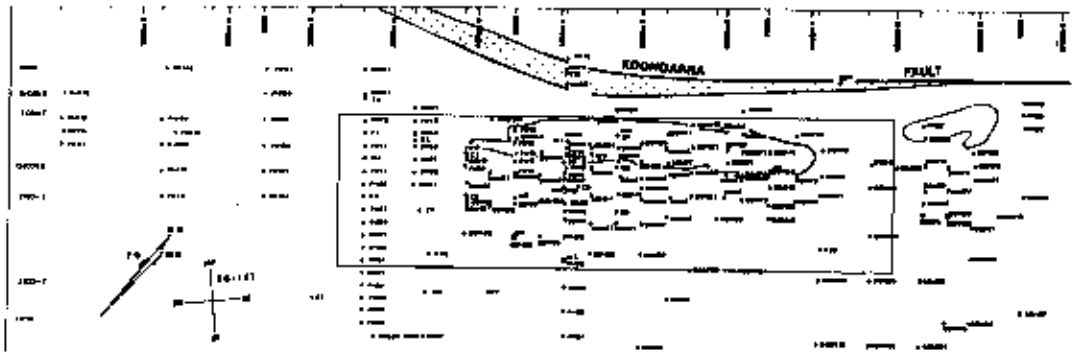

Figure 3.4. Location and size of 3-D block where uranium concentrations have been depicted.

Uranium is also found close to the surface south-west of the ore body. Unfortunately, this area is not well characterised, which is reflected by the appearance of areas in which the uranium concentration could not be predicted using the observed concentrations. Elevated uranium concentrations seem to extend as far as to the row of holes at 5865 mN (Figure 3.5a).

Uranium concentrations in the planes at 12 m and 21 m depths are shown in Figure 3.5b and 3.5c. The area with high uranium concentrations in the centre of the ore body is larger at these depths compared to what is found at the surface. The appearance of a separate area with high concentrations in the north-east part of the block at these depths is most likely an artifact caused by the lack of data for this particular part of the site. The dispersion of uranium in the south-westerly direction is more pronounced at these depths than in the surface layer.

At a depth of 30 m (Figure 3.5d), the uranium concentration in the centre of the ore body appears to be lower than closer to the surface, and the area with elevated concentration is not as broad as at more shallow depths. At still larger depths, 39 m (Figure 3.5e), the shape of the zone with elevated concentrations is similar to that at 30 m depth. The weathering front is located at approximately 30 m depth. At the 30 m level and below, essentially no dispersion of uranium has taken place. The area with elevated concentrations is therefore more narrow than at depths above 30 m, at which the rock is weathered and uranium dispersion has occurred. The south-westerly dispersion plume seems to vanish at depths below 30 m.

The dispersion of uranium in the weathered zone above 30 m depths is more clearly seen in Figure 3.5d, which depicts the uranium distribution in north-west to south-east cross-section at about 6110 mN and in a north-east to south-west at about 3160 mE. In both cross-sections the area with elevated concentrations is more enlarged above 30 m depth than below. In the north-east to south-west cross-section a band with zero concentrations is present that reflects the lack of observation points at this location.

The result from the kriging of observed uranium concentrations indicates that uranium dispersion has occurred in the weathered zone in the direction from the fault towards south-east. In addition, the results indicate the presence of a uranium dispersion plume more to the south. This latter finding is consistent with interpretations of hydrogeologic and groundwater chemistry data which suggest that the direction of the present day groundwater flow is more toward the south than south-east.

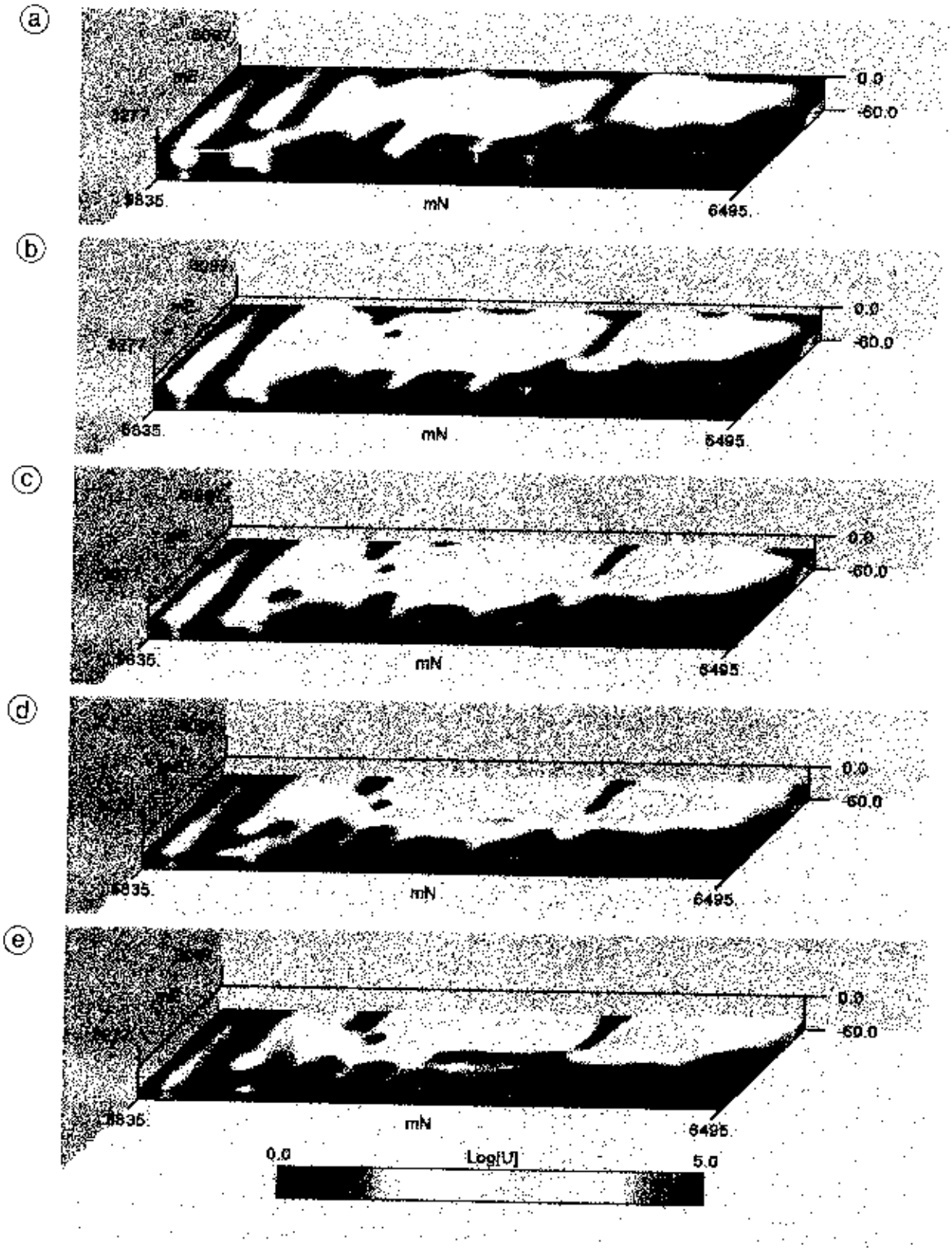

Figure 3.5. Kemakta. Plan view of uranium concentrations (mg/kg), a) at surface, b) at 12 m depth, c) at 21 m depth, d) at 30 m depth and e) at 39 m depth according to the colour scale.

Uranium Concentrations in Small Samples and in 5 m Cores

The large data base from the exploratory drilling include average uranium concentrations in 5 m long sections of drill cores, but contains no information on the distribution between different uranium isotopes or the concentration of thorium. Data are only available from radiochemical analyses of very small samples. To investigate the representativeness of data from analyses of small samples, uranium concentrations from these analyses were compared with corresponding data from analyses of the 5 m cores from the exploratory drilling.

The observed uranium concentrations in solid phase in the transect 6110 mN (Figure 3.2) from small sample analyses and from the exploratory drillcore logs are shown in Figure 3.6. The uranium concentrations of small samples at different areas of the site were generally quite similar to the average concentrations of the 5 m cores. The uranium concentrations in the small sample seemed to be somewhat higher at depths above 20 m in the ore zone and the dispersion fan. Both sets of data gave the same picture of the shape and location of the concentration front. From this analysis it can be concluded that the uranium concentration in the solid phase at the selected transect is equally well represented by the two sets of data.

A similar comparison between data from small and large samples in a direction deviating about 45 degrees from transect 6110 mN towards south, is shown in Figure 3.7. In this direction, the large sample data indicate higher uranium concentrations in the ore zone at depths between 10 and 20 m than is apparent from the small sample data. Both sets of data give a similar view of the shape and location of the concentration front. Further out from the ore zone the large sample data show higher concentrations than the small sample data.

The main difference between the observed uranium concentration versus distance in the two studied directions is the concentration level at distances beyond 200 m from the upstream boundary of the ore zone (3100 mE). In the transect 6110 mN, i.e. in the south-east direction from the upstream boundary, the concentration is approximately one tenth of the concentration in the south direction (Figures 3.6 and 3.7). This is another indication of that uranium has migrated a longer distance in the south direction than in the south-east direction.

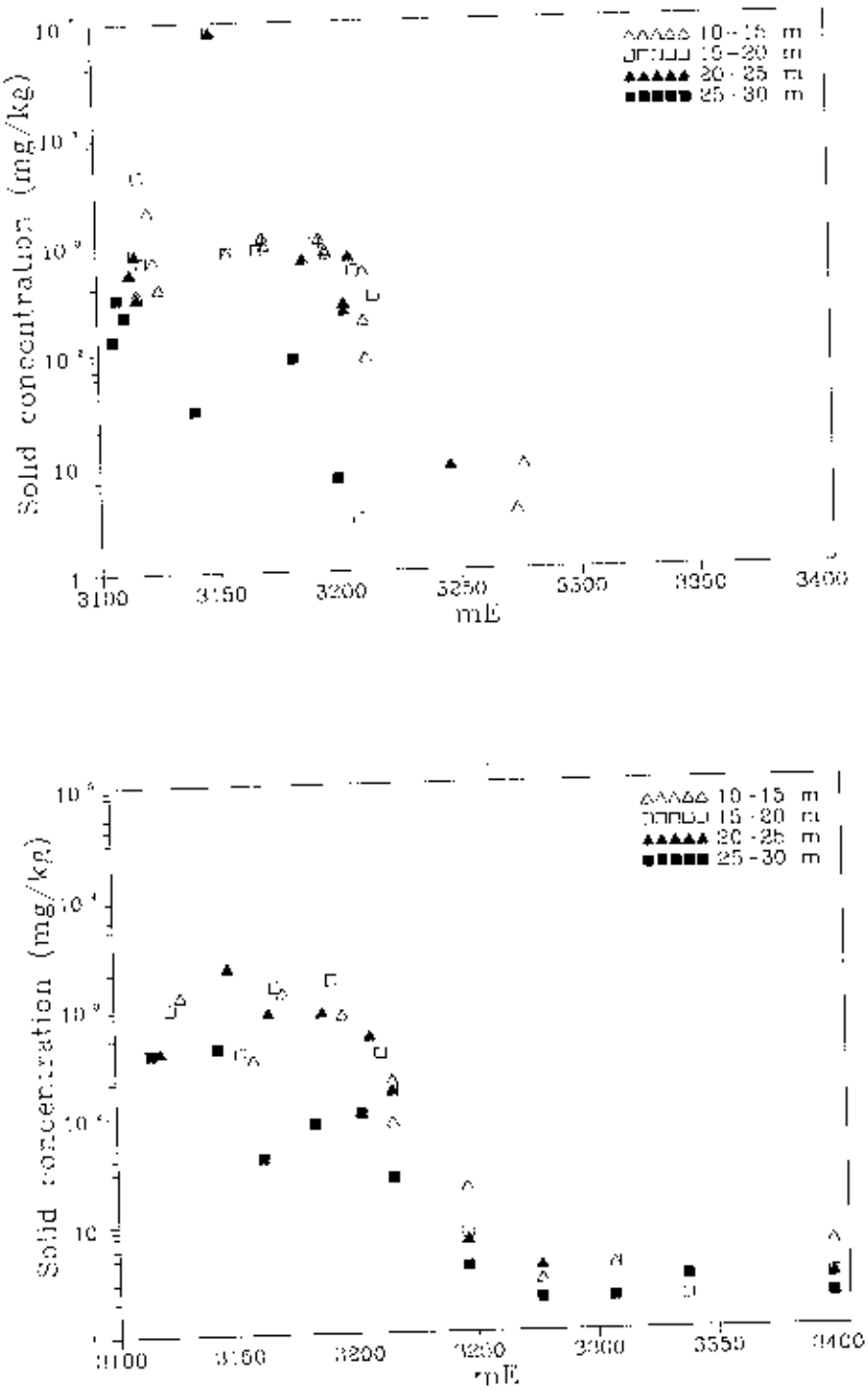

Figure 3.6. Kemakta. Uranium concentrations in solid phase in transect 6110 mN from the upstream boundary of the ore zone. Small sample analyses (upper) and average values over 5 m cores (lower).

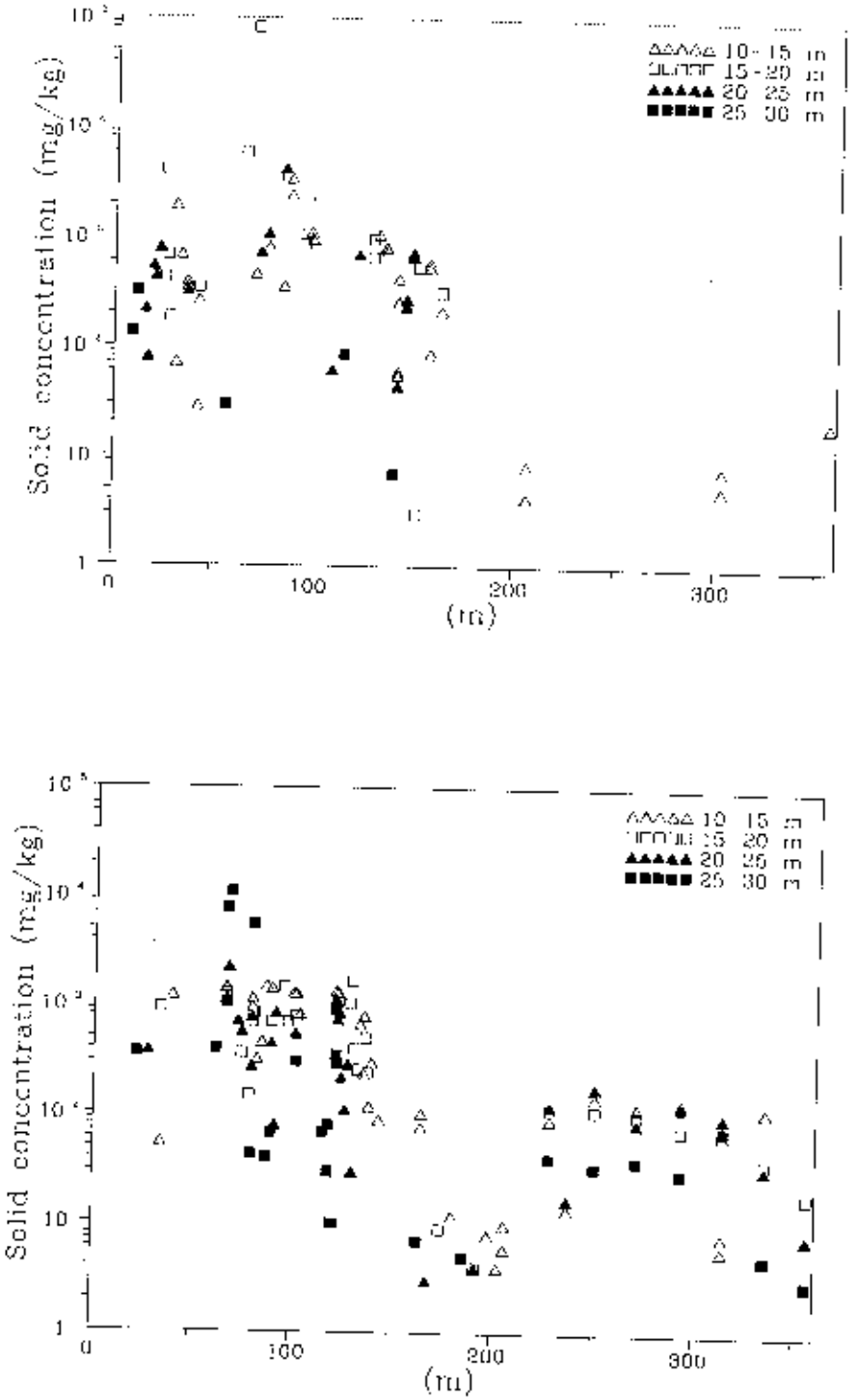

Figure 3.7 Kemakta. Uranium concentrations in solid phase in the S-direction from the upstream boundary of the ore zone. Small sample analyses (upper) and average values over 5 m cores (lower).

3.1.3 Radiochemical Data

A large amount of radiochemical data is available from analyses of bulk rock samples and individual mineral phases. As only small size samples have been analysed, they might not always be representative for larger volumes of the rock. Most data are obtained from samples at the section along the 6110 mN gridline. The relative distribution of uranium series nuclides may give some information on the evolution of the dispersion fan. Kemakta has analysed the activity ratios in bulk rock samples and in individual mineral phases that are presented at different locations and at different depths along the transect 6110 mN.

Bulk Rock Samples

Uranium concentrations and activity ratios for $^{234}U/^{238}U$ and $^{230}Th/^{234}U$ along the transect 6110 mN at different depth intervals are shown in Figures 3.8, 3.9 and 3.10. Between the the surface and 10 m depth, the activity ratio of $^{234}U/^{238}U$ is approximately 1 and it is independent of the distance from the upstream boundary of the ore zone, except close to the upstream boundary, where a few values are higher than 1 as can be seen in Figure 3.8. This deviation indicates a selective leaching of ^{238}U close to the upstream boundary of the ore zone. The $^{230}Th/^{234}U$ activity ratios of 1 to 2 close to the upstream boundary are probably the result of a selective leaching of uranium relative to thorium. The activity ratio seems to decrease with distance to values below 1 further away from the ore zone. This suggests a more recent deposition of uranium further away from the upstream boundary of the ore zone. When the uranium concentrations drop to very low values, the $^{230}Th/^{234}U$ activity ratios increase to values well above 1. This can again be the result of selective leaching of uranium over thorium. It should be noted that the uranium concentrations far away from the ore zone are very low and that the uncertainty in the data probably is large.

At depths between 10 and 20 m, the $^{234}U/^{238}U$ and $^{230}Th/^{234}U$ ratios seem to decrease slightly with distance from the upstream boundary of the ore zone (Figure 3.9). The fact that the $^{230}Th/^{234}U$ activity ratios were found to be above 1 close to the upstream boundary may indicate a selective leaching of uranium. Several of the $^{230}Th/^{234}U$ activity ratios are well above 1 at depths between 10 and 15 m further away from the ore body, where the uranium concentrations are low. This might as well be due to selective leaching of uranium or to uncertainties in the data because of low concentrations.

The activity ratios at depths between 20 and 25 m decrease with distance until the uranium concentration drops (Figure 3.10). This trend is not seen at depths between 25 and 30 m, but the zone with enhanced uranium concentrations is not so extended in the studied direction as it is closer to the surface at these depths. The $^{230}Th/^{234}U$ activity ratios near the upstream boundary of the ore zone do not indicate preferential leaching of uranium over thorium at the depth interval 25 to 30 m.

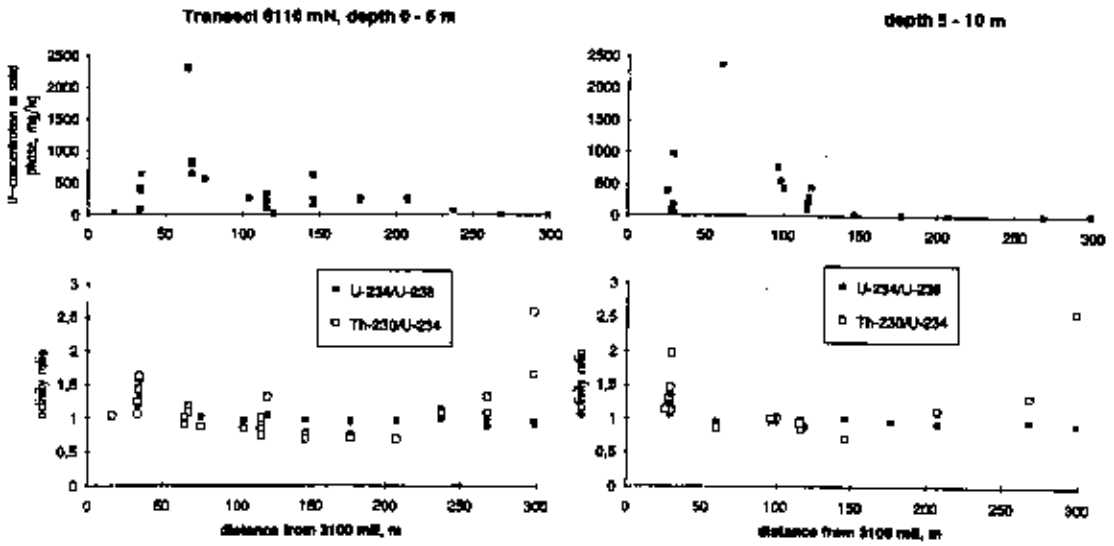

Figure 3.8. Kemakta. Uranium concentrations and activity ratios in bulk rock samples in the depth intervals 0–5 m (left) and 5–10 m (right).

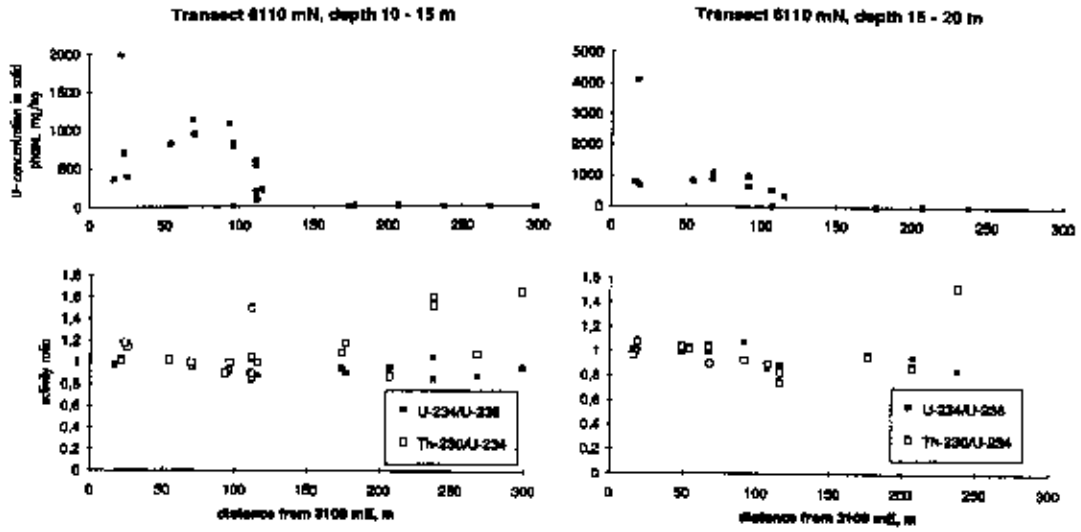

Figure 3.9. Kemakta. Uranium concentrations and activity ratios in bulk rock samples in the depth intervals 10–15 m (left) and 15–20 m (right).

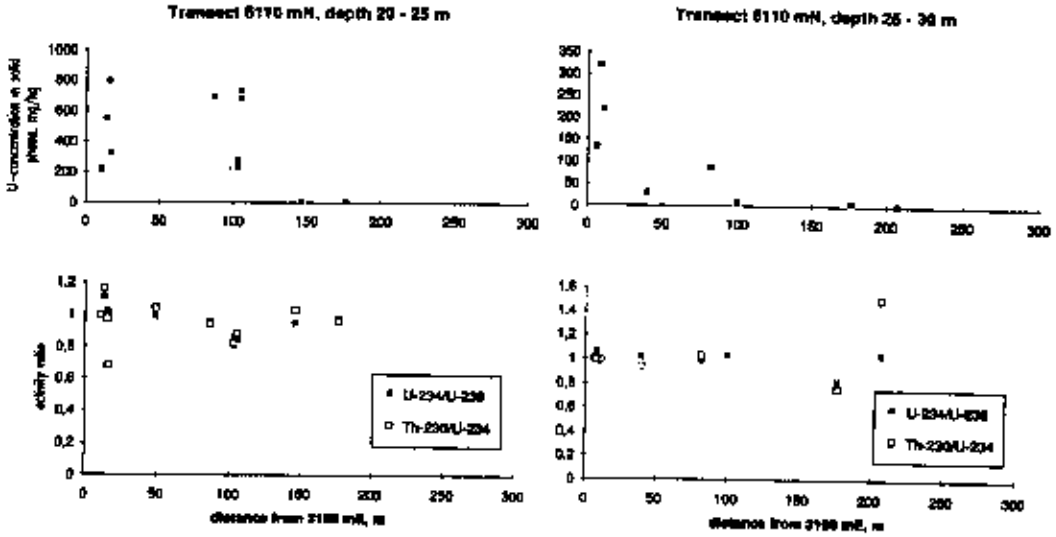

Figure 3.10. *Kemakta. Uranium concentrations and activity ratios in bulk rock samples in the depth intervals 20–25 m (left) and 25–30 m (right).*

Individual Mineral Phases

Uranium and thorium concentrations and activity ratios have been determined in 'amorphous' and 'crystalline' phases of drillcore samples using selective extraction procedures *[Duerden, 1992]*. The amorphous phase is defined as a poorly ordered material, such as ferrihydrite, accessible to and in approximate equilibrium with groundwater. This phase is in the following referred to as the *accessible* phase. The crystalline phases are highly ordered materials such as hematite, goethite, clays and quartz with contained species inaccessible to the groundwater. This phase is in the following referred to as the *inaccessible* phase. Species adsorbed to the surfaces of crystalline phases, mainly iron oxides and clays, are accessible to groundwater and are therefore considered belonging to the accessible phase.

Observed uranium concentrations and $^{234}U/^{238}U$ and $^{230}Th/^{234}U$ activity ratios in the accessible and inaccessible phases along the transect 6110 mN are shown in Figures 3.11 and 3.12. Most of the uranium seems to be contained in the inaccessible phase. The $^{234}U/^{238}U$ activity ratios in the inaccessible phase in the zone with high uranium concentrations are equal to or higher than 1, with the highest values close to the upstream boundary of the ore zone. The activity ratios show a similar trend in the accessible phase with a decrease with distance in the zone of high uranium concentrations, but the values are considerably lower and not exceeding 1. The few available data points in the depth interval 25–30 m, which is just above the base of weathering, are illustrated in Figure 3.12.

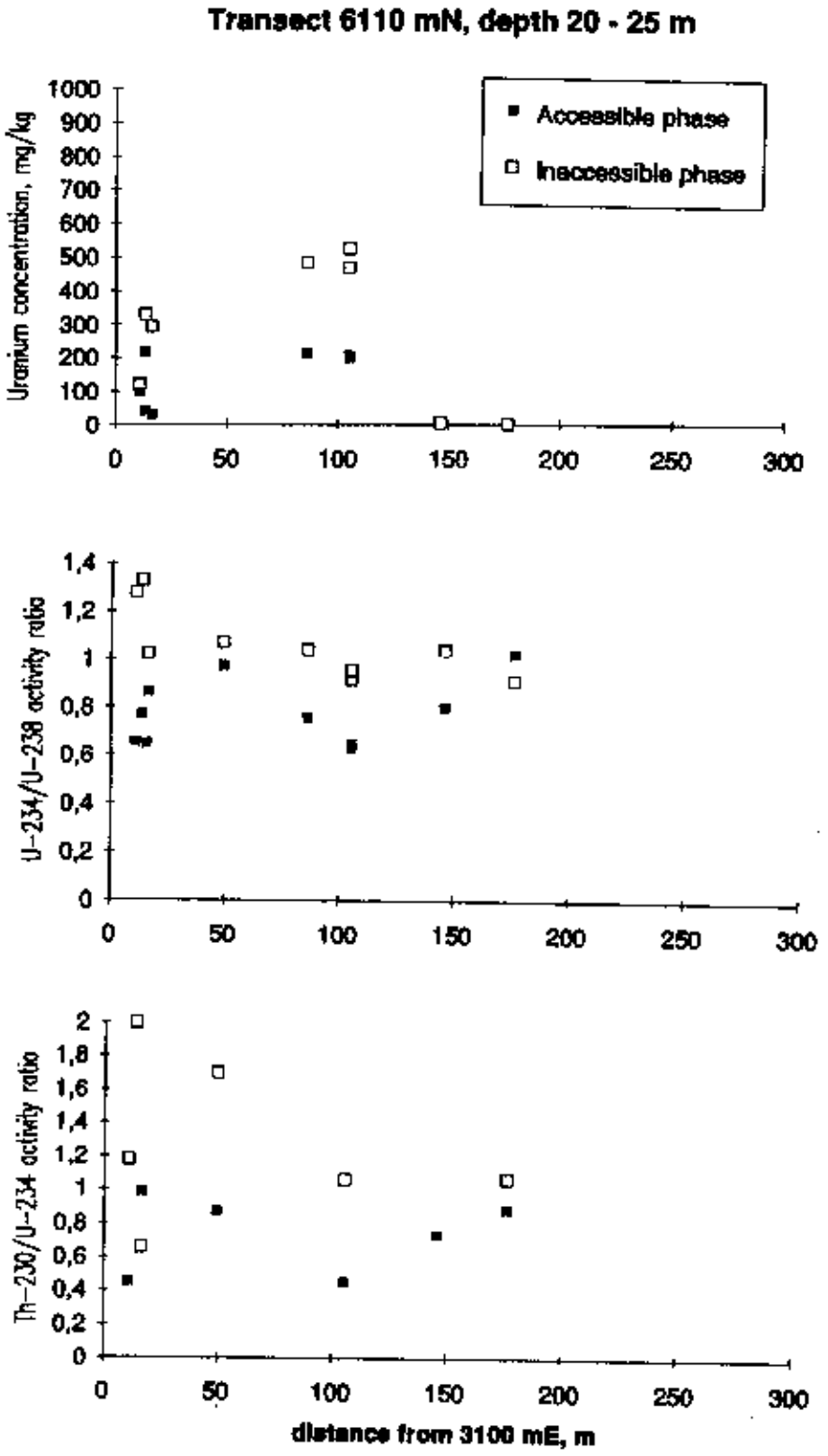

Figure 3.11. *Kemakta. Uranium concentrations and activity ratios in the accessible and inaccessible phase along the 6110 mN gridline in the depth interval 20–25 m.*

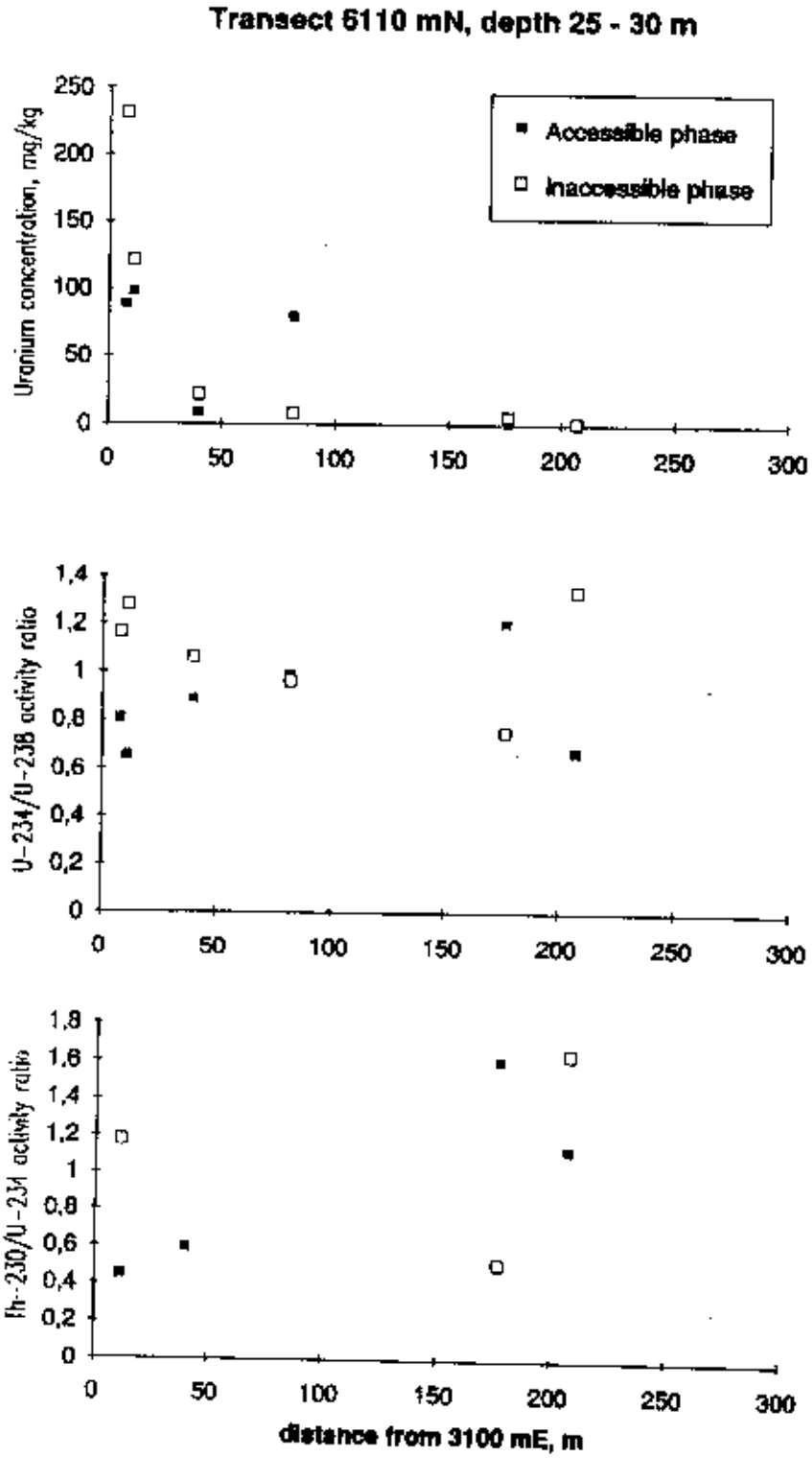

Figure 3.12. *Kemakta. Uranium concentrations and activity ratios in accessible and inaccessible phase along the 6110 mN gridline in the depth interval 25–30 m.*

The $^{234}U/^{238}U$ activity ratios illustrated in Figures 3.11 and 3.12 indicate an accumulation of ^{234}U in the inaccessible phase and a depletion in the accessible phase. This may be an effect of α-recoil, transferring ^{234}Th, the short-lived daughter nuclide of ^{238}U and parent nuclide of ^{234}U, into the inaccessible phase. The decrease in the activity ratio of both phases with distance from the upstream boundary of the ore zone suggests a more recent deposition of uranium that has moved downstream along the transect. At the distance where the uranium concentration steeply drops to low values, the activity ratios in the accessible phase start to increase with increasing distance, except at the depth interval 25 to 30 m. At approximately 200 m and further away from the upstream boundary of the ore zone the activity ratios in both the accessible and inaccessible phases are close to 1. This suggests that uranium in that area was deposited a long time ago, maybe when the primary ore was formed, and that the uranium concentrations there should be considered as being background levels.

The trend in the $^{230}Th/^{234}U$ activity ratio in the accessible phase is similar to that of the $^{234}U/^{238}U$ activity ratio with values close to 1 at the upstream boundary of the ore zone. The ratio has a minimum at the uranium concentration front and higher values are found at distances further away from the ore zone. This finding does not contradict the suggestion of a more recent deposition of uranium close to the concentration front. However, the activity ratios well above 1 at long distances are not consistent with the assumption of background levels of uranium in this area. It is rather an indication of a preferential removal of uranium over thorium that has taken place more recently. The general trend towards $^{230}Th/^{234}U$ activity ratios above 1 in the inaccessible phase can be due to recoil transfer of ^{230}Th from accessible to inaccessible phase.

Review of Radiochemical Data. Conclusions

The observed activity ratios, especially in the accessible phase, decrease with distance from the upstream boundary of the ore zone within the dispersion fan, but increase at distances beyond the concentration front, as the uranium concentration reaches background levels. The activity ratios in the accessible phase are generally lower than in the inaccessible phase, indicating a more recent deposition of uranium in the accessible phase and/or a preferential transfer of ^{234}U and ^{230}Th from the accessible to the inaccessible phase, for example as a result of α-recoil.

The data seem to follow the same pattern in the entire weathered zone, except in the surface layer just above the base of weathering. Due to present day monsoonal climate of the area, the hydraulic conditions in the near-surface layer vary between a dry, unsaturated state during the dry season and flooding causing high flow rates close to the surface during the wet season. During the dry season, the water table may be lowered as much as 10 m. This fluctuation in the water table and the variation in water flow in the surface layer may influence the redistribution of uranium and the activity ratios in the upper 10 m of the weathered zone.

Just above the base of weathering the data indicate a shorter migration distance for uranium than in the rest of the weathered zone. This is probably because the conditions at the interface between weathered and unweathered rock, such as minimal weathering of the rock and low water flux, are not favourable for uranium dissolution and migration.

3.2 RIVM

One of the most important features of the uranium mineralisation at Koongarra is the occurrence of abundant secondary uranium minerals, principally within the dispersion fan above ore body 1. At present, it is believed that the dispersion of uranium started, when the lower boundary of the weathered zone reached the top of the ore body, and that it has virtually stopped in those parts of the formation that are completely weathered and turned into clayey material. The dispersive transport is therefore assumed to take place in the transition zone of the weathering, where the flow velocity is highest and thus the dispersion rate is largest. Flow and transport are assumed to be mainly horizontal in the transition zone. Thus, one may identify three different layers:

- a top, fully weathered layer, in which no significant dispersion takes place
- an intermediate, partially weathered layer (the transition zone) moving downward as the weathering proceeds, in which the groundwater velocity is the highest and the dispersion rate is the largest
- a lower, unweathered zone, in which no dispersion of uranium occurs.

It might be expected that the magnitude and direction of the average flow velocity and transport have changed repeatedly during the past two million years, which is the estimated age of the dispersion fan. Such variations would result in different dispersion distances and directions at different depths. The form of the dispersion fan at different depths together with a reasonable estimate of the downward movement of the transition zone would then provide information about the direction and magnitude of flow and dispersion during the past two million years. However, this would be the case only if transport is negligible at all places, except in the transition zone of weathering. This hypothesis of transport taking place in the transition zone was tested by analysing available solid phase uranium concentration data. In addition, the distribution ratio of uranium between the solid phase and the water was studied.

The processes involved in the mobilization and immobilization of radionuclides must be understood prior to the modelling of radionuclide transport from the ore body. A preliminary geochemical study was therefore performed during INTRAVAL phase 1 to identify the processes that have resulted in the present occurrence of uranium in the Koongarra ore deposit.

3.2.1 Changes in dispersion distance and direction with depth

The concentration of uranium in the solid phase has been analysed and reported within the ARAP project. RIVM has presented all available data as contour plots at different depth intervals to get an overview. The migration distance and the main direction of dispersion were estimated from these plots (Figures 3.13a-f).

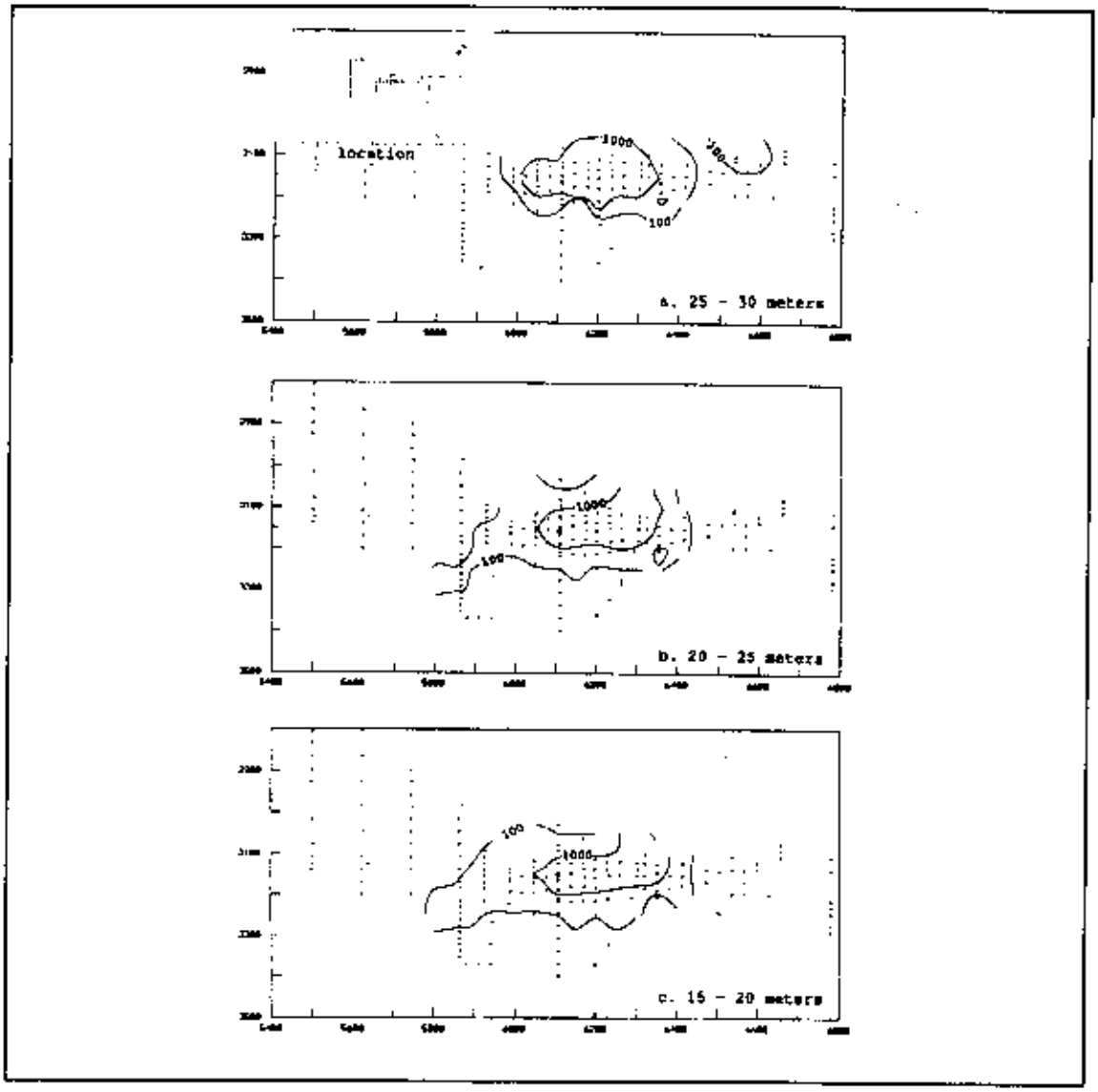

Figure 3.13 a–c RIVM. Contours of solid phase uranium concentrations (100 and 1000 mg/kg) at different depth intervals: a) 25–30 m, b) 20–25 m, c) 15–20 m.

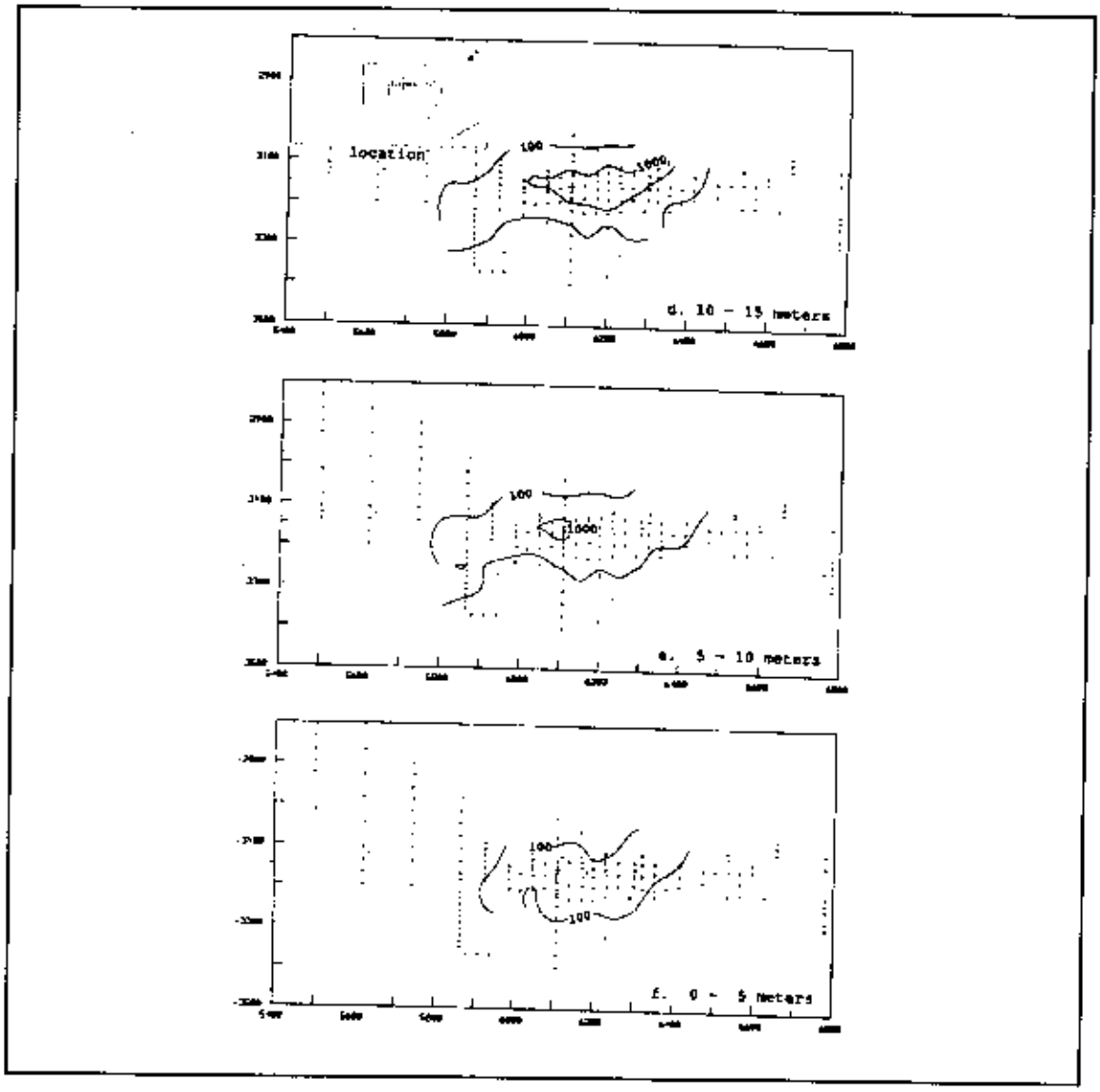

Figure 3.13 d-f RIVM. Contours of solid phase uranium concentrations (100 and 1000 mg/kg) at different depth intervals: d) 10–15 m, e) 5–10 m, f) 0–5 m.

The 100 and 1000 mg/kg contour lines of the solid phase uranium concentration are given in plan view. The contour lines in each figure represent measurements within a depth interval of 5 m, ranging from a depth of 30 m (the top of the unweathered schist) up to the present soil surface. Figure 3.13a shows the distribution of uranium in the primary ore body in the unweathered zone, as well as in the top of ore body 2 which is visible to the right of the main ore body. Figure 3.13b illustrates the uranium concentration contour lines just above the base of weathering. It can be seen that the nuclide transport has occurred in an approximately south-westerly direction. Note that north in the figure is upward and slightly to the right as illustrated in Figure 3.1. By comparing Figures 3.13a and 3.13b, it may be concluded that the base of weathering is the lower boundary for the region in which dispersion of uranium has occurred. The direction and distance of the dispersion of uranium is roughly the same at the depths

represented in Figures 3.13c to 3.13e, and in Figure 3.13b. However, the zone with uranium concentrations above 100 mg/kg is more extended in Figures 3.13d and 3.13e than in Figure 3.13b. From Figure 3.13f it appears that no primary ore is found within the first 5 m.

The dispersion direction and distance were estimated from the 100 ppm contour lines in Figures 3.13b to 3.13e and are summarised in Table 3.2. The transport distances and directions were estimated, assuming that borehole PH49 is located at the center of the ore body. This choice was based on the fact that this borehole is within the 1000 mg/kg contour at all depths. The transport distance was estimated by finding the point on the 100 mg/kg contour farthest away from PH49 in the general south-westerly direction. The compass bearing of the farthest point in relation to PH49 gives the main direction of the transport.

Table 3.2. RIVM. Estimates of dispersion direction and distance based on uranium concentrations in the solid phase.

Depth (m relative to 25 m AHD[1])	Main transport direction (degrees compass bearing)	Transport distance (m relative to PH49)
20–25	209°	335
15–20	214°	342
10–15	217°	340
5–10	221°	336

[1] AHD = Australian Height Datum

The results of this data analysis show that the direction and distance of dispersion is almost constant with depth. The farthest point on the 100 mg/kg uranium contour is between 335 m and 342 m away from PH49 and the direction from PH49 is between 209° and 221° compass bearing.

The following explanation for these observations can be made:

- The magnitude and direction of the average groundwater flow has not changed significantly during the past two million years.
- Other environmental factors have played an important role; vertical transport of uranium cannot be neglected, changes have occurred in groundwater pH over time, geochemical processes other than adsorption have been more influential, etc.

The shapes of the concentration distributions supports the hypothesis that groundwater movement and dispersion of uranium has taken place mainly in the transition zone. As there are no observations at Koongarra of a decrease of the dispersion distance with depth, there are no signs of a significant transport of uranium in the fully weathered top layer. Furthermore, the

shape of the concentration distribution indicates that the direction of groundwater flow does not seem to have changed significantly during the past few million years.

3.2.2 Distribution coefficients of uranium

The distribution ratio (R_d) of uranium is the ratio between the mass of uranium in the solid phase and the mass of uranium in solution:

$$R_d = \frac{\rho_s(1-n)}{n}\frac{Q}{C} \qquad \text{(Eq. 3.1)}$$

In which:

R_d = Distribution ratio [-]
ρ_s = Rock density [$M \cdot L^{-3}$]
n = Porosity [-]
Q = Bulk rock concentration [$M \cdot M^{-1}$]
C = Concentration in solution [$M \cdot L^{-3}$]

The quotient of Q and C is referred to as the partition coefficient P. In case of linear sorption, the P-value is constant (independent of C) and referred to as the distribution coefficient K_d ($L^3 \cdot M^{-1}$). Data analysis for Koongarra showed that the P-value calculated using the bulk rock uranium concentration, denoted by P_b, ranges from 1 to 52 m^3/kg *[Edis et al., 1992]*. Calculation of a partition coefficient based on the concentration of accessible uranium of the bulk rock phase, denoted by P_a, suggests a value in the range of 0.4 to 1 m^3/kg *[Edis et al, 1992]*. In the weathered zone, uranium appears to be mainly associated with secondary oxides of iron. The difference between the P_b and P_a values possibly reflects the fact that the early association of uranium with iron oxides becomes inaccessible (no longer in equilibrium with the solution) as a result of the aging of this mineral.

The use of bulk rock data for determining distribution coefficients, unambiguously overestimates the "equilibrium" adsorption of uranium onto the solid phases. A more realistic value may therefore be obtained using chemical extraction data and base the K_d-concept on the mass of uranium in the accessible phases of the rock. This thesis is supported by the similar activity ratios of $^{234}U/^{238}U$ in groundwater and accessible phases.

An examination of P-values at different locations along the dominant transport direction gave no evidence that the processes determining the distribution of uranium between the solid phase and the solution change with distance. This means that it might be a good approximation to use the average P_a-value as a K_d in the transport modelling, keeping in mind that this is a simplification of the processes occurring at Koongarra.

4. Models, Assumptions and Results for Migration Calculations

The migration distance of uranium has been simulated by Kemakta and RIVM for a number of parameter combinations and model concepts to test whether the observed migration distances could be predicted.

Both teams based their migration calculations on data that had been determined and reported within the ARAP project, e.g. porosity, K_d and rock densities, and the extensive hydrological work that was performed within ARAP as well as within INTRAVAL phase 1.

4.1 Kemakta

The Kemakta team focused their work on calculations of the dispersion of uranium and daughter nuclides in the weathered zone. The aim was to test the applicability of rather simple models that generally are used in performance assessment of radioactive waste repositories.

The modelling work was carried out in several iterations with increasing level of complexity. Each iteration included a review of available laboratory and field data, selection of the system to be modelled and a suitable model, and finally a comparison of modelling results with field observations.

In total three iterations were performed in which the following model concepts were applied:

- advection–dispersion model with linear sorption
- advection–dispersion model with linear sorption and chain-decay
- advection–dispersion model with linear sorption, chain-decay, α-recoil and phase transfer.

In the first modelling attempt, a simple 1-D advection–dispersion model including linear sorption according to the K_d-concept was used to simulate the dispersion of uranium in the weathered zone. This model may be considered as a simple performance assessment model.

In the second iteration, the system was extended to also include the transport of the daughter nuclides ^{234}U and ^{230}Th. In addition, an attempt was made to consider α-recoil in a very simple manner by assigning a higher K_d-value to ^{234}U than to ^{238}U. Furthermore, the sensitivity of the results to different combinations of groundwater flux and migration time was studied, as well as the effects of alternating periods of flow and no flow.

In the third and final iteration, the model was even further extended to include transfer of radionuclides between different phases of the rock. Additionally, a more detailed model description of α-recoil was used. This model is based on the assumption that radionuclides in the groundwater are sorbed to accessible phases of the weathered rock (amorphous iron oxides and clays) and that sorbed radionuclides are further included in inaccessible crystalline phases of the rock by recoil effects and recrystallisation of amorphous iron oxides and clays.

As the migration modelling by Kemakta was made during a fairly long time period, the recommended values for some of the parameters included in the calculations have changed, as more information became available. This is reflected in the values for the porosity, distribution

coefficients, water flux, dispersion length and source concentration which have been regularly updated and might therefore be different in the different iterations.

4.1.1 Advection–Dispersion Model with Linear Sorption

A simple approach was applied in these initial calculations. The system examined was the part of the weathered zone located below the water table. The basic assumptions were that this part of the weathered zone is homogeneous and that the system has been static at present conditions over the time-scale considered.

Uranium in the groundwater was assumed to be transported with groundwater flowing in the weathered zone. The processes included were: 1-D advection, hydrodynamic dispersion, and sorption. The weathered zone was assumed to be porous, and sorption of uranium to the solid phase was assumed to occur instantaneously in proportion to the uranium concentration in the groundwater (the K_d-concept). Only migration of ^{238}U was considered in these calculations.

The uranium migration was further assumed to have persisted during 2 million years. Radioactive decay was not considered due to the very long half-life of ^{238}U, $4.47 \cdot 10^9$ years.

The uranium migration in the weathered zone was modelled using the advection–dispersion equation:

$$\epsilon_f R \frac{\partial c}{\partial t} = D_L \frac{\partial^2 c}{\partial x^2} - u_0 \frac{\partial c}{\partial x} \qquad \text{(Eq. 4.1)}$$

$$D_L = \alpha \cdot u_0 + D_M \frac{\epsilon_f \cdot \delta_D}{\tau^2} \qquad \text{(Eq. 4.2)}$$

The retardation of uranium is defined as:

$$R = \frac{\epsilon_f + (1 - \epsilon_f) K_d \cdot \rho_s}{\epsilon_f} \qquad \text{(Eq. 4.3)}$$

and the relation between solid and liquid concentration of uranium is:

$$q = K_d \cdot c \qquad \text{(Eq. 4.4)}$$

where c = uranium concentration in the groundwater, (Bq/m^3)
D_L = dispersion coefficient, (m^2/year)
D_M = molecular diffusivity of uranium in water, (m^2/year)
K_d = distribution coefficient for uranium, (m^3/kg)

q = concentration of uranium in solid phase, (Bq/kg)
R = retardation of uranium (-)
t = time, (year)
x = length coordinate, (m)
u_0 = groundwater flux (Darcy velocity), (m^3/m^2,year)
α = dispersion length, (m)
δ_D = constrictivity of flow paths, (-)
ϵ_f = flow porosity, (m^3/m^3)
ρ_s = solid density, (kg/m^3)
τ^2 = tortuosity of flow paths, (-)

The initial and boundary conditions applied are:

$c = 0$ for $t = 0$ and $x > 0$
$c = c_0$ for $x = 0$ and $t \geq 0$
$c = 0$ for $x = \infty$ and $t \geq 0$.

The advection–dispersion equation was solved using the numerical code TRUMP *[Edwards, 1972]* which is based on an integrated finite difference method and solves, in general, for transient potential distributions in multidimensional systems with advection, conduction and source terms.

Data

The porosity and solid density values were set to 30% and 2500 kg/m^3, respectively. The value of the flow porosity is about twice as large as recently reported for matrix flow in the weathered zone *[Emerson, 1992]*. However, the model output is much less sensitive to these parameters than to the water flux and the distribution coefficient.

Two values of the distribution coefficient, K_d, were used in the calculations, 0.1 and 10 m^3/kg. These values were chosen based on experimentally determined distribution coefficients *[Sekine and Ueno, 1989]*.

As the hydrology at the site is not very well known, calculations were carried out for different values of the water flux. The uncertainty in the hydrology is reflected in the values of the water flux, ranging from $3.2 \cdot 10^{-4}$ to 10 m/yr which have been reported by different groups in the ARAP. The following values of the water flux were used in the calculations:

10^{-3} m/yr — This value is of the same magnitude as the Darcy fluxes in the weathered layer calculated by Lever and Morris *[Lever and Morris, 1990]* using the NAMMU code and assuming a highly permeable fault and an aquitard weathered layer. A similar value is obtained using hydraulic heads and hydraulic conductivities reported by Raffensberger and Garven *[Raffensperger and Garven, 1989]*.

0.01 and 0.1 m/yr — These values were chosen based on Darcy fluxes in the weathered zone ($4.7 \cdot 10^{-2}$ m/yr) calculated for the case of a highly permeable fault and a weathered layer that is an aquifer compared to the unweathered layer *[Lever and Morris, 1990]*.

1 and 10 m/yr — These values are of the same magnitude as fluxes estimated by Australian Groundwater Consultants (2–10 m/yr) and previously used in modelling the radionuclide transport at Koongarra *[Lever, 1986]*.

The assigned values of the flow porosity and water fluxes give transport velocities ranging from 0.0033 to 33 m/yr.

A dispersion length of 1 m and a molecular diffusivity of uranium of $6.3 \cdot 10^{-2}$ m^2/yr ($2 \cdot 10^{-9}$ m^2/s) were chosen in these initial calculations. The value of the dispersion length is representative for transport distances of 10 to 100 m, according to a compilation made *[Gelhar et al. 1985]*. Any possible effects of constrictivity and tortuosity of the flow paths were neglected in the calculations.

The concentration of dissolved uranium at the source was assumed to be constant in time at a level of 1000 mg/m^3. This value is somewhat higher than the highest concentration that has been measured in groundwater samples from drill holes penetrating the ore body, but somewhat lower than an estimate of the uranium solubility of 1200 mg/m^3 obtained with a simple speciation calculation. This calculation was carried out using the geochemical code EQ3 and assuming a groundwater composition according to results from an analysis of water samples taken from hole PH49 in May 1988. Calculations were also performed with a source concentration of 100 mg/m^3. This concentration is somewhat lower than the mean value in the samples from hole W1.

The uranium source was assumed to be located at 3100 mE, which is approximately where the outer extension of the ore body, towards the fault, is found.

The data used in the calculations are summarised in Table 4.1.

Table 4.1. Kemakta. Advection-dispersion model with linear sorption. Data used in the calculations.

Porosity (m^3/m^3)	0.30
Solid density of rock (kg/m^3)	2500
Distribution coefficient (m^3/kg)	0.1, 10
Water flux (m/yr)	10^{-3}, 10^{-2}, 10^{-1}, 1, 10
Dispersion length (m)	1
Molecular diffusivity (m^2/s)	$2 \cdot 10^{-9}$
Concentration of uranium at the source (mg/m^3)	100, 1000

Results

The calculated solid concentration of uranium at different distances from the source together with available small sample data from the depth interval 10–30 m in holes located along the transect at about 6110 mN are shown in Figures 4.1 and 4.2. The results from the calculations are also compiled in Table 4.2.

The results presented in Figure 4.1 illustrate that a K_d-value of 0.1 underpredicts the solid uranium concentration in the dispersed fan. A K_d-value of 10, (Figure 4.2), overpredicts the solid uranium, if the concentration of dissolved uranium at the source is 1000 mg/m^3, but gives a prediction that agrees fairly well with observed values, if the source concentration is 100 mg/m^3.

The migration distance is independent on the source concentration. The migration distance is well predicted for the combination of a K_d-value of 0.1 and a Darcy flux of 10^{-2} m/yr. Higher water fluxes overpredict and lower water fluxes underpredict the migration distance. The combination of a K_d-value of 10 and a Darcy flux of 1 m/yr predicts the migration distance fairly well, whereas a higher water flux overpredicts and a lower water flux underpredicts the migration distance.

With this model, the migration distance is dependent on the ratio Darcy flux to the distribution coefficient, K_d, and the maximum solid concentration level is dependent on the product of the liquid source concentration and the distribution coefficient. This means that a Darcy flux of 0.1 m/yr, a K_d-value of 1 m^3/kg and a source concentration of 1000 mg/m^3 will give a concentration curve similar to the one shown in Figure 4.1, with a Darcy flux of 1 m/yr, a K_d-value of 10 m^3/kg and a source uranium concentration of 100 mg/m^3.

All these modelling results are calculated for a migration time of 2 million years. A change in this entity will affect the migration distance and the steepness of the concentration front. The migration distance is directly proportional to the time of migration. For example, migration during 1 million years will result in migration distances half as long as those obtained for 2 million years. A shorter migration time will also result in a steeper concentration front, while the front will be more dispersed if the time of migration is longer than 2 million years.

Changing the location of the source to 3150 mE, which is approximately where the interface between the ore body and the dispersion fan is found, does not improve the results to any large extent.

Table 4.2. Kemakta. Advection-dispersion model with linear sorption. Calculated migration distances for a travel time of 2 million years. The observed migration distance is about 120 m.

K_d (m^3/kg)	Darcy flux (m/yr)				
	10^{-3}	10^{-2}	10^{-1}	1	10
Concentration of dissolved uranium at the source, 1000 (mg/m^3)					
0.1 [1]		~120	>200	>200	>200
10 [2]			10	~120	>200
Concentration of dissolved uranium at the source, 100 (mg/m^3)					
0.1 [1]		~120	>200	>200	>200
10 [3]			10	~120	>200

1) All cases predicted a too low solid uranium concentration level.
2) All cases predicted a too high solid uranium concentration level.
3) All cases predicted a fairly good solid uranium concentration level.

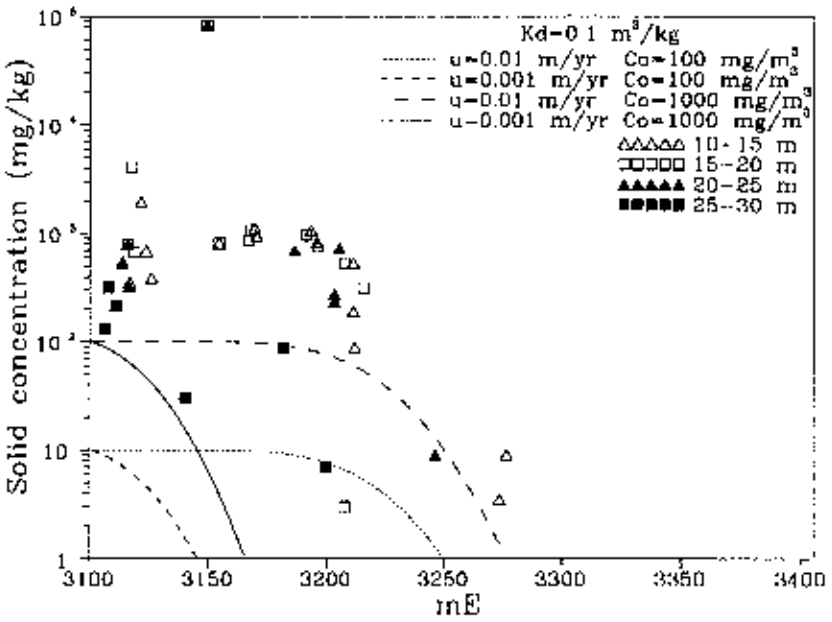

Figure 4.1. Kemakta. Advection–dispersion model with linear sorption. Predicted and observed uranium concentrations along the transect 6110 mN. Source located at the outer extension of the ore body. K_d=0.1 m^3/kg.

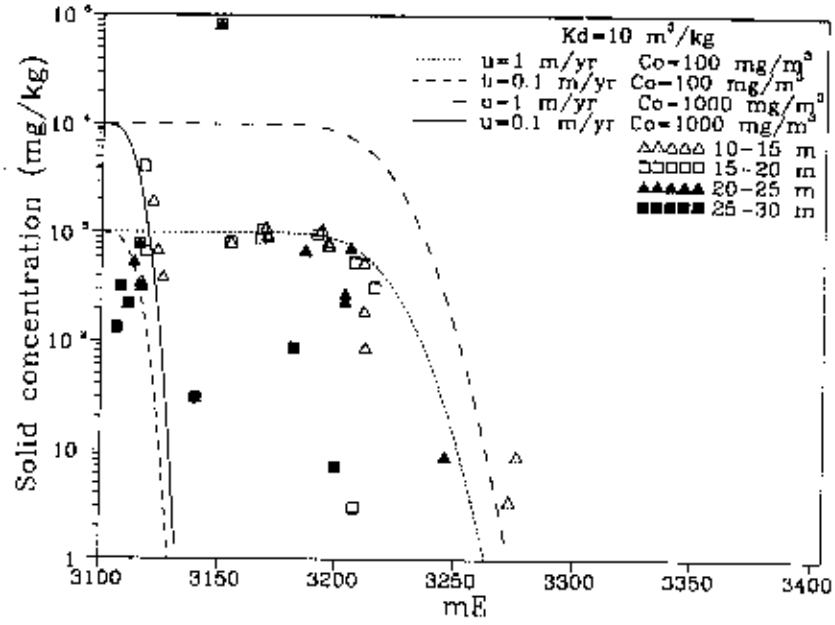

Figure 4.2. Kemakta. Advection–dispersion model with linear sorption. Predicted and observed uranium concentrations along the transect 6110 mN. Source located at the outer extension of the ore body. K_d=10 m³/kg.

Advection–Dispersion Model with Linear Sorption. Conclusions

Calculations with the simplest model gave results that were quite similar to what has been measured. It should be noted that the migration distance in this simple model concept is determined by the ratio between Darcy flux and K_d. Likewise the maximum solid concentration is determined by the product of K_d and source uranium concentration. This implies that there are an infinite number of combinations of K_d-values, Darcy flux values and liquid source concentrations that will give the same results.

4.1.2 Advection–Dispersion Model with Linear Sorption and Chain Decay

In the second iteration of the modelling work, the system was extended to include also transport of the ^{238}U daughter nuclides, ^{234}U and ^{230}Th. Otherwise the modelled system and the assumptions made were the same as in the first modelling attempt, except for some changes of updated input data in accordance with recommendations from ARAP as well as from conclusions drawn from previous calculations.

The advection–dispersion equation (Eq. 4.1) was extended to include chain decay, assuming that the migration of nuclide *i* in a porous medium with instantaneous and linear sorption is expressed as:

$$\epsilon_f R_i \frac{\partial c_i}{\partial t} = D_L \frac{\partial^2 c_i}{\partial x^2} - u_0 \frac{\partial c_i}{\partial x} - \epsilon_f R_i \lambda_i c_i + \epsilon_f R_{i-1} \lambda_{i-1} c_{i-1} \qquad \text{(Eq. 4.5)}$$

with the dispersion coefficient, D_L, defined by Eq. 2. The retardations of nuclide i and parent nuclide $i-1$ are defined as:

$$R_i = \frac{\epsilon_f + (1 - \epsilon_f) K_{d,i} \rho_s}{\epsilon_f} \qquad R_{i-1} = \frac{\epsilon_f + (1 - \epsilon_f) K_{d,i-1} \rho_s}{\epsilon_f}$$

(Eqs. 4.6 and 4.7)

and the relations between solid and liquid concentration of the nuclides are:

$$q_i = K_{d,i} c_i \qquad q_{i-1} = K_{d,i-1} c_{i-1} \qquad \text{(Eqs. 4.8 and 4.9)}$$

where c_i = concentration of nuclide i in the groundwater, (Bq/m^3)
c_{i-1} = concentration of parent nuclide $i-1$ in the groundwater, (Bq/m^3)
$K_{d,i}$ = distribution coefficient for nuclide i, (m^3/kg)
$K_{d,i-1}$ = distribution coefficient for parent nuclide $i-1$, (m^3/kg)
R_i = retardation factor of nuclide i, (-)
R_{i-1} = retardation factor of parent nuclide $i-1$, (-)

q_i = concentration of nuclide i in solid, (Bq/kg)
q_{i-1} = concentration of parent nuclide $i-1$ in solid, (Bq/kg)
λ_i = decay constant of nuclide i, (year^{-1})
λ_{i-1} = decay constant of parent nuclide $i-1$, (year^{-1})

The initial and boundary conditions applied were:

$c_i = 0$ for $t = 0$ and $x > 0$
$c_i = c_0$ for $x = 0$ and $t \geq 0$
$c_i = 0$ for $x = \infty$ and $t \geq 0$.

The advection-dispersion equation including sorption and chain decay was solved using the numerical code TRUCHN *[Rasmuson et al., 1982]*, which is an extended version of the code TRUMP *[Edwards, 1972]*.

Data

The same values for the porosity and the solid density, 30% and 2500 kg/m^3, were used as in the first modelling attempt. The dispersion coefficient was calculated assuming a dispersion length of 1 or 10 m, and a molecular diffusivity for the radionuclides of $6.3 \cdot 10^{-2}$ m^2/year ($2 \cdot 10^{-9}$ m^2/s). The dispersion lengths are representative for transport distances in porous media of 10 to 100 m and 10 to 1000 m, respectively *[Gelhar et al., 1985]*.

The distribution coefficient for uranium in this second iteration was set to 1 m^3/kg, based on experimentally determined distribution coefficients and field observations of the partitioning between liquid and solid phase. Distribution coefficient values of 5, 10 and 100 m^3/kg were used for thorium. A water flux of 0.1 m/yr was chosen, based on the results from the first calculations, since this flux together with the used distribution coefficient for uranium resulted in a reasonable transport distance for a migration time of 2 million years.

The uranium concentration at the source was assumed to be constant over time at a level of 1000 mg/m^3 (12 000 Bq/m^3). The two uranium isotopes, ^{238}U and ^{234}U, were assumed to be in radioactive equilibrium. The concentration of ^{230}Th in the groundwater at the source was assigned a value, based on the assumption that ^{230}Th is in radioactive equilibrium with the uranium isotopes at all times. This may not be the case initially when the mobilisation of uranium and thorium starts, but the results from the calculations presented below show that the migration of thorium is not very sensitive to the thorium concentration at the source.

The observed activity ratios between ^{234}U and ^{238}U indicate a retention of ^{234}U relative to ^{238}U. This could be due to α-recoil of the short-lived ^{234}Th into the solid phase making ^{234}U, the daughter nuclide of ^{234}Th, more attracted to the solid phase than ^{238}U, the parent nuclide of ^{234}Th. This effect was simulated in a simple manner in one calculation by assigning a higher K_d-value for ^{234}U than for ^{238}U, 1.5 m^3/kg and 1 m^3/kg, respectively. In addition, calculations were carried out to study possible changes in the activity ratios due to different natural background levels of uranium and daughter nuclides in the rock in the weathered zone. Two values of the background levels were used, 12 mBq/kg and 12 Bq/kg.

The data used in the calculations are summarised in Table 4.3.

Table 4.3. Kemakta. Advection-dispersion model with linear sorption and chain-decay. Data used in the calculations.

porosity (m^3/m^3)	0.30
solid density of rock kg/m^3)	2500
distribution coefficients (m^3/kg)	
uranium	1[a)]
thorium	5, 10, 100
water flux (m/yr)	10^{-1}
dispersion length (m)	1, 10
molecular diffusivity (m^2/s)	$2 \cdot 10^{-9}$
source concentration (mg/m^3)	
uranium	1000
thorium	in equilibrium

a) to simulate α-recoil, K_d=1.5 for ^{234}U

Results

Figures 4.3 to 4.9 show the modelling results and the observed activity data in the depth interval 10–30 m along the 6110 mN transect. The uranium source was assumed to be located at the outer extension of the ore body (3100 mE).

The two calculated concentration curves for ^{238}U depicted in Figure 4.3 show the influence of the dispersivity. A dispersion length of 1 m seems to better represent the measured ^{238}U data than a dispersion length of 10 m. The same observation was done for the ^{234}U activity data as illustrated in Figure 4.4.

A good agreement with measured activities at the front was obtained, when α-recoil was simulated by a higher K_d for ^{234}U (K_d=1.5) than for ^{238}U (K_d=1.0), see Figure 4.4. However, the calculated peak values close to the source cannot be found in the observed data. A comparison of calculated and observed activity ratios $^{234}U/^{238}U$ gives a somewhat different picture (Figure 4.5). Because of the higher K_d, ^{234}U will, compared to ^{238}U, be enriched in the solid phase close to the source, resulting in activity ratios above 1, and delayed at longer distances from the source, resulting in an activity ratio which decreases below 1. This tendency can also be seen in the measured data, although much less pronounced. However, at longer distances than 100–150 m from the assumed location of the source, the observed activity ratios no longer decrease with distance from the source, as the predicted curve suggests. The observed activity ratios close to 1 at these longer distances may be an indication of the presence of background levels of uranium at those locations. If both uranium isotopes are sorbed to the same extent, then radioactive equilibrium is expected between the isotopes and the activity ratio will be maintained at a constant value of 1, as illustrated in Figure 4.5.

The calculated and observed activity content of ^{230}Th in the solid phase at different locations in the transect 6110 mN are shown in Figure 4.6. As for the uranium isotopes, the steeper concentration front obtained with the lower value of the dispersion length is more in agreement with the measured data. The transport of ^{230}Th is very slow. The transport distance after 2 million years is indicated

by the front of the peak near the source in the calculated curves. The main dispersion of ^{230}Th is caused by the migration and subsequent decay of uranium to thorium which is strongly sorbed at the locations where it is formed. Because of this, the calculated results are not very sensitive to the thorium concentration at the source, except at locations very close to the source. Furthermore, the calculated results for longer distances are not sensitive to the choice of K_d-value for thorium, since all selected values are higher than the K_d-values of uranium. This is illustrated in Figure 4.6 by the identical shape and location of the concentration fronts obtained for the K_d-values 10 and 100 m^3/kg. The somewhat shorter migration distance obtained in the calculation with a K_d of 5 m^3/kg is solely dependent on the higher K_d-value, 1.5 m^3/kg, assumed for ^{234}U in this calculation.

The calculated and observed activity ratios between ^{230}Th and ^{234}U are shown in Figure 4.7. The assumption that secular equilibrium between ^{230}Th and the uranium isotopes is established in the water at the source before the migration of the radionuclides starts, results in high ^{230}Th to ^{234}U activity ratios close to the source. This trend is difficult to see in the observed data. The calculated decrease in the activity ratio with distance from the source is also indicated in the observed data up to a distance of about 100 to 150 m from the source. Beyond this distance the observed ratios, contrary to the calculated ratios, seem to increase with distance and almost all values are above 1. However, the concentrations of both uranium and thorium at these locations are low.

The trend in the observed $^{230}Th/^{234}U$ activity ratio in Figure 4.8 has been simulated by assuming a background level of uranium, not accessible to groundwater, in the rock around the ore body. However, the fit to the actual values is poor. The fact that the observed ratios at distances longer than 150 m from the source are larger than 1, implies that the background content of uranium has been accessible to groundwater and that leaching of uranium relative to thorium has occurred.

The predicted uranium concentration in the solid phase was also compared with observed concentrations in the north to south direction, i.e., in a direction deviating 45 degrees from the transect at 6110 mN. The result is shown in Figure 4.9. The observed data are plotted as a function of the distance from the gridline 3100 mE in the south direction. The concentration front is steep also in this direction, with a shape similar to the predicted curve, assuming a dispersion length of 1 m. However, the prediction underestimates the migration distance as well as the maximum concentration level.

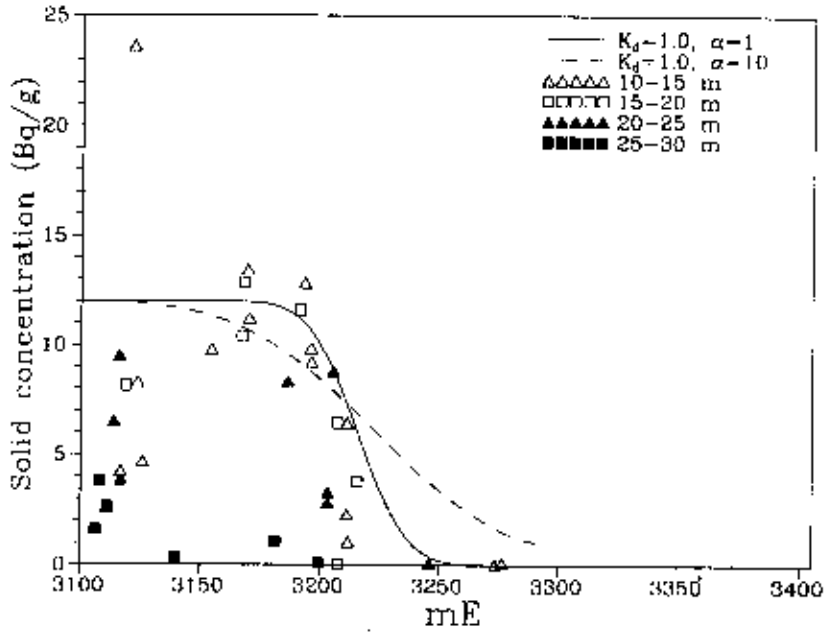

Figure 4.3. *Kemakta. Advection–dispersion with linear sorption and chain decay. Predicted and observed ^{238}U-concentrations at 10–30 m depth along the transect 6110 mN. Linear scales.*

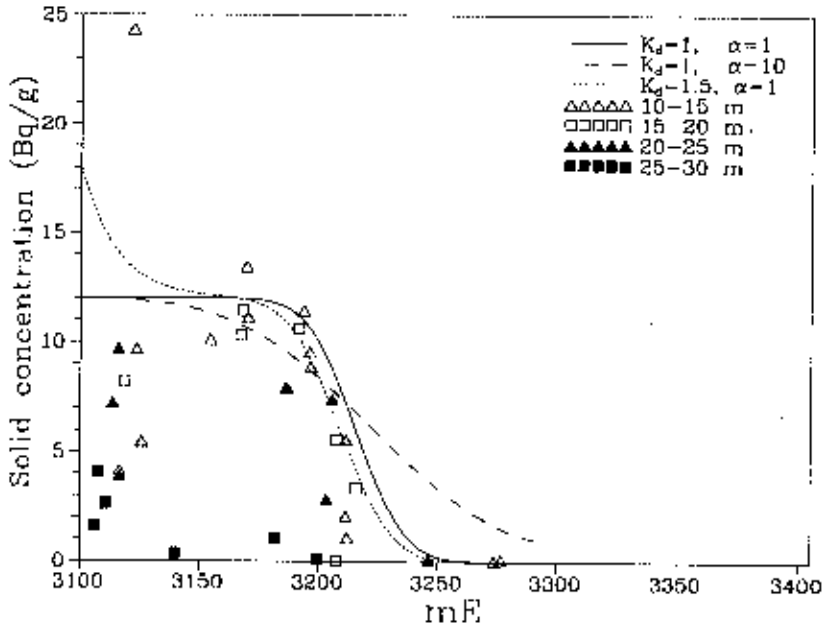

Figure 4.4. *Kemakta. Advection–dispersion with linear sorption and chain decay. Predicted and observed ^{234}U-concentrations at 10–30 m depth along the transect 6110 mN. Linear scales.*

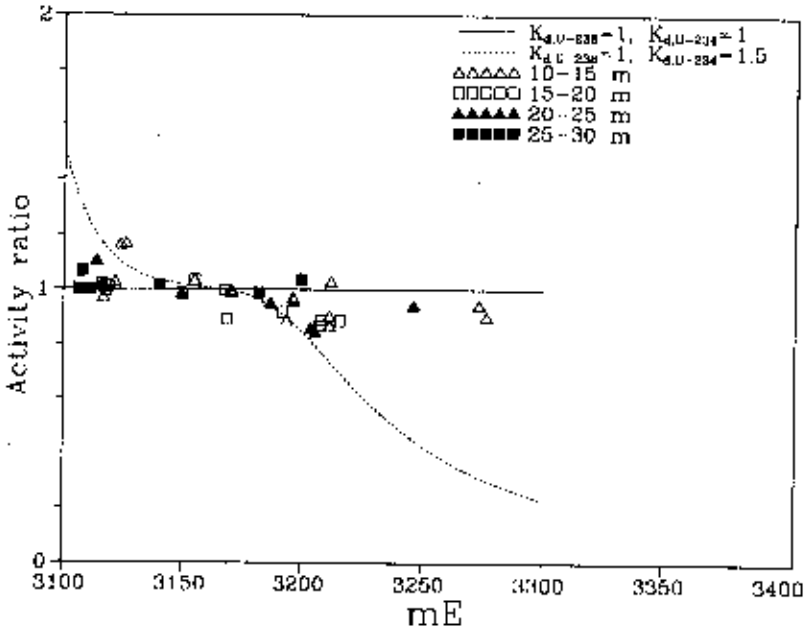

Figure 4.5. *Kemakta. Advection–dispersion with linear sorption and chain decay. Predicted and observed $^{234}U/^{238}U$ activity ratios at 10–30 m depth along the transect 6110 mN.*

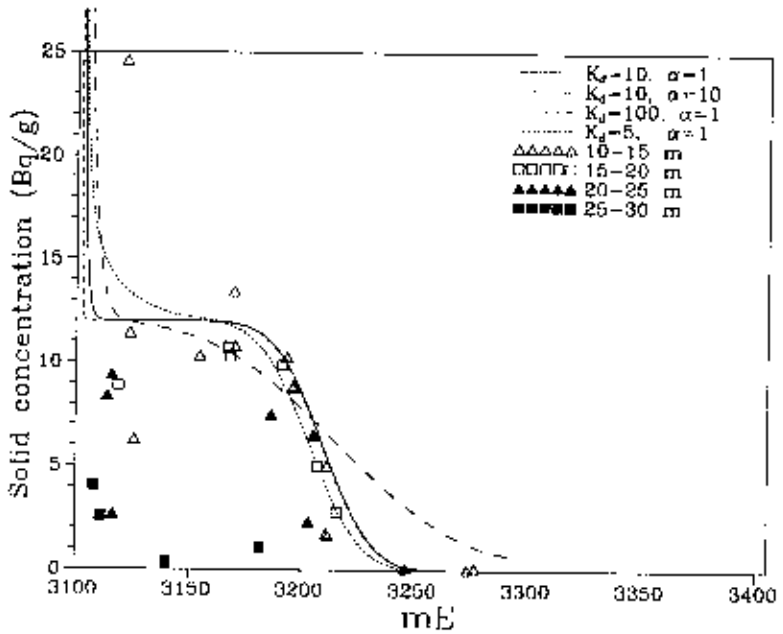

Figure 4.6. *Kemakta. Advection–dispersion with linear sorption and chain decay. Predicted and observed ^{230}Th-concentrations along the transect 6110 mN. Source located at the outer extension of the ore body. K_d = 0.1 m^3/kg.*

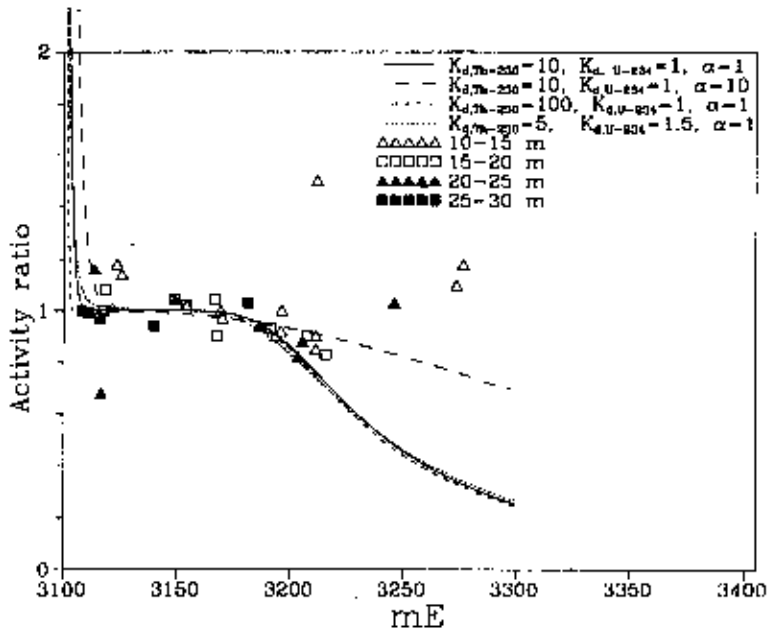

Figure 4.7. *Kemakta. Advection–dispersion with linear sorption and chain decay. Predicted and observed $^{230}Th/^{234}U$ activity ratios at 10–30 m depth along the transect 6110 mN.*

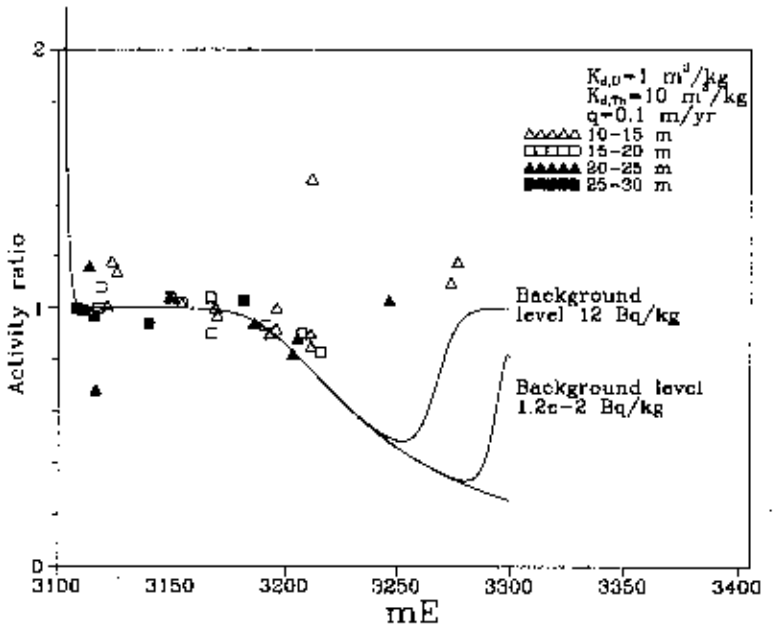

Figure 4.8. *Kemakta. Advection–dispersion with linear sorption and chain decay. Predicted and observed $^{230}Th/^{234}U$ activity ratios. Effects of background concentration of uranium not accessible to groundwater.*

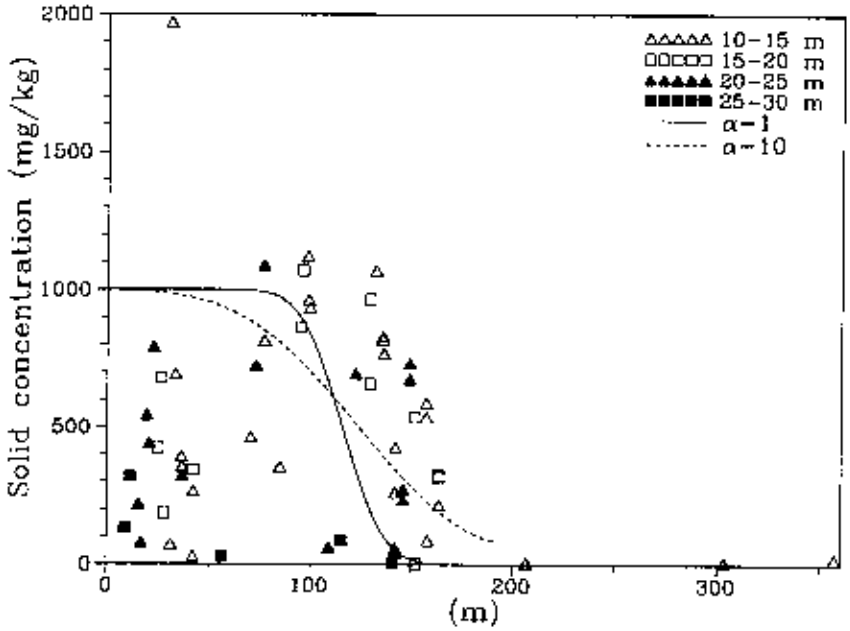

Figure 4.9. *Kemakta. Advection–dispersion with linear sorption and chain decay. Predicted uranium concentrations, K_d = 1 m^3/kg and water flux = 0.1 m/yr. Observed concentrations in small samples from 10-30 m depth as a function of distance from 3100 mE in north-south direction.*

Influence of Migration Time on Activity Ratios

As mentioned earlier, it is possible to obtain almost identical simulations of the uranium concentration versus distance with different combinations of the values of the distribution coefficient, source concentration, water flux and migration time. However, the activity ratio $^{234}Th/^{234}U$ versus distance from the source is dependent on the migration time, irrespective of the other parameter values.

To investigate if the assumed migration time of millions of years seems reasonable, the $^{230}Th/^{234}U$ activity ratio at different distances from the source was calculated on different assumptions regarding the migration time. In all calculations the K_d-value for uranium was set to 1 m^3/kg and a value of 10 m^3/kg was chosen for thorium. As in the previous calculations, the source concentration of dissolved uranium was 1000 mg/m^3 and radioactive equilibrium between ^{238}U, ^{234}U and ^{230}Th was assumed at the source. Different values of the water flux were used, dependent on the assumed migration time, since the basic criteria was that the calculated uranium concentration versus distance should match the observed. The following combinations of water flux and migration time were used:

Table 4.4. Kemakta. Values of Water Flow and Migration Time.

Migration time (Myr)	Water flux (m/yr)
0.2	1
1	0.2
2	0.1
4	0.05

The uranium migration distance for all these parameter combinations are very similar and all match the observed migration distance quite well. The $^{230}Th/^{234}U$ activity ratios are depicted in Figure 4.10. Here, the difference between the different cases is significant. A comparison between the predicted curves and the observed data indicates that a migration time of 0.2 million years is too short, and that a migration time in the order of million years gives a better match to the observed data.

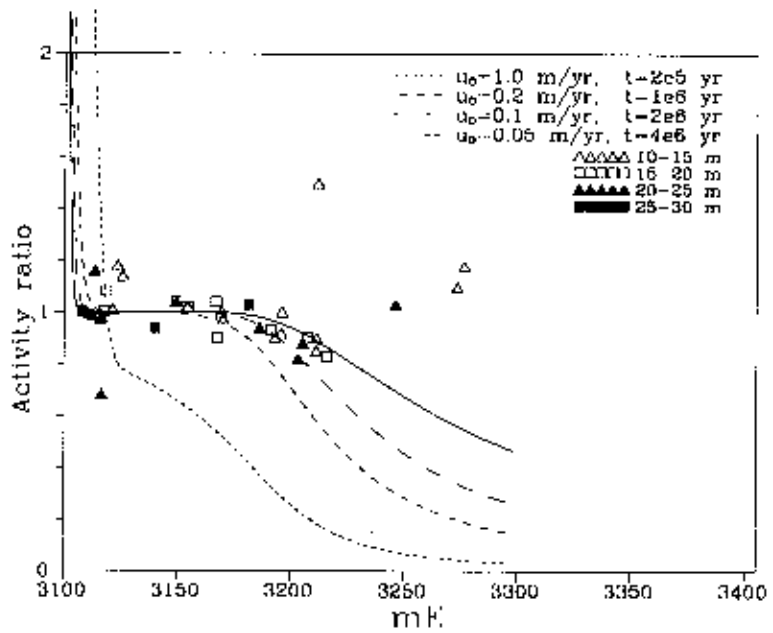

Figure 4.10. Kemakta. Advection–dispersion with linear sorption and chain decay. Predicted and observed $^{230}Th/^{234}U$ activity ratios. Effects of different combinations of water flux and migration time.

Influence of Alternating Periods of Flow and no Flow on Activity Ratios

The climate in the Koongarra area has varied over time. It has been dry, almost desert-like, with minimal water flow in the weathered zone during glacial periods. The flow rates have probably been significantly higher during the interglacial periods due to heavy rainfalls.

Calculations were performed, assuming alternating periods of flow and no flow during 2 million years, in order to study the impact of variations in the water flow. The duration of the wet periods were set to 25 000 years, and each wet period was followed by a 75 000 year long dry period. As has been shown earlier, a fair agreement between predicted and observed uranium concentrations is obtained with an average water flux of 0.1 m/yr during 2 million years. This means that the water flux during the wet periods has to be 0.4 m/yr to give an equally good match to the observed uranium concentrations, in this case with alternating periods of flow and no flow.

Predicted and observed $^{230}Th/^{234}U$ activity ratios are shown in Figure 6.15. In addition to the results obtained with alternating flow and no flow over the entire time period of 2 million years, the activity curves obtained are depicted assuming average water flux during 1.8 million years and then two cycles with flow and no flow. The result obtained for a constant water flux of 0.1 m/yr over the whole period is also shown for comparison. As could be expected, the activity ratios are higher at the migration front after a dry period than after a wet period. However, alternating periods with flow and no flow during the first 1.8 Myr does not seem to influence the decrease in activity ratio with distance as illustrated by the almost identical curves for the cases with alternating flow over the entire time period and alternating flow only during the last 200 000 years.

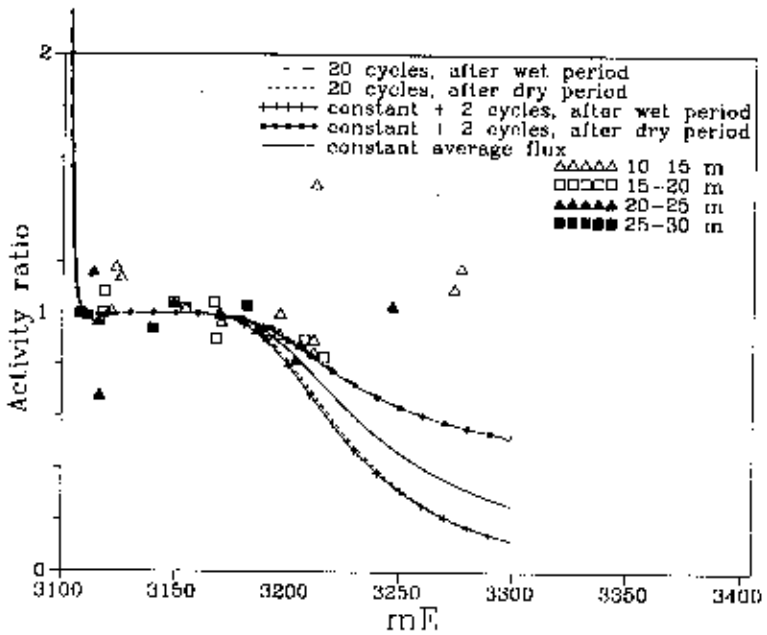

Figure 4.11. Kemakta. Advection–dispersion with linear sorption and chain decay. Predicted and observed $^{230}Th/^{234}U$ activity ratios, cases with alternating periods of flow and no flow.

Advection–Dispersion Model with Linear Sorption and Chain Decay. Conclusions.

The model extended to include chain-decay made it possible to get an independent estimation of the migration time by studying the $^{230}Th/^{234}U$ activity ratio. This ratio indicated that the migration time has been in the order of million years. With a migration time of 200 000 years, the activity ratios were under-predicted over the entire migration distance.

It was not possible to simulate the observed decrease in the $^{234}U/^{238}U$ activity ratio unless a higher retardation of ^{234}U relative to ^{238}U was assumed. This difference in retardation between the isotopes could be an effect of α-recoil.

The simulation of variable climatic conditions by assuming alternating periods of flow and no flow showed that the flow conditions during the last 200 000 years are important to the results, given that an average flow rate can be used for times prior to 200 000 years ago.

4.1.3 Advection–Dispersion Model with Linear Sorption, Chain Decay, α-recoil and Phase Transfer

Measurements of uranium and thorium concentrations and activity ratios in different mineral phases in the weathered zone at Koongarra indicate that uranium associated with amorphous iron oxides, such as ferrihydrite, and sorbed onto iron oxides and clay minerals is accessible to, and at near equilibrium with, the groundwater. Crystalline phases of iron oxides, such as goethite and hematite, and very resistant minerals, such as quartz and mica, also contain uranium. The suggested mechanism for entrapment of uranium in crystalline iron oxides involves uranium adsorption onto ferrihydrite before it is transformed to a more crystalline form. High $^{234}U/^{238}U$ activity ratios in crystalline phases further suggest α-recoil emplacement from amorphous and surface sites.

In this third iteration, the advection-dispersion model was extended in order to investigate the influence of phase transfer and α-recoil on the activity ratios.

Assumptions and Model Description

Two solid phases, the accessible and the inaccessible phase, were considered in these calculations. In practice, the accessible phase corresponds to amorphous iron minerals and clays and the inaccessible phase to crystalline iron minerals and other minerals, for example quartz. The accessible phase was assumed to be porous and reversible sorption is assumed to occur instantaneously in proportion to the nuclide concentration in the groundwater (the K_d-concept). The inaccessible phase was assumed to have no direct interaction with the groundwater. The nuclide can enter the inaccessible phase either by phase transfer, crystallisation of amorphous iron, or by α-recoil. The interactions between the different phases and nuclides included in this modelling concept are illustrated schematically in Figure 4.12.

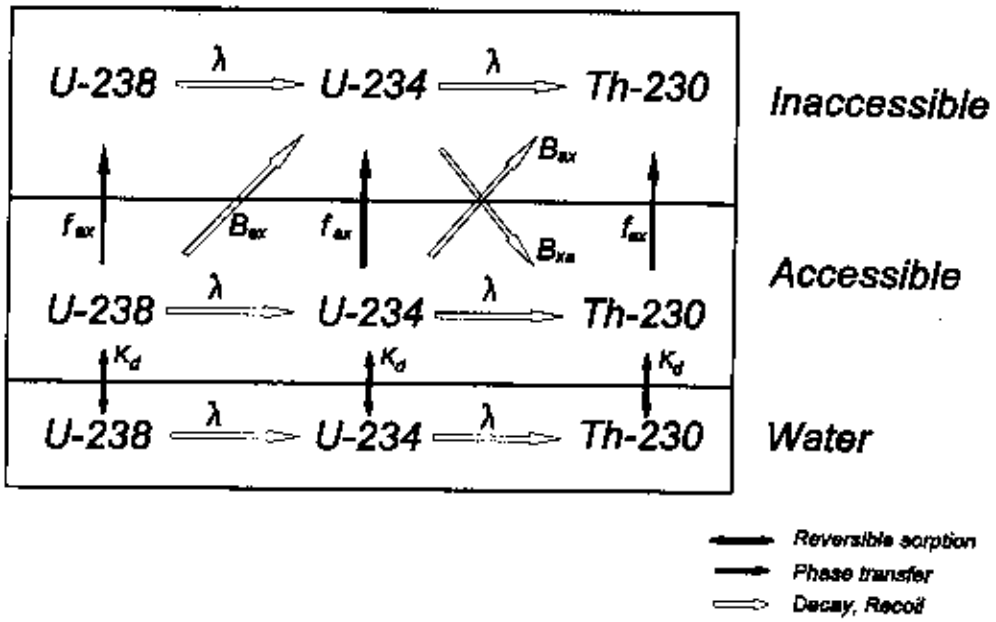

Figure 4.12. Kemakta. Advection–dispersion model with linear sorption, chain decay, α-recoil and phase transfer. Schematic picture of the interactions between the different phases and nuclides.

The equations describing the migration of nuclide *i* are:

$$\epsilon_f R_i \frac{\partial c_i}{\partial t} = D_L \frac{\partial^2 c_i}{\partial x^2} - u_0 \frac{\partial c_i}{\partial x} - \epsilon_f R_i \lambda_i c_i - f_{ax}(K_{d,i} c_i - X_i) + \\ + \epsilon_f R_{i-1}(1 - B_{ax})\lambda_{i-1} c_{i-1} + B_{xa} \lambda_{i-1} X_{i-1} \qquad \text{(Eq. 4.10)}$$

$$\frac{\partial X_i}{\partial t} = -\lambda_i X_i + f_{ax}(K_{d,i} c_i - X_i) + (1 - B_{xa})\lambda_{i-1} X_{i-1} + \epsilon_f R_{i-1} B_{ax} \lambda_{i-1} c_{i-1} \qquad \text{(Eq. 4.11)}$$

where

B_{ax}	=	recoil factor (recoil from accessible to inaccessible phase)
B_{xa}	=	recoil factor (recoil from inaccessible to accessible phase)
c_i	=	concentration of nuclide *i* in the groundwater, (Bq/m^3)
c_{i-1}	=	concentration of parent nuclide *i-1* in the groundwater, (Bq/m^3)
f_{ax}	=	phase transfer rate (from accessible to inaccessible phase) (year^{-1})
D_L	=	dispersion coefficient, (m^2/year)
t	=	time, (year)
X_i	=	concentration of nuclide *i* in the inaccessible solid phase (Bq/kg)
X_{i-1}	=	concentration of parent nuclide *i* in the inaccessible solid phase (Bq/kg)
x	=	length coordinate, (m)
ϵ_f	=	flow porosity, (m^3/m^3)

λ_i = decay constant of nuclide *i*, (year^{-1})
λ_{i-1} = decay constant of parent nuclide *i-1*, (year^{-1})

The dispersion coefficient, D_L, is defined in Eq.4.2 and the retardation factors, R_i and R_{i-1}, and the relations between the nuclide concentration in accessible phase and water are defined by Eqs. 4.5 and 4.6, respectively.

The initial and boundary conditions applied are:

$c_i = 0, X_i = 0$ for $t = 0$ and $x > 0$
$c_i = c_0$ for $x = 0$ and $t \geq 0$
$c_i = 0$ for $x = \infty$ and $t \geq 0$.

The transport equations were solved with the numerical code TRUCHN *[Rasmuson et al., 1982]*, which was modified to account for phase transfer and α-recoil.

Data

A water flux of 1 m/yr was used in these calculations, based on analyses of the specific discharge in the weathered zone *[Townley, 1992]*. A dispersion length of 1 m was assumed as in the previous calculations, but the porosity was changed to 15% to be in accordance with the most recent reported values *[Emerson, 1992]*.

Two values of the distribution coefficient for uranium between accessible solid phase and water were studied, 3 m^3/kg and 10 m^3/kg. These values were chosen based on earlier recommendations regarding the magnitude of the distribution coefficient between accessible solid phase and water. However, more recent recommendations are lower, 0.5–2 m^3/kg *[Golian and Lever, 1992]*. This indicates that the distribution coefficients used in these calculations might be too high. This is further discussed in connection with the presentation of the results. The recommended K_d-values for thorium are on average 4 orders of magnitude higher than for uranium, which implies that thorium is almost immobile. This has been achieved in the calculations by assigning a K_d-value of 100 m^3/kg for thorium.

The recommended range for the α-recoil factor that accounts for the part of the decay events resulting in daughter radionuclide transfer between phases, is 0.1–0.4 for the accessible to inaccessible transfer (B_{ax}) and 0.00–0.05 for the inaccessible to accessible transfer (B_{xa}) *[Golian and Lever, 1992]*. Based on these recommendations, B_{ax}-values of 0.3 and 0.4, and B_{xa}-values of 0 and 0.05 were selected to be used in the calculations.

Analyses of the activity ratio data for different phases and modelling results indicate that the phase transfer rate has to be comparable with the decay constants of ^{230}Th and ^{234}U, i.e. $8.66 \cdot 10^{-6}$ yr^{-1} and $2.83 \cdot 10^{-6}$ yr^{-1}, respectively *[Golian and Lever, 1992]*. In the present calculations phase transfer rates of 0, 10^{-7} and 10^{-6} yr^{-1} were studied. It should be noted that the transfer rate of a radionuclide is not identical to the phase transformation rate.

The data used in the calculations are summarised in Table 4.5 and the different calculation cases are summarised in Table 4.6.

Table 4.5. Kemakta. Advection–dispersion model with linear sorption, chain decay, α-recoil and phase transfer. Data used in the calculations.

porosity (m^3/m^3)	0.15
solid density of rock (kg/m^3)	2500
distribution coefficients (m^3/kg)	
uranium	3, 10
thorium	100
water flux (m/yr)	1
dispersion length (m)	1, 10
molecular diffusivity (m^2/s)	$2 \cdot 10^{-9}$
α-recoil factor	
accessible phase to inaccessible phase	0.3, 0.4
inaccessible phase to accessible phase	0.00, 0.05
phase transformation rate (1/yr)	$0, 10^{-7}, 10^{-6}$
source concentration (mg/m^3)	
uranium	100
thorium	in equilibrium

Table 4.6. Kemakta. Advection–dispersion model with linear sorption, chain decay, α-recoil and phase transfer. Summary of the calculation cases.

Case	B_{ax} (-)	B_{xa} (-)	f_{ax} (yr^{-1})	K_d (uranium) (m^3/kg)
1	0.3	0	0	10
2	0.4	0	0	10
3	0.4	0.05	0	10
4	0.4	0	10^{-7}	10
5	0.4	0	10^{-6}	10
6	0.4	0	10^{-6}	3

Results

The results from the modelling are shown in Figures 4.13 to 4.19. The source is assumed to be located at the outer extension of the ore body (3100 mE), and the results are compared with observed small sample data from depths between 10 and 30 m along the 6110 mN gridline.

The calculated concentration curves for uranium in the bulk rock, accessible and inaccessible, are depicted together with observed data in Figure 4.13. In the cases with no phase transfer ($f_{ax} = 0$, Cases 1, 2 and 3), the migration distance agrees fairly well with observed data. These cases overlap and they are also identical to the results obtained in the previous modelling with a water flux of

1 m/yr and a K_d-value for uranium of 10 m^3/kg. This is to be expected, since α-recoil only influences the migration of ^{234}U, and the concentration of ^{234}U is negligible compared to the concentration of ^{238}U.

In the case with high phase transfer rate and high sorption capacity ($f_{ax} = 10^{-6}$ and $K_d = 10$, Case 5), the calculated migration distance is too short. By lowering the K_d-value ($K_d = 3$ and $f_{ax} = 10^{-6}$, Case 6) the migration distance is increased, but too much in comparison with observed data. In addition, the shape of the concentration versus distance curve is not in agreement with observed data. If, instead, the phase transfer rate is lowered ($K_d = 10$ and $f_{ax} = 10^{-7}$, Case 4), both the migration distance and the shape of the concentration trend are fairly well simulated.

The influence of recoil and phase transfer on the $^{234}U/^{238}U$ activity ratios in the accessible phase is illustrated in Figure 4.14. The results show that the phase transfer rate does not affect the activity ratios in the accessible phase, while both the recoil factor and the distribution coefficient have an influence. The difference in the results between the different calculation cases are smaller than the scatter in the observed data.

The calculated and observed $^{230}Th/^{234}U$ activity ratios in the accessible phase are shown in Figure 4.15. The observed data indicate an almost immediate decrease from a value close to 1 near the source to values as low as 0.2 at the uranium concentration front 100 m from the source. The calculated curves do not reflect this trend. Close to the source, the values are well below 1 and remain constant until about 100 m from the source, when the values decrease, except in the case with the lower K_d-value (Case 6), where the values are independent of distance. Beyond the concentration front, where the uranium concentrations are low, the observed activity ratios increase towards 1 and even above 1. As has been shown earlier, the calculated activity ratios will increase towards 1 at distances beyond the concentration front, if the background level is considered in the calculations.

A comparison between the calculated and observed $^{234}U/^{238}U$ activity ratios in the inaccessible phase (Figure 4.16) shows that only the higher phase transfer rate, 10^{-6} yr^{-1}, gives results that are close to the observed data. This is also the case for the $^{230}Th/^{234}U$ activity ratio in the inaccessible phase, as is illustrated in Figure 4.17.

The predicted activity ratios are compared with observed data in the bulk rock in Figures 4.18 and 4.19. The small decrease in observed $^{234}U/^{238}U$ activity ratio with distance (Figure 4.18) is fairly well simulated in all calculation cases. The observed $^{230}Th/^{234}U$ activity ratios (Figure 4.19) are also fairly well simulated by all calculated curves which are almost identical. The only curve that significantly differs from the others is the case with a lower K_d-value ($K_d = 3$, Case 6).

The presently recommended K_d-value for uranium in the accessible phase is lower than the values that have been used in the calculations that are presented above. The results shown in Figure 4.13 do not suggest that the match between calculated and observed uranium concentrations in bulk rock would be improved with a still lower K_d-value, at least not without increasing the phase transfer rate. However, to study the effect of lowering the K_d and at the same time increasing the phase transfer rate, the uranium concentration in bulk rock was calculated, assuming a K_d of 1 m^3/kg and a phase transfer rate of 10^{-5} yr^{-1}. The fit to the observed data was not improved, neither the migration distance, nor the shape of the migration front.

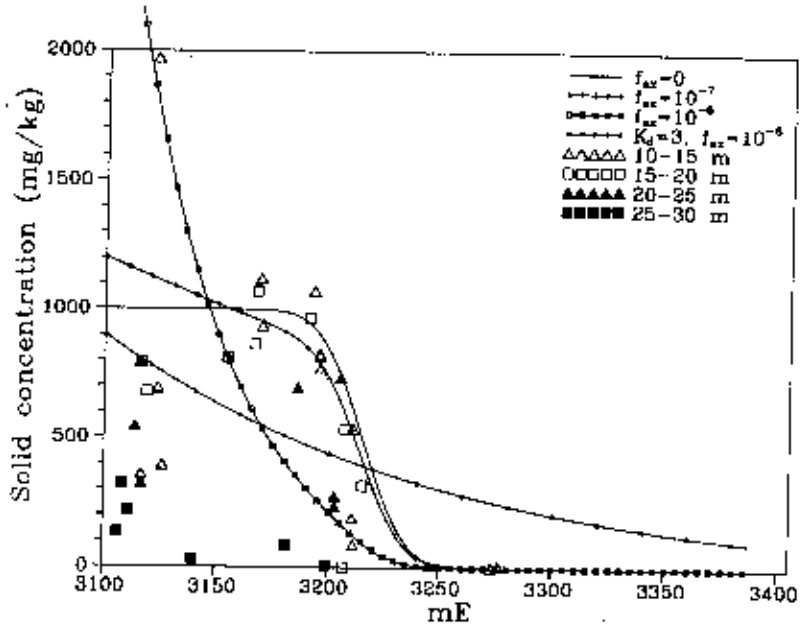

Figure 4.13. *Kemakta. Advection–dispersion model with linear sorption, chain decay, α-recoil and phase transfer. Predicted and observed bulk rock uranium concentrations. (Cases 1–3 overlap).*

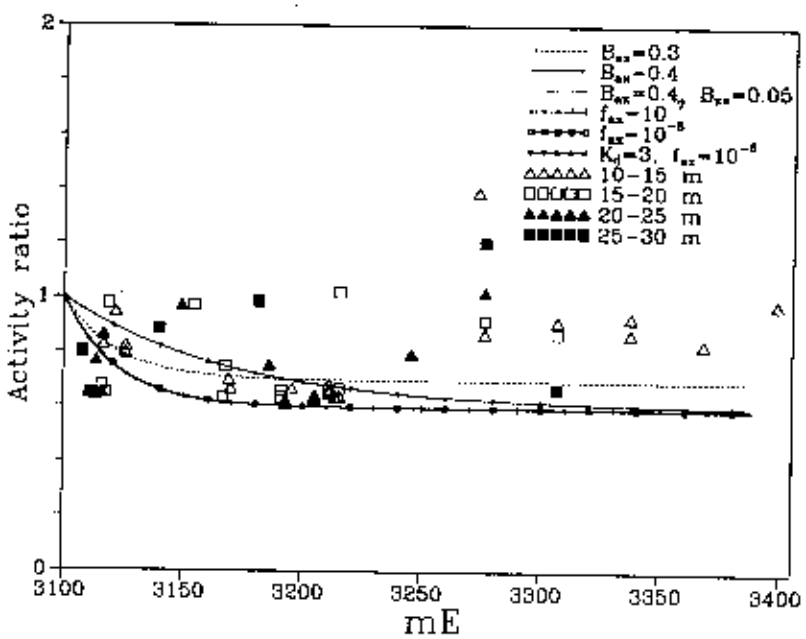

Figure 4.14. *Kemakta. Advection–dispersion model with linear sorption, chain decay, α-recoil and phase transfer. Predicted and observed $^{234}U/^{238}U$ activity ratios in the accessible phase. (Cases 2–4 overlap).*

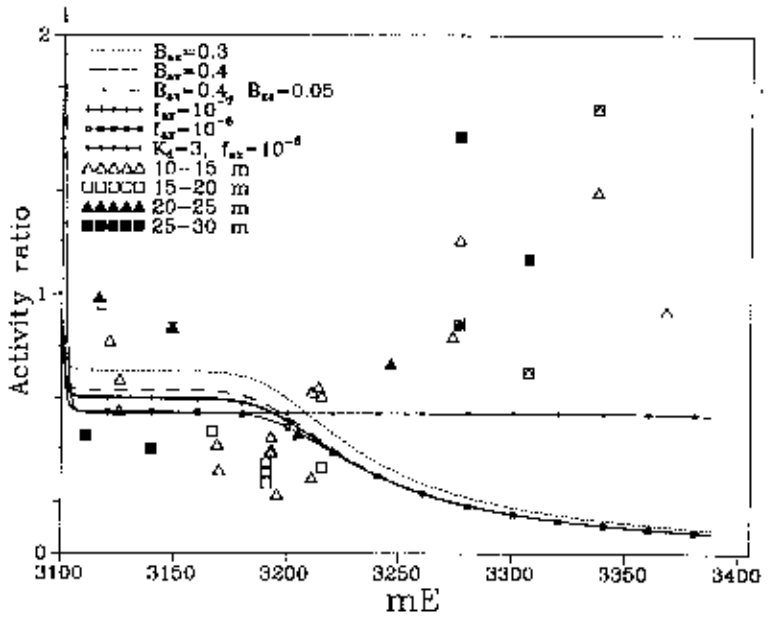

Figure 4.15. *Kemakta. Advection–dispersion model with linear sorption, chain decay, α-recoil and phase transfer. Predicted and observed $^{230}Th/^{234}U$ activity ratios in the accessible phase. (Cases 2 and 4 overlap).*

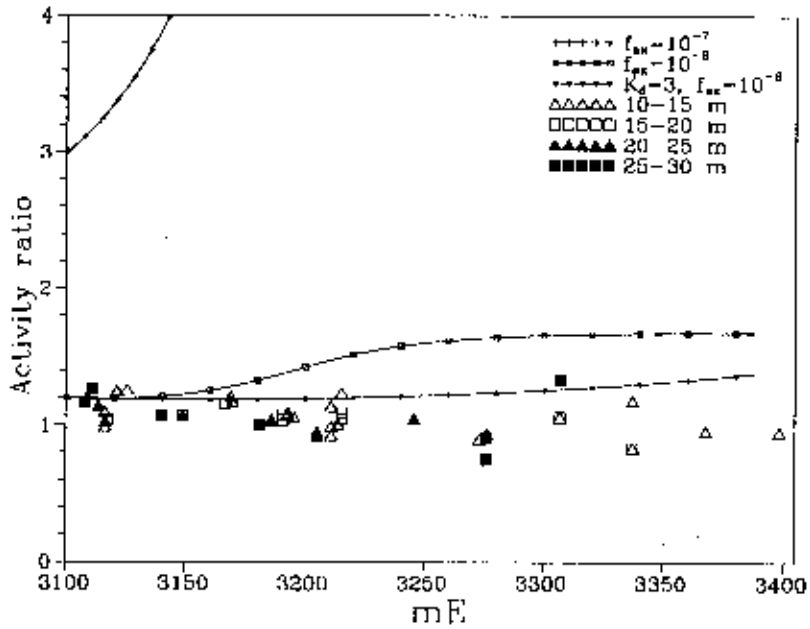

Figure 4.16. *Kemakta. Advection–dispersion model with linear sorption, chain decay, α-recoil and phase transfer. Predicted and observed $^{234}U/^{238}U$ activity ratios in the inaccessible phase.*

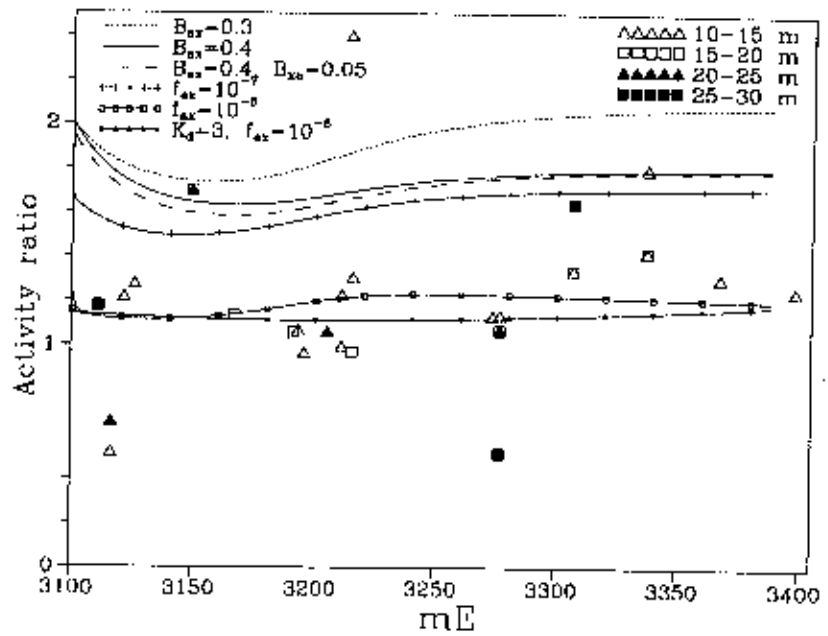

Figure 4.17. *Kemakta. Advection–dispersion model with linear sorption, chain decay, α-recoil and phase transfer. Predicted and observed $^{230}Th/^{234}U$ activity ratios in the inaccessible phase.*

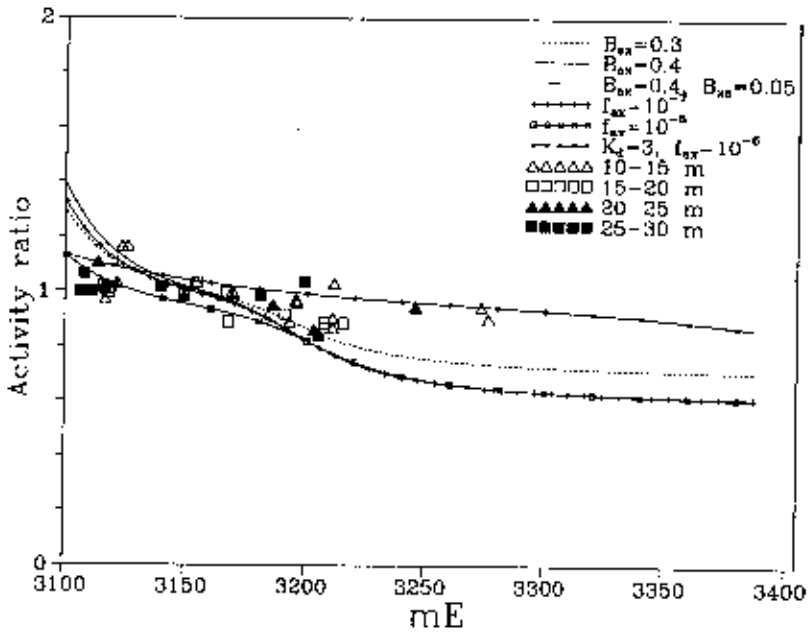

Figure 4.18. *Kemakta. Advection–dispersion model with linear sorption, chain decay, α-recoil and phase transfer. Predicted and observed $^{234}U/^{238}U$ activity ratios in bulk rock.*

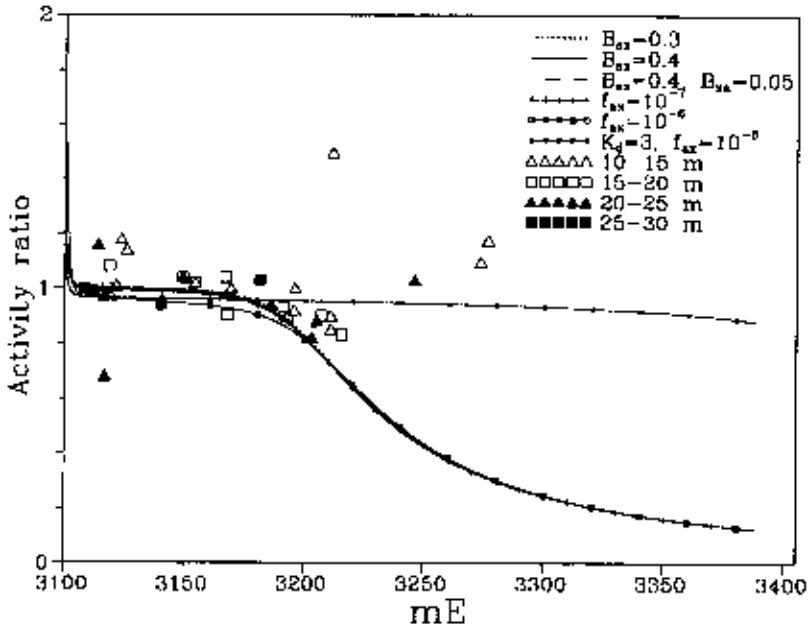

Figure 4.19. *Kemakta. Advection–dispersion model with linear sorption, chain decay, α-recoil and phase transfer. Predicted and observed $^{230}Th/^{234}U$ activity ratios in bulk rock.*

Advection-Dispersion Model with Linear Sorption, Chain Decay, α-recoil and Phase Transfer. Conclusions

Comparisons between calculated and observed data suggest that the results are not significantly improved by including phase transfer and α-recoil in the model, at least not with the particular combination of phase transfer rates and K_d-values used in the calculations. Adding only the process of α-recoil gave similar results as the simple advection–dispersion–reversible sorption model, while the introduction of phase transfer gave results that were less in agreement with observed data.

4.1.4 Summary of Results

The results obtained with the 1-D advection–dispersion model with reversible sorption were in fair agreement with measured uranium and thorium concentrations. The uranium migration curve can be simulated almost equally well using different combinations of the input parameters; water flux, distribution coefficient, concentration of uranium in water at the source and migration time. The shape of the concentration front is better simulated with a dispersion length of 1 m than 10 m. Some combinations of input data that gave results in fair agreement with the observed data in transect 6110 mN, are listed in Table 4.7.

Table 4.7. Kemakta. Advection-dispersion model with linear sorption. Summary of input parameters giving almost the same migration curve for uranium.

Water flux (m/yr)	K_d (m^3/kg)	c_0 (mg/kg)	t (Myr)
1	10	100	2
0.1	1	1000	2
0.01	0.1	10000	2
1	1	1000	0.2
0.2	1	1000	1
0.05	1	1000	4

It was not possible to simulate the observed decrease in the $^{234}U/^{238}U$ activity ratio unless a higher retardation of ^{234}U relative to ^{238}U was assumed. This difference in retardation between the uranium isotopes could be an effect of α-recoil.

The observed decrease in the $^{230}Th/^{234}U$ activity ratio was fairly well simulated by the model for migration times in the order of millions of years. With a migration time of 200 000 years, the activity ratios were under-predicted over the entire migration distance.

It was not possible to improve the match between calculated and observed uranium concentrations by extending the model to include also α-recoil and radionuclide transfer between amorphous and crystalline mineral phases of the rock. Adding the process of α-recoil gave similar results as the simple advection–dispersion–reversible sorption model, while the introduction of phase transfer gave results that were less in agreement with observed data.

The extended model simulated the observed decrease in activity ratios in bulk rock with distance from the source fairly well. However, the advection–dispersion–reversible sorption gave an equally good match to the data, when a higher retardation of ^{234}U relative to ^{238}U was assumed.

The general trend with most of the observed activity ratios in the accessible phase below 1 and in the inaccessible phase above 1 was fairly well simulated by the extended model. The calculated activity ratios in the accessible phase were not very sensitive to variations in phase transfer rate, recoil factor and K_d-value in the sense that the difference between the calculated results was smaller than the scatter in the observed data. The choice of parameter values seems to have significantly larger influence on the predicted activity ratios in the inaccessible phase.

The mobility of ^{230}Th in groundwater is small due to strong sorption. This means that the concentration of ^{230}Th at longer distances from the source is entirely dependent on the migration and decay of uranium.

The simulation of variable climatic conditions by assuming alternating periods of flow and no flow in the advection–dispersion–reversible sorption model showed that the time period when variations in flow conditions are of importance to the results is limited to the last 200 000 years. An average flow rate may therefore be used for times prior to 200 000 years ago.

4.2 RIVM

4.2.1 General

The analysis of the ARAP data that was reported in Chapter 3.2 suggests that the migration of radionuclides in the fully weathered zone and in the unweathered zone of the Koongarra ore deposit is negligible. RIVM has therefore focused its attention on the transition zone between the highly weathered and the unweathered rock, when developing the conceptual transport model. The transition zone was modelled as a two-dimensional region bounded by the Koongarra fault, the Koongarra Creek and two non-perennial creeks perpendicular to the Koongarra fault, as illustrated in Figure 4.20. Migration calculations have been performed for two cases: a stationary transition zone and a transition zone that moves downward with time.

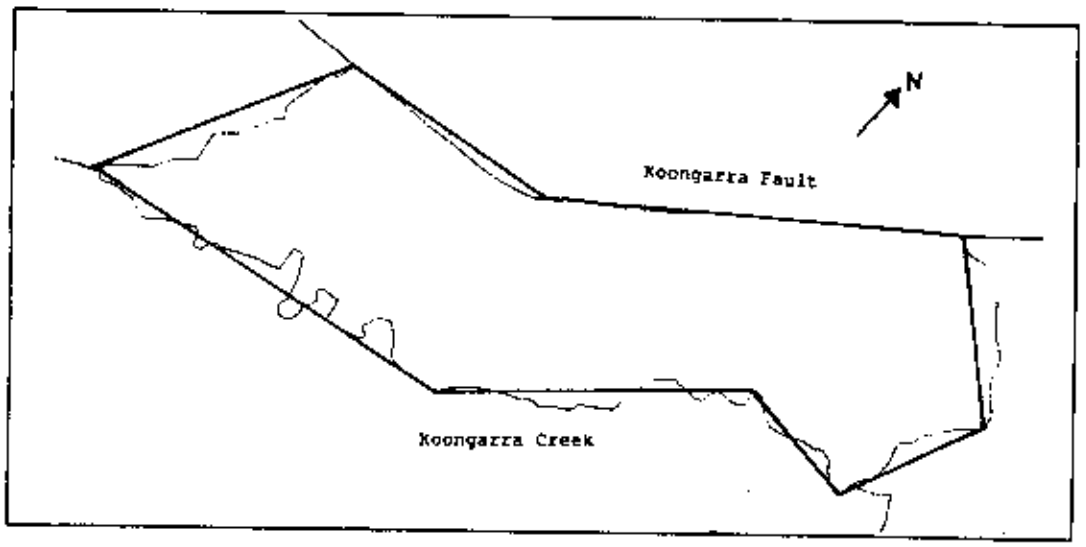

Figure 4.20 RIVM. Location of the modelling region.

The modelling study is based on a sensitivity analysis in which the effect of various parameters and processes on the transport of uranium in the weathering zone are investigated. The three main parameters and processes considered were: the velocity distribution, the downward movement of the transition zone, and a few geochemical processes. All simulations were performed using the mathematical model METROPOL *[Sauter et al., 1993]*.

The governing partial differential equations incorporated the movement of the weathering zone and hence the loss of uranium at the top of the zone and the entering of clean schist at the bottom of the zone (Figure 4.21). Diffusion of uranium from the highly weathered zone into the transition zone was also included.

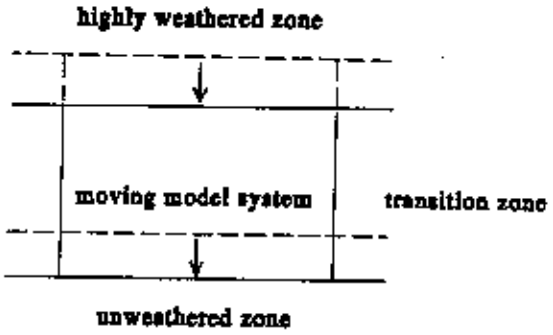

Figure 4.21 RIVM. Schematic illustration of the moving transition zone.

4.2.2 Processes and Equations

The processes considered for the description of the transport of uranium in the transition zone were:

- advective transport
- diffusive and dispersive transport
- adsorption/desorption
- decay
- dissolution.

Diffusive and dispersive mass transport were assumed to be given by a Fickian type relation, where the dispersion tensor was defined in the classical way as a function of the liquid velocity.

The following simplifying assumptions were made in the development of the governing mass balance equation for uranium:

- The porous medium is saturated and has spatially varying properties that are constant over time.
- Uranium concentration does not influence the liquid density.
- Decay of uranium can be described by a first order relationship.
- Adsorption/desorption can be described by a linear isotherm.
- No external sources and sinks are present.
- Uranium is not produced by decay of other species.

Based on these assumptions, the three-dimensional mass balance equation for uranium can be written as:

$$nRp\frac{\partial \omega}{\partial t} + \nabla\cdot(\rho\omega q + J) + nR\rho\lambda\omega = S \qquad \text{(Eq 4.12)}$$

where:
n = porosity [-]
R = retardation factor [-]
ρ = liquid density [$M\cdot L^{-3}$]
ω = mass fraction of uranium in liquid phase [-]
q = Darcy velocity [$L\cdot T^{-1}$]
J = diffusive/dispersive mass flux of uranium [$M\cdot L^{-2}\cdot T^{-1}$]
λ = decay constant of uranium [T^{-1}]
S = source term related to the dissolution process [$M\cdot L^{-3}\cdot T^{-1}$]

The retardation factor R is related to the adsorption equilibrium distribution constant K_d by:

$$R = 1 + \frac{\rho_s(1-n)}{n}K_d \qquad \text{(Eq. 4.13)}$$

where ρ_s is the mass density of the solid phase [$M\cdot L^{-3}$].

The diffusive/dispersive uranium mass flux is given by:

$$J = -\rho D\cdot\nabla\omega \qquad \text{(Eq. 4.14)}$$

with the dispersion tensor D defined by:

$$D = (nD_m + \alpha_T|q|)\,I + (\alpha_L-\alpha_T)\frac{q\,q}{|q|} \qquad \text{(Eq. 4.15)}$$

where:
D_m = effective diffusion coefficient [$L^2\cdot T^{-1}$]
I = unit tensor [-]
α_L = longitudinal dispersivity [L]
α_T = transversal dispersivity [L]

The effect of tortuosity of the porous medium is included in the molecular diffusion coefficient D_m.

The source term, S, is related to the mineral dissolution rate by:

$$S = \frac{\partial Q}{\partial t}\rho_s(1-n) \qquad \text{(Eq. 4.16)}$$

where Q is the amount of mineral present in the solid phase [$M \cdot M^{-1}$].

The dissolution rate of a mineral follows from the following equation:

$$-\frac{\partial Q}{\partial t} = \frac{n}{\rho_s(1-n)}\rho K\,(\omega_{eq}-\omega) \qquad \text{(Eq. 4.17)}$$

where:

ω_{eq} = equilibrium concentration of a mineral under given conditions ($M \cdot L^{-3}$)

K = rate constant of dissolution (T^{-1})

It was assumed that the decrease of the mineral content in the solid phase with time could be neglected compared to the total amount of mineral present in the solid phase.

The dissolution will stop in a closed system after a certain time because no discharge will take place, given that ω becomes equal to ω_{eq} in equation (4.17). In an open system, transport of the dissolved mineral may be a constant "sink" and thereby act as a constant driving force to the dissolution process. However, a dynamic equilibrium may still be reached in an open system if sources and sinks are equal.

Combining equations (4.16) and (4.17) gives:

$$S = n\rho K(\omega_{eq} - \omega) \qquad \text{(Eq. 4.18)}$$

Substitution of equations (4.14) and (4.18) in equation (4.12) gives the fully three-dimensional mass balance equation for dissolved uranium. The resulting equation was integrated over the thickness of the moving transition zone of weathering. In doing so, the following assumptions were made:

- The thickness of the transition zone does not change with time.
- The transition zone moves downward with a constant rate.
- The liquid velocity and the velocity of the transition zone are equal at the top and the bottom of the zone.
- The liquid density is constant.
- The local value of the retardation factor equals the average value.

The final two-dimensional form of the integrated mass balance equation is:

$$n\rho R\frac{\partial\omega}{\partial t} + \rho\mathbf{q}\cdot\nabla\omega + \nabla\cdot\mathbf{J} + \lambda Rn\rho\omega + \frac{2(1-R)mw}{b}\rho\omega + n\rho K\omega = \\ = n\rho K\omega_{eq} + \frac{2(1-R)mw}{b}\rho\omega_{bot} \qquad \text{(Eq. 4.19)}$$

where w is the downward velocity of the transition zone ($L\cdot T^{-1}$), b the thickness of the transition zone (L), and ω_{bot} the mass fraction of uranium in the liquid phase just below the transition zone ($M\cdot L^{-3}$).

The average diffusive–dispersive uranium mass flux $\mathbf{J}$ was assumed to be obtained from the two-dimensional forms of equations (4.14) and (4.15). When estimating the amount of uranium entering the zone at the bottom and the amount leaving the zone at the top, the diffusive mass flux was neglected, while it was assumed that the uranium mass fraction as a function of depth in the zone is linear.

4.2.3 Model Domain

As illustrated in Figure 4.20, the model domain is bounded by the Koongarra fault, Koongarra Creek and two non-perennial creeks perpendicular to the Koongarra fault. These boundaries coincide with assumed hydrological boundaries. The finite element mesh of the modelling region used by RIVM is shown in Figure 4.22. The mesh was refined in the ore body region to improve the modelling accuracy.

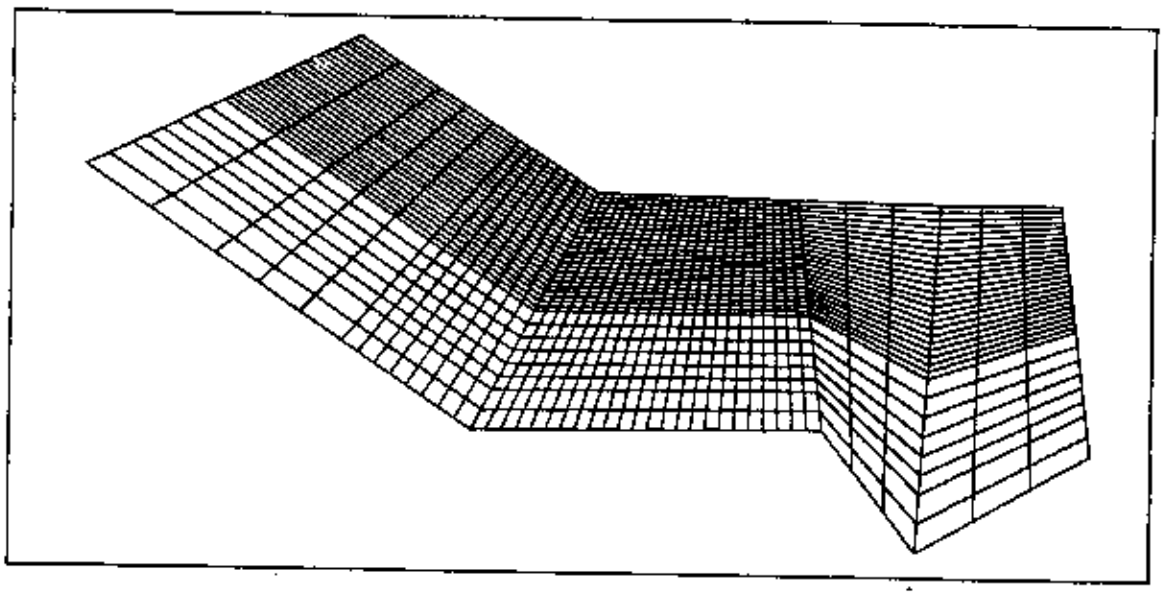

Figure 4.22 RIVM. The finite element mesh representing the model area.

4.2.4 Boundary and Initial Conditions

A no-dispersive and no-diffusive flux boundary condition was employed at all boundaries of the model domain. The concentration in each nodal point located in the ore body region was prescribed a constant concentration of 500 µg/l in the preliminary modelling attempts that studied migration in a stationary transition zone.

In the modelling study that included a moving transition zone, the uranium concentration in the ore body region as a function of time is determined by equation 4.18. Values for K_d, K, ω_{eq} and ω_{bot} have to be assigned to each of the nodal points in the modelling region. K_d was set to zero in the ore body region, because the dominant mechanisms in this region were assumed to be dissolution and precipitation. ω_{bot}, ω_{eq} and K were assigned a value of zero in all nodal points outside of the ore body, since no dissolution was assumed to occur there. Inside the ore body region, values of ω_{bot}, ω_{eq} and K were assigned to each nodal point.

It was assumed that the initial location of the moving transition zone was above the ore body, given that the initial uranium concentration was set to zero everywhere. The weathering front, i.e. the bottom of the transition zone, was assumed to be at the upper boundary of the ore body region at the start of the model simulation.

4.2.5 Model Input and Parameter Estimation

The parameter values used in the modelling exercise are presented in Table 4.8. The parameters were selected in such a way that, as much as possible, they correspond to the present values in the transition zone of weathering. This is in accordance with the simplified model assumption that the conditions do not vary in time along the downward moving weathering front.

Table 4.8 Model parameters for calculations of uranium transport with the moving transition zone model

Parameter	Value	Source
Effective average velocity (q) (PH49) (m/y)	1.3	model calculation (Townley and Barr, 1992)
	0.56	calculated velocity field 17
	0.053	calculated velocity field 11
Flow direction (PH49) (degrees compass bearing)	216°	data analysis
	210°	calculated velocity field 17
	209°	calculated velocity field 11
Longitudinal dispersivity (α_L) (m)	30	assumed
Transversal dispersivity (α_T) (m)	3	assumed
Porosity (n)	0.15	field data (Emerson, 1989)
Rock Density (ρ_s) (kg/m^3	2660	field data (Emerson, 1989)
Distribution coefficient (K_d) (m^3/kg)	0.7	data analysis (Edis *et al*, 1992)
downward velocity of transition zone of weathering (w) (m/y)	0	assumed
	$1.1 \cdot 10^{-5}$	estimated based on data
	$5.5 \cdot 10^{-6}$	assumed
	$1.7 \cdot 10^{-5}$	assumed
thickness of transition zone (b) (m)	5	estimated present thickness of the transition zone (Emerson, 1989)
mean dissolution constant (K) (y^{-1})	6.5	assumed
	$3.0 \cdot 10^{-2}$	assumed
	$3.0 \cdot 10^{-3}$	fitting parameter
	$3.0 \cdot 10^{-4}$	assumed
mean equilibrium concentration ($C_{eq} = \rho^* \omega_{eq}$) (µg/l)	500	highest concentration measured
	650	assumed
	1300	estimated based on calculations
	1950	assumed
bottom concentration ($C_{bot} = \rho^* \omega_{bot}$) (µg/l)	0	assumed
	500	assumed
	650	assumed
	1300	assumed

Velocity Field

A velocity field constant in time and space was employed in the preliminary modelling attempts. It was not possible to determine the present day velocity field because available hydrological data are scarce and incomplete, especially with regard to the boundary conditions. As a consequence, RIVM did not attempt to calculate the velocity field for past periods. The mathematical model METROPOL was used to calculate different velocity fields for the present transition zone by varying the boundary conditions. In this way, a sensitivity analysis for different boundary conditions was performed. Boundary conditions were chosen based on hydrological modelling results presented by Townley and Barr *[Townley and Barr, 1992]*.

The boundary conditions, K_X and K_Y values used for determining the different velocity fields, and the travel time of particles starting in the ore body to leave the model domain, are summarised in Table 4.9. The Koongarra fault was assumed to be a no-flow boundary in all simulations. The two perennial creeks perpendicular to the fault were assumed to be either no-flow boundaries or no-flow boundaries along their upper, and constant head boundaries along their lower reaches. In the latter case, the head was assumed to decrease linearly with downstream distance. The Koongarra Creek was assumed to be a constant head boundary with the head varying linearly with downstream distance. A constant influx was considered over the whole modelling area due to leakage through the highly weathered zone.

On the basis of the calculated velocity fields, it was concluded that the direction and velocity of the particles were mainly controlled by the ratio between K_X and K_Y and the recharge (leakage through the weathered zone).

Patterns of the particle tracking, isohypses and velocity vectors for simulations no. 11 and 17 are shown in Figures 4.23 and 4.24. These two velocity fields were chosen based on the present knowledge of transport directions in Koongarra *[Payne et al., 1992, van de Weerd et al., 1993]*.

Table 4.9 *Boundary conditions and K_X and K_Y values used for determining the different velocity fields.*

nr.	h_L (m)	h_R (m)	$Grad_L$ (-)	$Grad_R$ (-)	RE ($m \cdot y^{-1}$)	K_X ($m \cdot y^{-1}$)	K_Y ($m \cdot y^{-1}$)	$T.T.$ (y)
1	16.0	23.0	0.001	0.001	$3.65 \cdot 10^{-3}$	$3.65 \cdot 10^{2}$	$3.65 \cdot 10^{2}$	$2.05 \cdot 10^{2}$
2	16.0	23.0	0.001	0.001	$3.65 \cdot 10^{-3}$	$3.65 \cdot 10^{1}$	$3.65 \cdot 10^{2}$	$1.79 \cdot 10^{3}$
3	16.0	23.0	0.001	0.001	$3.65 \cdot 10^{-3}$	$1.83 \cdot 10^{2}$	$3.65 \cdot 10^{2}$	$3.73 \cdot 10^{2}$
4	16.0	23.0	0.001	0.001	$3.65 \cdot 10^{-3}$	$3.65 \cdot 10^{2}$	$3.65 \cdot 10^{2}$	$4.05 \cdot 10^{2}$
5	16.0	23.0	0.001	0.001	$3.65 \cdot 10^{-3}$	$3.65 \cdot 10^{2}$	$3.65 \cdot 10^{2}$	$2.36 \cdot 10^{2}$
6	16.0	19.5	0.001	0.001	$3.65 \cdot 10^{-3}$	$3.65 \cdot 10^{2}$	$3.65 \cdot 10^{2}$	$5.23 \cdot 10^{2}$
7	16.0	19.5	0.001	0.001	$3.65 \cdot 10^{-3}$	$3.65 \cdot 10^{1}$	$3.65 \cdot 10^{2}$	$4.05 \cdot 10^{3}$
8	16.0	19.5	0.001	0.001	$3.65 \cdot 10^{-3}$	$1.83 \cdot 10^{2}$	$3.65 \cdot 10^{2}$	$8.88 \cdot 10^{2}$
9	16.0	19.5	0.001	0.001	$3.65 \cdot 10^{-3}$	3.65	$3.65 \cdot 10^{2}$	$1.10 \cdot 10^{4}$
10	16.0	19.5	0.001	0.001	$3.65 \cdot 10^{-3}$	$3.65 \cdot 10^{2}$	$3.65 \cdot 10^{2}$	$1.10 \cdot 10^{3}$
11	16.0	23.0	0.001	0.001	$3.65 \cdot 10^{-3}$	3.65	$3.65 \cdot 10^{2}$	$1.02 \cdot 10^{4}$
12	16.0	17.8	0.001	0.001	$3.65 \cdot 10^{-3}$	$3.65 \cdot 10^{2}$	$3.65 \cdot 10^{2}$	$1.25 \cdot 10^{3}$
13	16.0	17.8	0.001	0.001	$3.65 \cdot 10^{-3}$	$3.65 \cdot 10^{1}$	$3.65 \cdot 10^{2}$	$8.60 \cdot 10^{3}$
14	16.0	17.8	0.001	0.001	$3.65 \cdot 10^{-3}$	3.65	$3.65 \cdot 10^{2}$	$1.08 \cdot 10^{4}$
15	16.0	23.0	0.001	0.001	$3.65 \cdot 10^{-3}$	3.65	$3.65 \cdot 10^{2}$	$1.08 \cdot 10^{3}$
16	16.0	23.0	0.001	0.001	$3.65 \cdot 10^{-3}$	3.65	$3.65 \cdot 10^{2}$	$1.88 \cdot 10^{4}$
17	16.0	23.0	0.001	0.001	$3.65 \cdot 10^{-3}$	$3.65 \cdot 10^{1}$	$3.65 \cdot 10^{2}$	$1.27 \cdot 10^{3}$
18	16.0	23.0	0.001	0.001	$3.65 \cdot 10^{-3}$	$3.65 \cdot 10^{2}$	$3.65 \cdot 10^{2}$	$1.91 \cdot 10^{2}$
19	16.0	23.0	0.002	0.002	$3.65 \cdot 10^{-3}$	$3.65 \cdot 10^{1}$	$3.65 \cdot 10^{2}$	$2.05 \cdot 10^{3}$
20	16.0	23.0	0.004	0.004	$3.65 \cdot 10^{-3}$	$3.65 \cdot 10^{1}$	$3.65 \cdot 10^{2}$	$2.65 \cdot 10^{3}$
21	16.0	23.0	0.001	0.001	$3.65 \cdot 10^{-3}$	$3.65 \cdot 10^{1}$	$3.65 \cdot 10^{2}$	$1.80 \cdot 10^{3}$
22	16.0	19.5	0.001	0.001	$3.65 \cdot 10^{-3}$	$3.65 \cdot 10^{1}$	$3.65 \cdot 10^{2}$	$1.07 \cdot 10^{3}$
23	16.0	19.5	0.001	0.001	$3.65 \cdot 10^{-3}$	$3.65 \cdot 10^{1}$	$3.65 \cdot 10^{2}$	$2.47 \cdot 10^{3}$
24	16.0	23.0	NF	NF	$3.65 \cdot 10^{-3}$	$3.65 \cdot 10^{2}$	$3.65 \cdot 10^{2}$	$3.92 \cdot 10^{2}$
25	16.0	23.0	NF	NF	$3.65 \cdot 10^{-3}$	$3.65 \cdot 10^{1}$	$3.65 \cdot 10^{2}$	$2.96 \cdot 10^{3}$
26	16.0	23.0	NF	NF	$3.65 \cdot 10^{-3}$	$3.65 \cdot 10^{1}$	$3.65 \cdot 10^{2}$	$1.23 \cdot 10^{3}$
27	16.0	23.0	NF	NF	$3.65 \cdot 10^{-3}$	$3.65 \cdot 10^{2}$	$3.65 \cdot 10^{2}$	$3.45 \cdot 10^{2}$

No.: simulation number
h_L, h_R: head at downstream and upstream ends of Koongarra creek
$Grad_L$, $Grad_R$: Gradient in lower part of the left and right non-perennial creeks
RE: recharge (= leakage from "above")
K_X, K_Y: permeability in the X and Y direction
$T.T.$: Travel time of a particle started in the orebody to leave the model domain
NF: No-flow boundary.

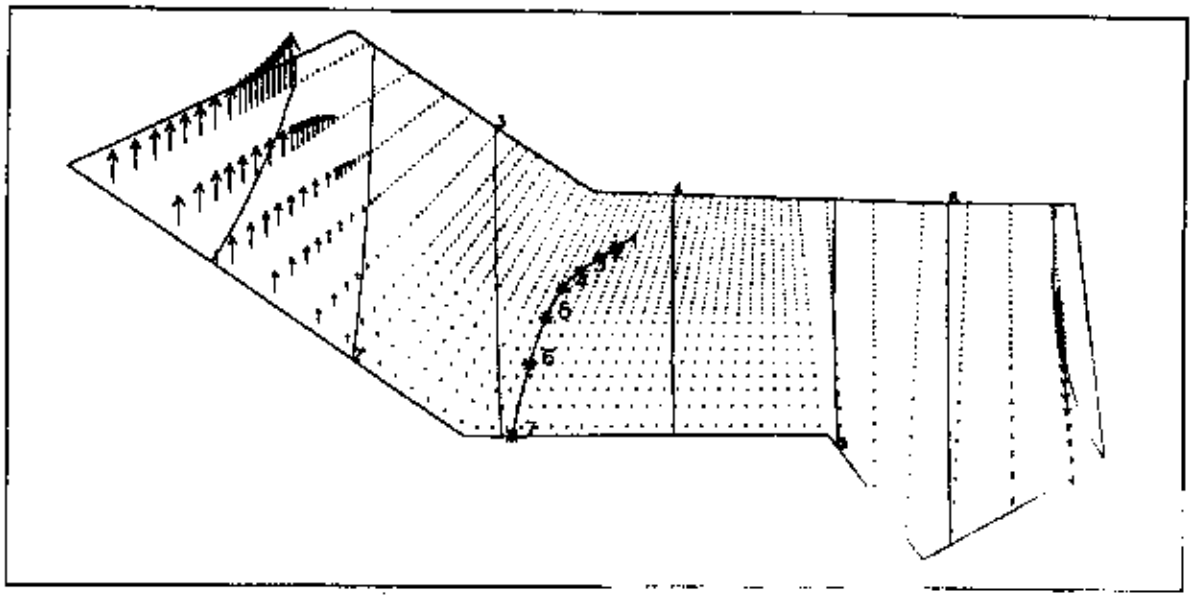

Figure 4.23 *RIVM. Particle tracks, isohypses and velocity vectors for simulation no. 11. Vectors: 1 cm = 5.5 m/y; Isohyps [illegible] 7, Hydraulic head [illegible]-23 m; Particle tracks *: every 1 000 000 [illegible]*

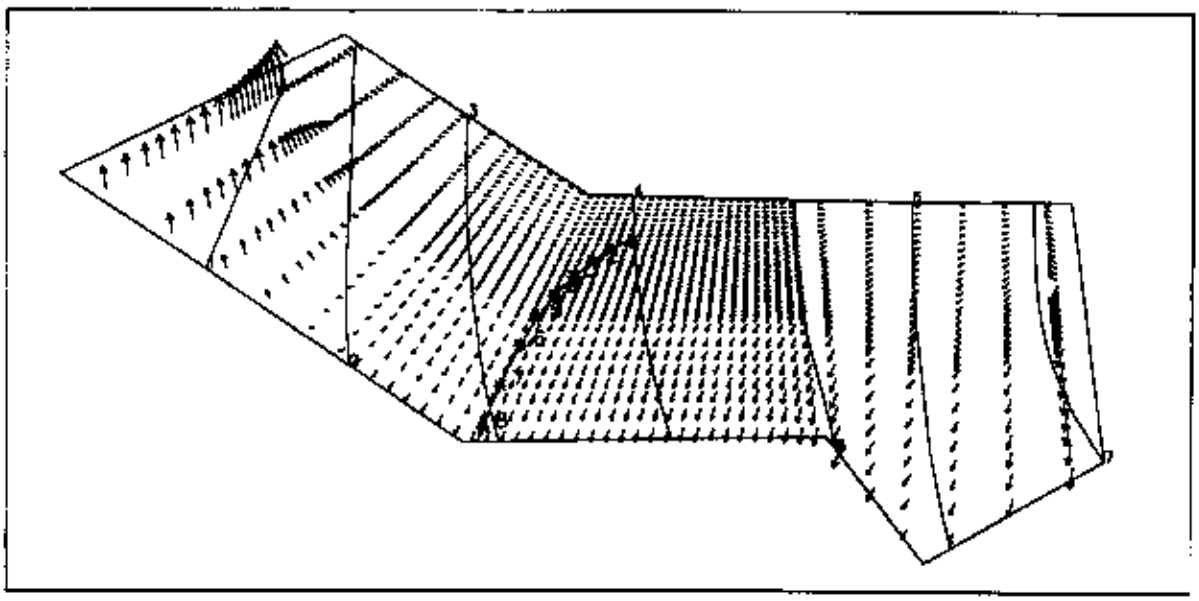

Figure 4.24 *RIVM. Particle tracks, isohypses and velocity vectors for simulation no. 17. Vectors: 1 cm = 7.5 m/y; Isohyps no. 1–7, Hydraulic head: 17–23 m; Particle tracks *: every 100 000 years.*

Rate of Downward Movement of the Transition Zone of Weathering

The history of the ore body region, based on the scenario formulation of Skagius and Wingefors *[Skagius and Wingefors, 1992], is* summarized below. Uranium series disequilibria data on the secondary dispersion fan mineralisation indicate that the weathering front reached the top of the ore body sometime in the interval 1–3 million years ago. The onset of the Pleistocene ice age, beginning around 1.6 million years ago, and the climate changes accompanying this event, may have aided the penetration of weathering down to the ore body. The lowering of the sea level from 1.8 million years onwards would have increased stream gradients, resulting in increased erosion rates. Some 20 m of schists above the Koongarra ore body was stripped off and thus allowed the weathering front to penetrate the top of the primary ore.

Combination of these data leads to the following considerations:

- The earliest possible time at which the weathering front reached the top of the ore body was 1.8 million years ago.
- The base of weathering is at present positioned about 25 metre below the former top of the ore body.
- No ore is present in the top 5 m.

If it is assumed that the transition zone has moved about 20 metres downward over a time period of 1.8 million years, then a mean velocity of $1.1 \cdot 10^{-5}$ m/y is obtained. However, it cannot be reasonable to assume a constant downward velocity of the transition zone during the past 1.8 million years, since this time period involves cycles of alternative cold and warm climates in combination with advancing and retreating ice sheets, and falling and rising sea levels. An increase in rainfall would, for example, potentially increase the erosion, raise the water table, and increase both the groundwater flow and the dispersion of uranium down-slope in the weathered zone. Nevertheless, it was considered acceptable to work with an average value of the movement of the transition zone, since data on dry and wet periods and sea levels fluctuations are not available or too uncertain to provide any reasonably good estimate of the variations in the weathering front velocity.

Equilibrium Concentration of Uranium

The preliminary modelling attempts, that were based on a stationary transition zone, used a constant uranium source concentration of 500 µg/l. This value was chosen because it is close to one of the highest uranium concentrations found at Koongarra (borehole M1, 489 µg/l).

The equilibrium concentration of uranium in the calculations that included the moving transition zone was based on geochemical calculations in order to obtain a more realistic equilibrium concentration. The calculations were based on that the primary uranium mineral, uraninite, is in equilibrium with the groundwater in the orebody. Based on the results from these calculations, the equilibrium concentration of uranium was assumed to be equal to the

minimum value calculated for borehole PH49, $1.3 \cdot 10^{-3}$ g/l, which is located in the centre of the ore body. This borehole is within the 1000 mg/kg contour line of solid phase uranium concentrations at every depth as illustrated in Figures 3.13a–f.

4.2.6 Results

The results from the simulations with and without movement of the transition zone of weathering and with and without a spatially variable velocity field are presented in this section. As the number of measured uranium concentrations in the liquid phase are scarce, the calculated values of liquid phase concentrations were converted into solid phase concentrations by using the K_d value in order to compare the modelling results with the present conditions. By using these converted concentrations, contour plots of the simulation results could be compared with solid phase uranium concentration contours from section 3.2.1. This conversion is not possible within the ore body, since the solid phase concentration in this region is not determined by sorption but by the concentration of uranium minerals.

Modelling Uranium Transport in the Present Transition Zone – Effect of Variations in the Velocity Field

The results from simulations 1, 2 and 3, with a stationary transition zone, are presented in Figures 4.25, 4.26 and 4.27. A velocity field constant in time and space was used in model simulation 1 (Figure 4.25). This simulation is similar to earlier reported calculations *[Van de Weerd et al, 1993]*, because the dissolution rate is high enough to maintain the equilibrium concentration in the ore body. The spatially varying velocity fields selected in section 4.2.4 were used in simulations 2 and 3 (Figures 4.26 and 4.27). These simulations show the effect of variations in the velocity field on the transport of uranium.

A summary of the model parameters used for simulations no 1, 2 and 3 is given in Table 4.10. All other parameters values are given in Table 4.8.

Table 4.10 *RIVM. Model parameters used for transport calculations in the present transition zone.*

Sim. no.	Sim. times y	v_{eff} (PH49) m/y	Direction (PH49) compass bearing	K y^{-1}	ω_{eq} µg/l	ω_{bot} µg/l	w m/y
1 a	$1.0 \cdot 10^5$						
b	$4.5 \cdot 10^5$	1.3	215	6.5	500	500	0
c	$1.8 \cdot 10^6$						
2 a	$1.0 \cdot 10^5$						
b	$4.5 \cdot 10^5$	0.56	210	6.5	500	500	0
c	$1.8 \cdot 10^6$						
3 a	$1.0 \cdot 10^5$						
b	$4.5 \cdot 10^5$	0.053	209	6.5	500	500	0
c	$1.8 \cdot 10^6$						

The equilibrium and the bottom concentrations were chosen to be close to one of the highest concentrations found at Koongarra (borehole M1, 489 µg/l). The dissolution rate constant was set very high to reach the equilibrium concentration. The results are illustrated in Figures 4.25, 4.26 and 4.27. Three different simulation times were applied.

It can be seen in Figures 4.25, 4.26 and 4.27 that the calculated dispersion of uranium gradually increases with increasing simulation time. The calculated concentration distribution pattern after 450 000 years (Figures 4.25 and 4.26) shows a qualitatively good agreement with the pattern found for the present transition zone (Figure 5b).

The spreading of uranium in simulation 3 (Figure 4.27) is very limited due to the very low effective velocities used in this simulation (Figure 4.23). This illustrates that the present dispersion distance is not reached even after a simulation period of two million years due to the low velocities. The magnitude of the effective velocity is thus very important for the dispersion distance.

The flow velocity and direction of transport is only provided for borehole PH49 in Table 4.10. However, the magnitude of the effective velocity and the direction of flow may vary in space in a spatially variable velocity field. Figures 16 and 17 give an indication of the change in direction and effective velocity along a particle track starting in the ore body. The change in direction and degree of spreading between 450 000 years and 1800 000 years in Figure 4.26 may be explained by the higher effective velocity and the change of the flow direction towards the Koongarra Creek. The results show that a spatially variable velocity field may have a great impact on the dispersion.

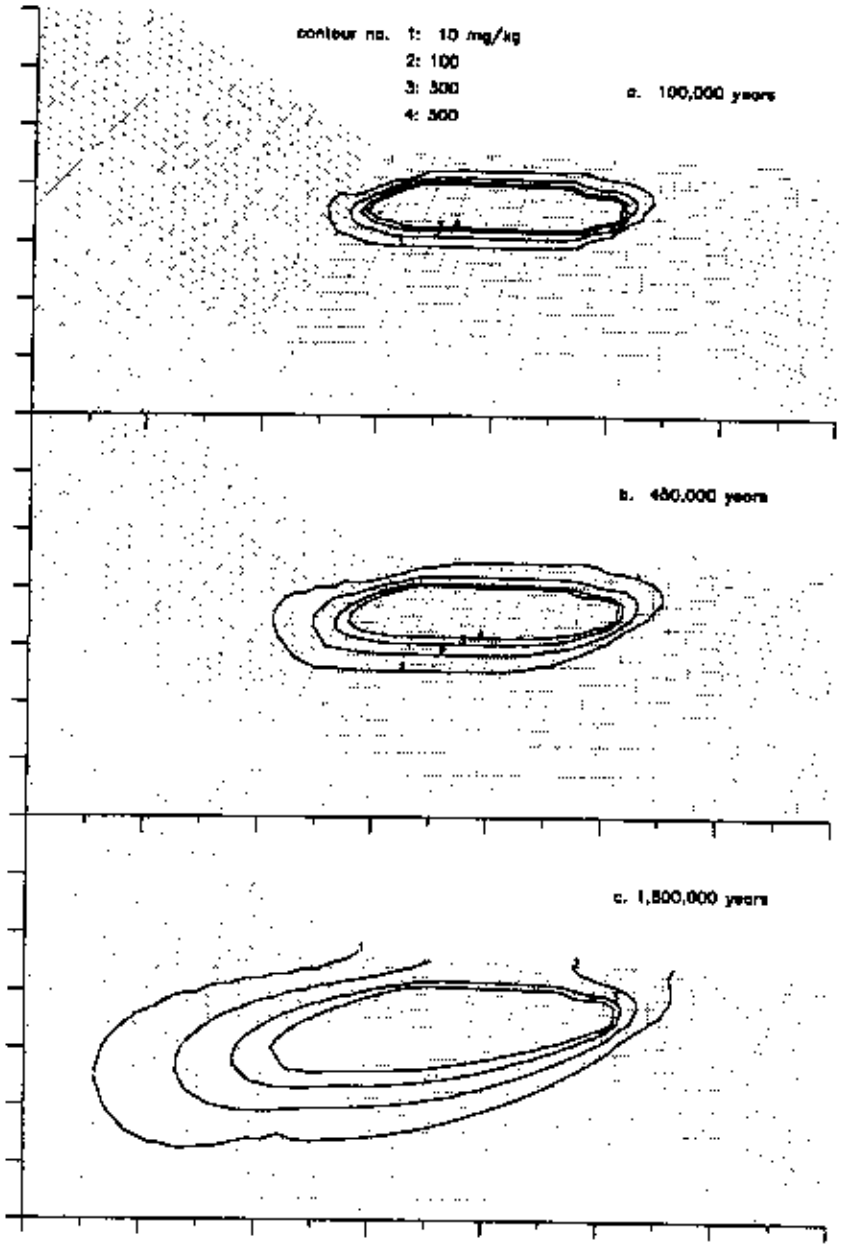

Figure 4.25 *RIVM. Results of simulation 1, with a stationary transition zone and a velocity field constant in time and space. Contour plots of solid phase uranium concentrations at different simulation times.*

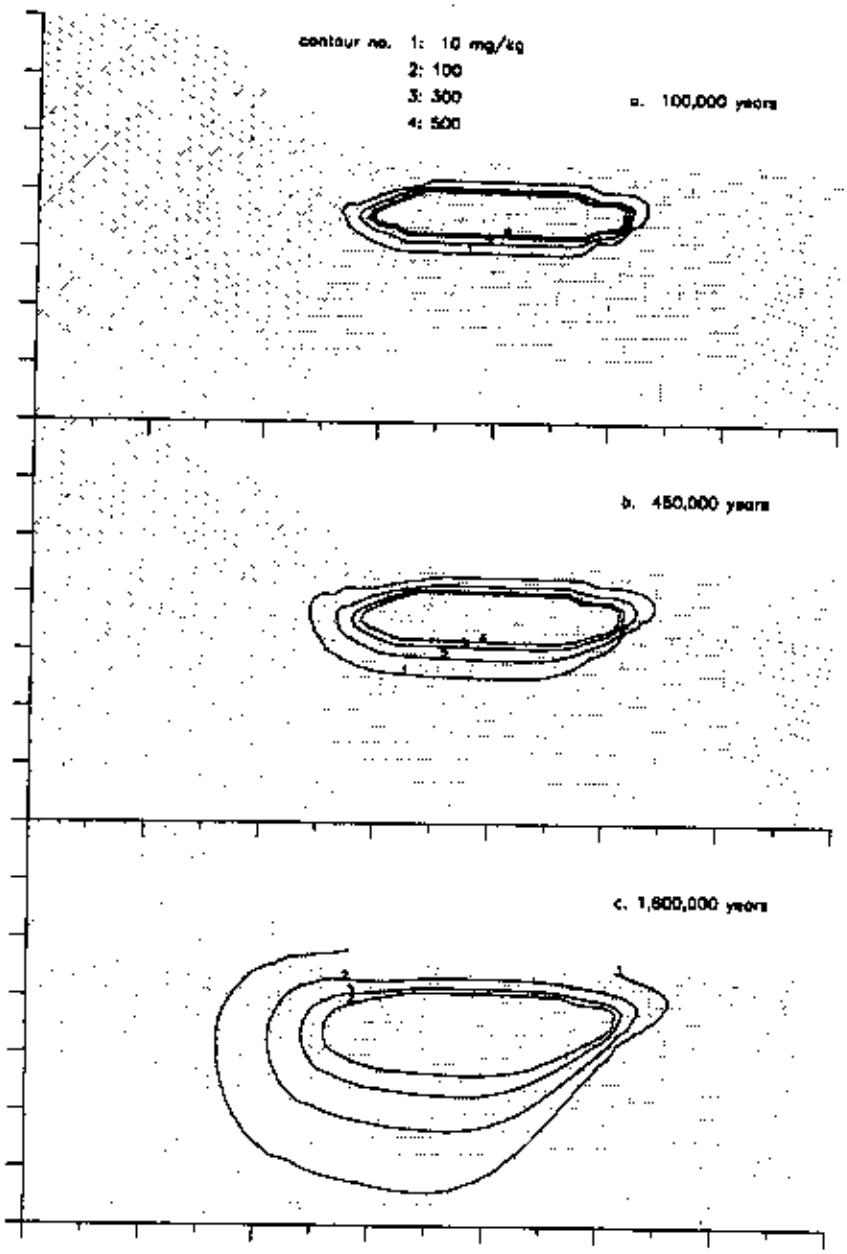

Figure 4.26 *RIVM. Results of simulation 2, with a stationary transition zone and a spacial variable velocity field. Contour plots of solid phase uranium concentrations at different simulation times.*

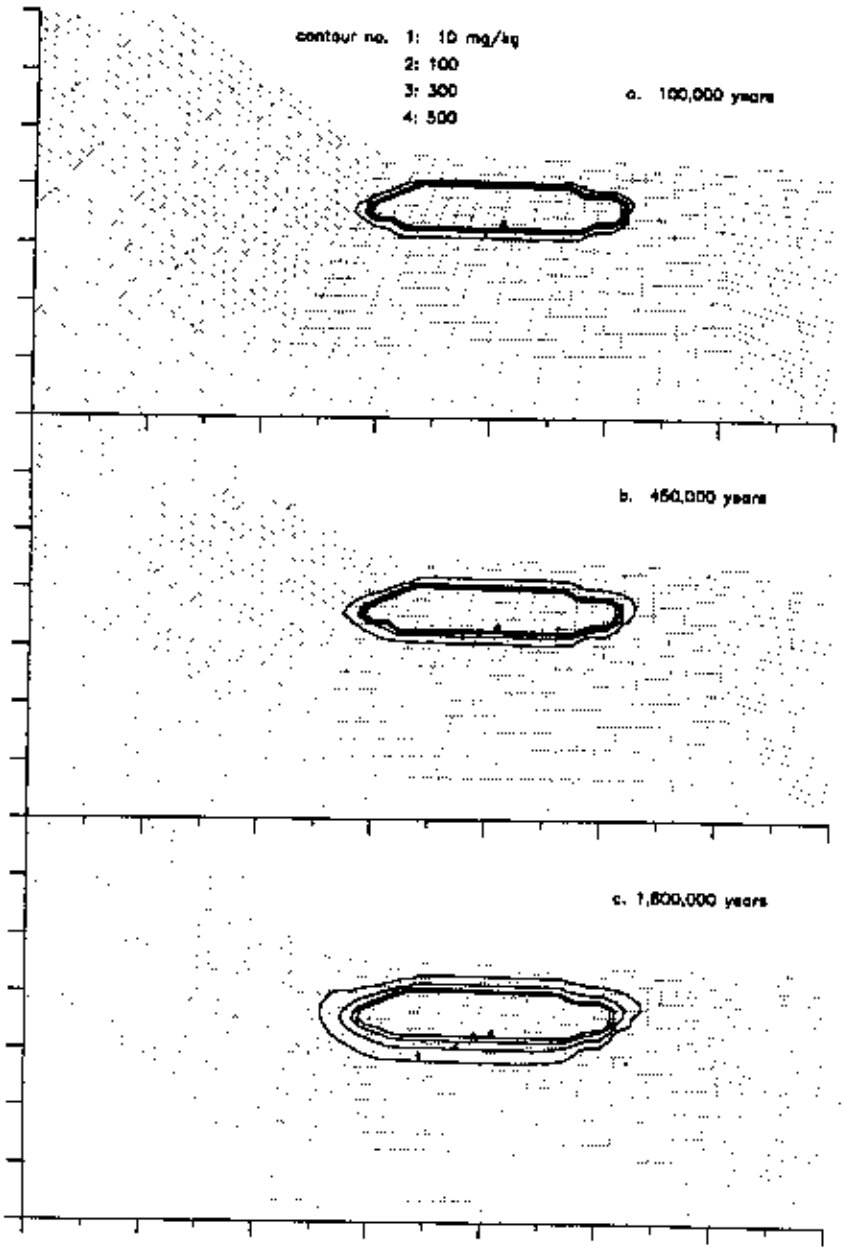

Figure 4.27 *RIVM. Results of simulation 3, with a stationary transition zone and a spatial variable velocity field. Contour plots of solid phase uranium concentrations at different simulation times.*

The boundary conditions used for the calculation of the velocity field are very uncertain. They may be valid for the present transition zone, but are unknown in the past. This being the case, the calculations with the moving transition zone were performed with a velocity field that was constant in time and space.

The results of simulations no. 4 to 12 which involve a moving transition zone are presented in Figures 4.28 to 4.31. Simulation no. 4 should be considered as a base case using the parameters derived in section 4.2.4. The bottom concentration and the dissolution rate constant were used as fitting parameters and selected in such a way that the aqueous concentration reached in the ore body was close to the highest aqueous concentration measured in the present transition zone at Koongarra (489 µg/l). Different combinations of K and ω_{bot} will lead to this concentration. The value of ω_{bot} was set to 650 µg/l because ω_{bot} was expected to be in the range 0 and 1300 µg/l. The value of K was then adjusted in order to get a concentration close to 489 µg/l. The parameter values used in the calculations are summarised in Table 4.11.

Table 4.11 RIVM. Model parameters used for model calculations with a moving transition zone and a velocity field constant in time and space.

Simulation no.	Sim. time y	K y^{-1}	ω_{eq} µg/l	ω_{bot} µg/l	w *m/y*
4	$1.8 \cdot 10^{6}$	$3.0 \cdot 10^{-3}$	1300	650	$1.1 \cdot 10^{-5}$
5	$3.6 \cdot 10^{6}$	$3.0 \cdot 10^{-3}$	1300	650	$5.5 \cdot 10^{-6}$
6	$1.2 \cdot 10^{6}$	$3.0 \cdot 10^{-3}$	1300	650	$1.7 \cdot 10^{-5}$
7	$1.2 \cdot 10^{6}$	$3.0 \cdot 10^{-3}$	650	650	$1.1 \cdot 10^{-5}$
8	$1.2 \cdot 10^{6}$	$3.0 \cdot 10^{-3}$	1950	650	$1.1 \cdot 10^{-5}$
9	$1.2 \cdot 10^{6}$	$3.0 \cdot 10^{-3}$	1300	0	$1.1 \cdot 10^{-5}$
10	$1.2 \cdot 10^{6}$	$3.0 \cdot 10^{-3}$	1300	1300	$1.1 \cdot 10^{-5}$
11	$1.2 \cdot 10^{6}$	$3.0 \cdot 10^{-43}$	1300	650	$1.1 \cdot 10^{-5}$
12	$1.2 \cdot 10^{6}$	$3.0 \cdot 10^{-2}$	1300	650	$1.1 \cdot 10^{-5}$

A planar view of the dispersion of uranium for simulation 4, 5 and 6 after different simulation periods is given in Figures 4.28, 4.29 and 4.30. The simulation times were chosen in such a way that the lower boundary of the transition zone was positioned at the present depth of the weathering front at the end of the simulation. The uranium dispersion at depth intervals 5–10 m, 10–15 m, 15–20 m and 20–25 m is illustrated in Figures 4.28a–d, 4.29a–d and 4.30a–d. The evolution of the aqueous uranium concentration for a nodal point (positioned in the moving transition zone) in the ore body and in the dispersion fan is given in Figure 4.31 for simulations 7 to 12.

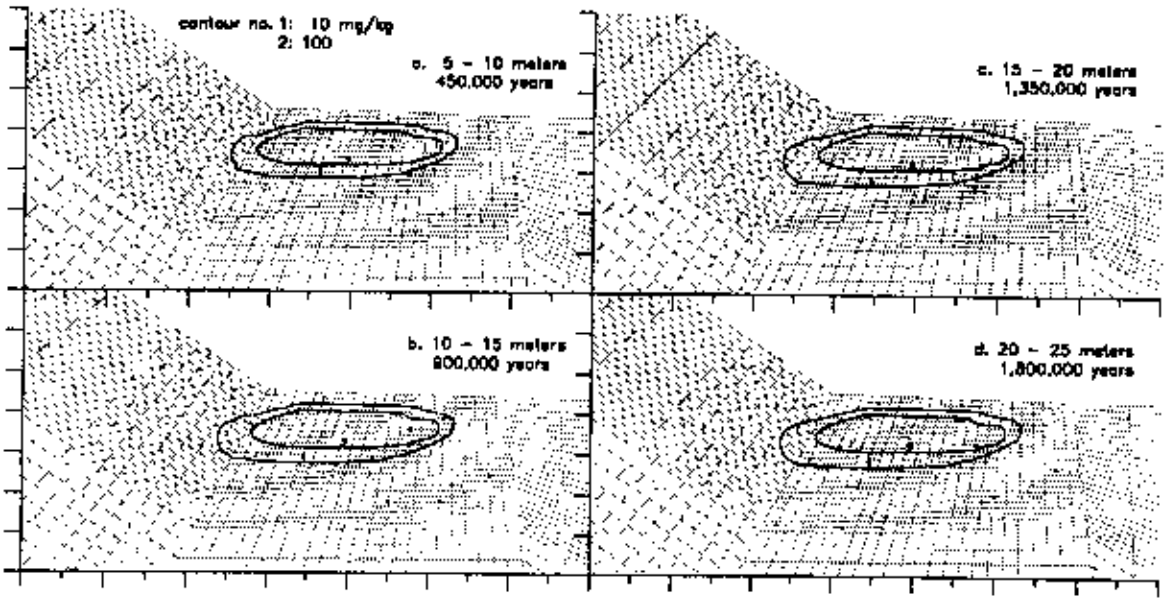

Figure 4.28 RIVM. Results of simulation 4, with a velocity constant in time and space and a moving transition zone ($w = 1.1 \cdot 10^{-5}$ m/y).

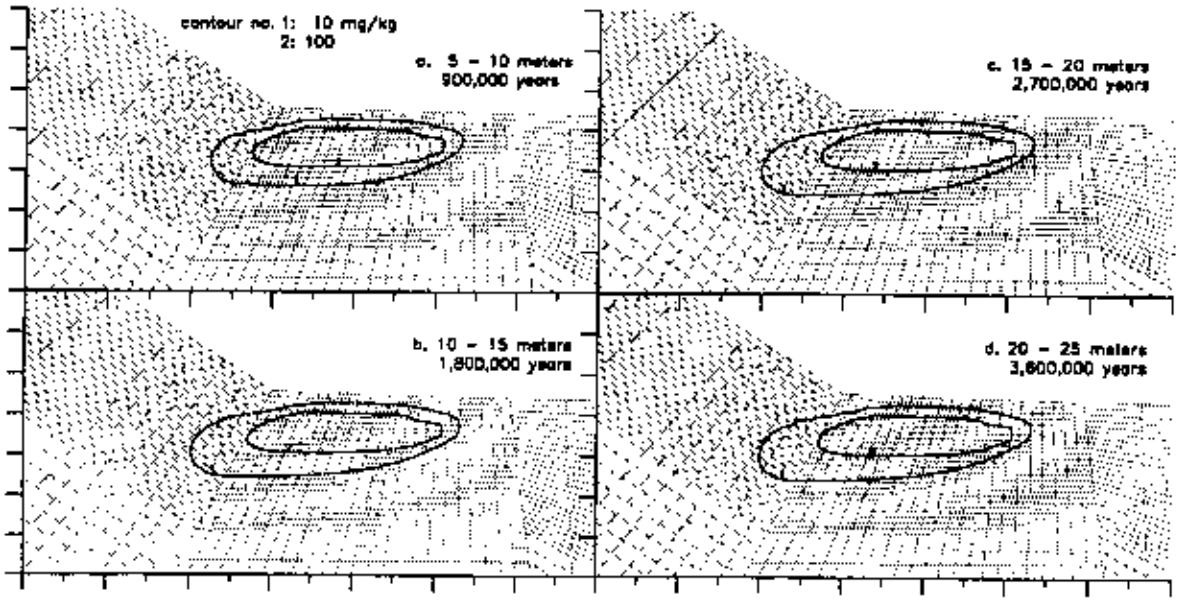

Figure 4.29 RIVM. Results of simulation 5, with a velocity constant in time and space and a moving transition zone ($w = 5.5 \cdot 10^{-6}$ m/y).

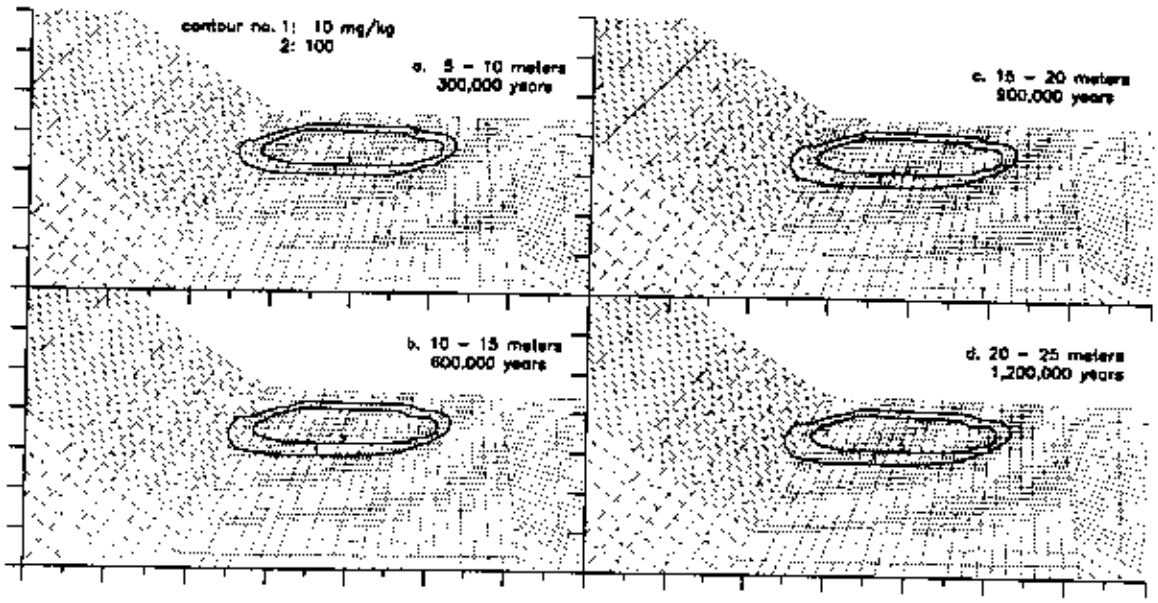

Figure 4.30 RIVM. Results of simulation 6, with a velocity constant in time and space and a moving transition zone ($w = 1.7 \cdot 10^{-5}$ m/y).

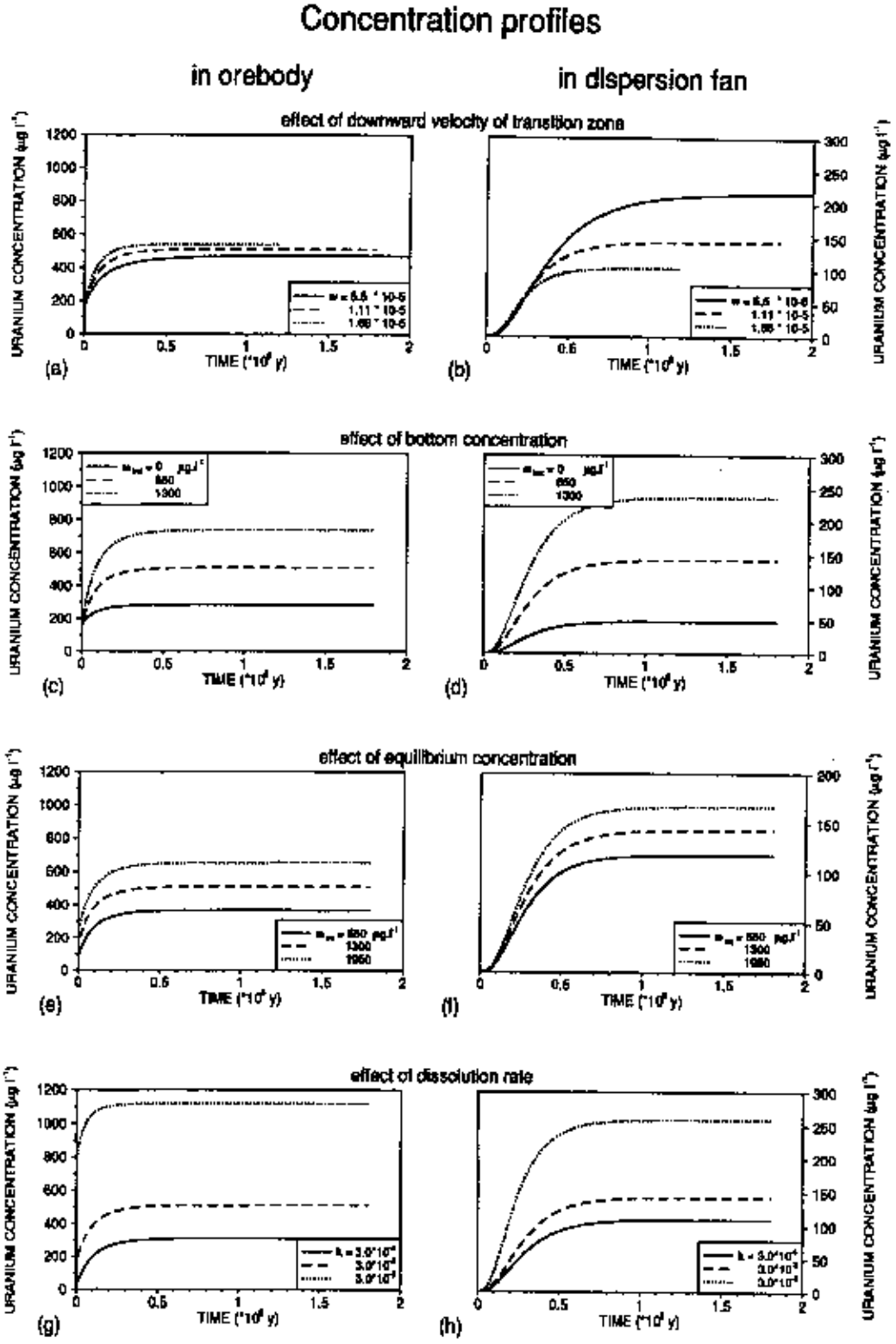

Figure 4.31 *RIVM. Results of simulations 4–12. Evolution of the aqueous uranium concentration in a nodal point in the ore body (PH 49) and outside the ore body (DDH 54) as a function of simulation parameter values.*

From a comparison of the results of simulation 4 (Figure 4.28) with the solid phase uranium contours (Figure 3.13) it can be concluded that the dispersion distance of the simulation is not in accordance with the dispersion distance found in Koongarra. A steady state situation is reached after a simulation period of 900 000 years and a depth ranging from 10 to 15 m. However, the maximum dispersion of uranium, as illustrated in Figure 3.13, is already reached at a depth ranging from 5 to 10 m. The 10 mg/kg contours in Figure 4.28c–d are in qualitative agreement with the 100 mg/kg contour of Figure 3.13. By varying some of the model parameters, it may be possible to reach a better "fit" of the solid phase uranium contours. For example, increasing the effective velocity will lead to more dispersion, and if the effective velocity or K-value are increased the maximum dispersion distance will be reached earlier.

It can be seen in Figures 4.28, 4.29 and 4.30 that a steady state situation is reached in the transition zone after a certain simulation time. The sources and sinks of uranium are obviously equal after that time. There are two sources of uranium; the bottom concentration entering the transition zone in the ore body region at the lower boundary and the uranium formed by dissolution of the ore in the ore body region of the transition zone. The sink is the concentration of uranium leaving the transition zone at the upper boundary. With increasing dispersion distance, the sink term will increase, because the area over which the uranium leaves the system becomes larger. A steady state situation will therefore be reached at a certain dispersion distance.

The effect of the downward movement rate of the transition zone on the uranium dispersion can be assessed by comparing the results from simulations 4, 5 and 6. It can be seen in Figures 4.28, 4.29 and 4.30 that the dispersion distance decreases with increasing downward velocity.

Figures 4.31a and 4.31b illustrate that a change in the downward velocity of the transition zone will have a large impact on the concentrations in the dispersion fan, but it will hardly affect the concentrations in the ore body.

Figures 4.31e and 4.31f show that an increase in the equilibrium concentration will increase the concentrations reached in the ore body and dispersion fan. Obviously, "the dissolution source term" increases because a higher aqueous concentration of uranium is necessary to maintain the difference between ω and ω_{eq} (Equation 4.18).

The impact of the bottom concentration on the evolution of the uranium concentration is illustrated in Figures 4.31c and 4.31d. Apparently, an increasing bottom concentration gives higher concentrations in the ore body and dispersion fan. The bottom concentration is a source of aqueous uranium that will be more or less important depending on the downward velocity of the transition zone.

The impact of the dissolution rate constant on the evolution of the uranium concentration is treated in Figures 4.31g and 4.31h. An increase in the dissolution rate will increase the concentrations reached in the ore body and dispersion fan.

Results of Modelling. Conclusions

To assess the effect of the groundwater velocity field, three simulations were carried out neglecting the movement of the transition zone. The groundwater velocities were constant in time in the simulations, but both constant and spatially variable velocity fields were applied. A qualitatively fairly good agreement between calculated and measured uranium concentration in the solid phase was obtained for the constant velocity field case and one of the variable velocity field cases. These simulations showed that the uranium concentration distribution pattern is highly dependent on the velocity field. Furthermore, the use of a spatially variable velocity field could not be justified because of the large uncertainties in the boundary conditions.

The boundary conditions used for the calculation of the velocity field are very uncertain. They may be valid for the present transition zone, but are unknown for the past. This being the case, the calculations that included the downward movement of the transition zone were performed with a velocity field that was constant in time and space. Results from the simulations is illustrated in Figures 4.28, 4.29 and 4.30 at four different depths. A concentration distribution pattern that is almost constant with depth was observed in the simulations which is in agreement with the observations at Koongarra as illustrated in Figure 13a–f. One conclusion that can be drawn from these simulations is that the present situation in Koongarra can be simulated by including a moving transition zone. However, the calculated dispersion distance from the ore body was shorter than observed at Koongarra. It is believed that a better "fit" with the measured solid phase uranium concentration distribution could be obtained by changing some of the model parameters, like the groundwater velocity, the downward velocity of the transition zone, the adsorption distribution coefficient or the dissolution source term..

The results from the simulations show that with the use of a moving transition zone it is possible to simulate the present situation in Koongarra. However, the values of most parameters are very uncertain. The largest uncertainties are associated with the boundary conditions. We do not know how the system did evolve. Nor is it known if the Koongarra fault is a hydrological barrier. As a result of such uncertainties, the effective velocity, and its spatial and temporal variability, as well as the velocity of the moving transition zone are uncertain.

5 Uncertainties

In the models used in the INTRAVAL study, a number of simplifications of the complex system had to be made that may introduce uncertainties in the modelling results. One type of uncertainties is associated with the identification of processes, geometrical structures and other conditions that have lead to and influenced the mobilisation and dispersion of uranium and daughter nuclides from the primary ore body. Another area, still poorly understood, concerns the present and past day hydrogeology of the site, which implies that the assumptions regarding flow directions and types of flow paths are uncertain. It is even unknown whether the water flow, and thereby the uranium migration, has taken place in the entire weathered zone or only in a rather thin transition zone that has moved downward with time.

Still another type of uncertainty is introduced by the use of a rather simplified mathematical model and by the assumptions made in the calculations. For example, sorption was modelled by applying the K_d-concept, which signifies that sorption was assumed to be instantaneous, reversible and independent of the composition of the water along the transport path. This approach may not be entirely adequate to describe the effects of sorption. Another example concerns the mathematical description of processes leading to the observed distribution of uranium and thorium between different mineral phases of the rock. Accounting for these processes by merely assuming a phase transfer rate may be a too simplistic approach. Uncertainties are also introduced by making the assumptions that hydrogeological and hydrochemical conditions are constant over the space- and time-scale of interest, and that these conditions are determined by the present day situation. It should also be noted that the applied models are based on groundwater flow in a homogeneous media. This is a simplification of the actual system where probably a large part of the flow, at least in the unweathered zone and the transition zone, takes place in fractures.

A third type of uncertainty is associated with the data used as input to the model and with the data with which the model results are compared. Values of the downward velocity of the transition zone, the dissolution constant, the equilibrium concentration, the water flux, the distribution coefficient, the recoil factor and the phase transfer rate used in the modelling were based on the results from independent modelling and interpretations of site data. The difficulty in describing the present and past hydrology at the site introduces uncertainties in the estimates of water flux in the weathered zone. The recommended ranges of K_d-values are based on both laboratory experiments and field observations of the distribution of elements between water and solid phases. In the field, other processes in addition to sorption may have contributed to the observed distribution between water and solid phase, which makes K_d-values based on field observations uncertain. In addition, observations at the site have shown that most of the radionuclides in the rock are not directly accessible to groundwater and that they therefore cannot be treated as sorbed. A K_d-value based on the total amount of a radionuclide in the rock may thus be too high. Using a K_d-value based on the observed partitioning of radionuclides between water and amorphous phases may be more relevant both with respect to competing processes and accessibility, although still not without uncertainty.

The uncertainty in the observed data used for comparison and evaluation of the modelling results arises from the difficulty in assessing which data and form of data that should be used to best represent the modelling purpose. It is believed that the concentrations and activity ratios measured in bulk rock samples are more reliable than the radiochemical data given for the accessible and inaccessible phases separately. These latter data are obtained by a sequential extraction procedure on very small samples, and the separation into accessible and inaccessible phases of these samples

in the extraction procedure may not necessarily represent the actual separation between accessible and inaccessible phases of the rock at the site. Furthermore, the uranium concentrations in the groundwater show large variations between different sampling occasions. No clear trend could be found, such as an increasing or decreasing concentration with depth.

6 Discussions and Conclusions

6.1 Data Review

The review of the available solid uranium concentrations shows that the extension of the dispersed fan in the south direction from the fault is around 350 m, whereas the extension in the southeast direction is around 100 m. Information from different depths indicates that the pattern of the dispersion is similar at all depths in the weathered zone. This supports the hypothesis that groundwater movement and dispersion of uranium have taken place mainly in the transition zone. If significant transport had occurred in the fully weathered top layer, then the dispersion distance from the ore body should decrease with depth. Moreover, the concentration distribution pattern suggests that the direction and magnitude of the average groundwater flow have not changed significantly during the past few million years.

The hypothesis that groundwater movement and dispersion of uranium have taken place mainly in the transition zone is, however, not supported by the observed activity ratio $^{230}Th/^{234}U$. The similarity in the activity ratio profile at different depths in the weathered zone, with values below 1 at the uranium dispersion front, indicates that uranium migration has taken place at all depths in the weathered zone during the last 200 000 years. The similarity in both uranium concentration distribution pattern and $^{230}Th/^{234}U$ activity ratio profile at different depths could be explained by assuming an initially very fast downward movement of the weathering front down to the present base of weathering that initiated uranium migration at all depths in the weathered zone.

There appears to be a linear relationship between uranium in the accessible solid phase of the weathered rock and the uranium concentration in the groundwater. This suggests that the sorption process can be described by a linear adsorption isotherm with a distribution coefficient calculated from the measured concentration of accessible uranium in the solid phase and the uranium concentration in solution.

The activity ratios ($^{234}U/^{238}U$, $^{230}Th/^{234}U$) in the accessible phase are generally lower than in the inaccessible phase, which indicates a more recent deposition of uranium in the accessible phase and/or a preferential transfer of ^{234}U and ^{230}Th from the accessible to the inaccessible phase. The preferential transfer could be a result of α-recoil.

6.2 Migration Calculations

The model concepts that have been applied in this study are rather simple. The models used are performance assessment models accounting for advection, dispersion and linear sorption in one or two dimensions. The one-dimensional model was extended to include recoil and phase transfer. The vertical movement of the transition zone was included in the two-dimensional model.

One-dimensional Calculations

The dispersion distance and solid uranium concentrations calculated with the simplified one-dimensional advection–dispersion model including sorption were in fair agreement with observed migration distance and solid uranium concentrations in the dispersion fan. The applied model

involved extensive simplifications of the system, but the results showed that it is possible to simulate the observed migration distance and concentration levels with a few parameters having values consistent with what has been recommended by independent interpreters.

The model that was extended to include chain-decay made it possible to get an independent estimation of the migration time by studying the $^{230}Th/^{234}U$ ratio. The result indicated that the migration has continued for a time period in the order of millions of years.

The introduction of α-recoil and phase transfer allowed the model to simulate certain observed effects, e.g. the decrease in activity ratios in the bulk rock with distance and to explain the general trend with most of the observed activity ratios in the accessible phase falling below 1 and in the inaccessible phase above 1, but the model did not improve the match between calculated and observed uranium concentrations in the bulk rock.The model gave a description of the system that was more consistent with what is observed at the site. The fact that the number of free parameters is larger and that more data on the system are required compared to the more simple advection–dispersion–reversible sorption model may possibly explain the difficulty in improving the simulation results using this model.

Two-dimensional Calculations

Calculations of uranium transport in the present transition zone, not considering the moving transition zone, resulted in contour lines of the uranium concentration in the solid phase that were qualitatively in agreement with the contour lines from the observed concentrations. Taking into account the movement of the transition zone, a dispersion pattern that was stationary with depth was obtained in the weathered zone. This result is in agreement with the observations at Koongarra. However, the calculated dispersion length was shorter than the one measured. By calibration, a better estimate of the dispersion length could be obtained, e.g., by increasing the effective velocity and/or the dissolution rate of uranium. Thus, the two-dimensional study showed that it is possible to simulate the present situation in Koongarra using the concept of a moving transition zone.

Results from the ARAP

Modelling or the uranium migration was also carried out in the ARAP by ANSTO and other organisations. The migration modelling in the ARAP was performed using models ranging from rather simple advection–dispersion–linear sorption models to complex multi-phase models considering recoil and chemical transfer. The advection–dispersion–linear sorption models were found to simulate the observed extension of the uranium migration fairly well. The more complex multi-phase models considering recoil and chemical transfer gave a good description of the observed uranium concentrations and activity ratios in the different mineral phases of the rock. The migration modelling carried out in the ARAP as well as by RIVM and Kemakta in INTRAVAL indicated that the uranium migration has continued for a time period of about half a million up to a few million year. This is in fair agreement with results from geomorphological investigations which indicate that the arrival of the orebody at a depth suitable for the development of the dispersion fan occurred sometime in the last 1–6 million years *[Wyrwoll, 1992]*.

6.3 Validation Aspects

One of the main aims of this INTRAVAL study was to test and, if possible, validate simple and conservative models used in performance assessment of radioactive waste repositories. Although the results from the work are not sufficient to validate simple performance assessment models in a strict sense, it has been shown that even simple models are able to describe the present day distribution of uranium in the weathered zone at Koongarra, if they are based on established transport processes and reasonably selected parameter values.

6.4 Concluding Remarks

Studies of the Alligator Rivers Natural Analogue has demonstrated that the system is very complex. The interaction of many geochemical and geohydrological processes occurring over long times makes it difficult to construct a quantitative model of the history of the groundwater flow and nuclide transport. The study has shown the importance of a joint interpretation of different types of data and the necessity of an iterative procedure for data collection, data interpretation and modelling in order to get a consistent picture of the evolution of the site. Furthermore, the studies have shown that sorption is a major retardation mechanism, that uranium fixation in crystalline phases is a potentially important retardation mechanism in geologic media where significant alteration of the rock is expected, and that α-recoil may have an impact on the distribution of uranium isotopes in the water. Modelling simulations indicated migration times in fair agreement with independent geomorphological information.

A general conclusion from the studies is that rather simple and robust concepts and models seem able to adequately describe the long range migration processes that have occurred. On the other hand, for more detailed modelling and to attain a more comprehensive understanding the geochemical processes have to be taken into account to a greater extent.

Acknowledgement

This report is based on work that was mainly carried out by the National Institute of Public Health and Environmental Protection (RIVM) and Kemakta Konsult. The report was prepared by Kemakta with valuable support by Ms. Rikje van de Weerd at RIVM who supplied us with background material and gave helpful suggestions regarding the content. We would also like to thank Dr. Stig Wingefors at the Swedish Nuclear Power Inspectorate for useful proposals regarding the content.

References

Drever J.I., The Geochemistry of Natural Waters (2nd edition), Prentice-Hall, New Jersey, 1988.

Duerden P.(ed), The International INTRAVAL Project Phase 1 - Test Case 8 - The Alligator Rivers Natural Analogue. Swedish Nuclear Power Inspectorate (SKI)/OECD Nuclear Energy Agency, 1992.

Edghill R., The Distribution of Uranium and Thorium between Phases in Weathered Core from Koongarra, ARAP Progress Report, 1 June - 31 August, ANSTO, 1989.

Edgehill R., The Distribution of Uranium and Thorium between Phases in Weathered Core from Koongarra, ARAP 1st annual report, 1988-1989 (editor P Duerden), 1990.

Edis R. *et al.*, Chemistry and Mineralogy of Rocks and Soils, ARAP Final Report, Volume 8, OECD/NEA, 1992.

Edwards A.L., TRUMP: A Computer Program for Transient and Steady State Temperature Distributions in Multidimensional Systems, National Technical Information Service, National Bureau of Standards, Springfield, Va, USA, 1972.

Emerson D.W., Physical Property Measurements on Drillcore from the Koongarra Uranium Deposit, ARAP Progress Report, 1 June - 31 August, ANSTO, 1989.

Emerson D.W., Geophysics, Petrophysics and Structure, ARAP Final Report, Volume 4, OECD/NEA, 1992.

Gelhar L.W., Mantoglou A., Welty C., Rehfeldt K.R., A Review of Field-Scale Physical Solute Transport Processes in Saturated and Unsaturated Porous Media, Electrical Power Research Institute, EPRI EA-4190, Palo Alto, California, USA, 1985.

Golian C., Lever D.A., Radionuclide Transport, ARAP Final Report, Volume 14, OECD/NEA, 1992.

Lever D., Modelling Radionuclide Transport at Koongarra, In Australian Atomic Energy Commission Annual Report 1984-1985, AAEC/C55, 1986.

Lever D.A., Morris S.T., The Application of NAMMU to Modelling the Groundwater Flow at Koongarra, ARAP Progress Report, 1 December 1989 - 28 February 1990, ANSTO, 1990.

Nightingale T.J., Mobilisation of Uranium within the Weathered Zone of the Koongarra Uranium Deposit, ARAP Progress Report, 1 September 1987 - 30 April 1988, ANSTO, 1988.

Payne T.E., Field Trip - October 1989, ARAP Progress Report, 1 September - 30 November, ANSTO, 1989.

Payne T.E. *et al.*, Groundwater Chemistry, ARAP Final Report, Volume 7, ANSTO, 1992.

Raffensberger J., Garven G., Coupled Hydrogeochemical Modelling of Uranium Ore Deposit, ARAP Progress Report, 1 June - 31 August, ANSTO, 1989.

Rasmuson A., Narasimhan T.N., Neretnieks I., Chemical Transport in a Fissured Rock: Verification of a Numerical Model, Water Resour. Res., vol. 18, pp 1479-1492, 1982.

Sauter F.J., Leijnse A. and Beusen A.H.W., METROPOL User's guide, RIVM report no. 725205003, Bilthoven, 1993.

Sekine K., Murakami T., Yanase N., Ohnuki T., Isobe H., Kobayashi Y., Migration Behaviour of Uranium and Thorium Series Nuclides: Relevant to Alteration, ARAP Progress Report, 1 September - 30 November, ANSTO, 1988.

Sekine K., Ueno T., Uranium and Thorium Adsorption onto Pure Minerals, ARAP Progress Report, 1 September - 30 November, ANSTO, 1989.

Skagius K., Wingefors S., Scenarios, ARAP Final Report, Volume 16, OECD/NEA, 1992.

Skagius K., Lindgren M., Pers K. and Brandberg F., The Alligator Rivers Natural Analogue - Modelling of Uranium and Thorium Migration in the Weathered Zone at Koongarra, SKI 94:19, Swedish Nuclear Power Inspectorate, Stockholm, 1994.

Townley L.R., Barr A.D. Two-dimensional Regional Groundwater Flow near Koongarra, ARAP 3rd annual report 1990-1991, ANSTO, 1992.

Townley L.R., Hydrogeological Modelling, ARAP Final Report, Volume 6, OECD/NEA, 1992.

Van De Weerd H., Hassanizadeh S.M. and Richardson-van der Poel M.A., INTRAVAL Phase 2, Test Case 8 - Alligator Rivers Natural Analogue - Modelling of Uranium Transport in the Weathered Zone at Koongarra (Australia), RIVM report no. 725206010, Bilthoven, 1993.

Van De Weerd H., Leijnse A., Hassanizadeh S.M. and Richardson-van der Poel M.A., INTRAVAL Phase 2, Test Case 8, Alligator Rivers Natural Analogue - Modelling of Uranium Transport in the Weathered Zone at Koongarra (Australia), RIVM report no. 715206005, Bilthoven, 1994.

Wyrwoll K.-H., Geomorphology and Paleoclimatic History, ARAP Final Report, Volume 3, OECD/NEA, 1992.

Yanase N., Technical Report on Work carried out in the Lucas Heights Research Laboratory for the Alligator Rivers Analogue Project, ARAP Progress Report, 1 September 1987 - 30 April, 1988.

Yanase N., Distribution of Uranium and Actinium Series Radionuclides in Rocks and Groundwater, ARAP Progress Report, 1 May - 31 August, 1988.

Yanase N., Uranium Distribution in Mineral Phases of Rock by a five Phase Sequential Extraction Procedure, ARAP 1st annual report, 1988-1989 (editor P Duerden), 1990.

APPENDIX 1: Data Available from the Alligator Rivers site

An extensive experimental programme, including both field and laboratory investigations, has resulted in a large amount of data characterising the site. A compilation of the tests that have been carried out and the type of data acquired are given below.

Hydrogeology

Hydrogeologic data were obtained from drawdown and recovery tests, water pressure tests, aquifer tests and slug tests. Petrophysical properties were measured in the laboratory on core samples from different locations. The following types of data are available from different hydrogeological investigation:

- climatologic data, including precipitation and temperature
- surface water measurements, including stream flow
- location, elevation, geologic logs, casing and perforation details of all test holes and wells
- map showing test holes and wells as well as land-surface contours
- aquifer test results, including water-level drawdowns, discharge measurements and water quality of discharge
- periodic water-level measurements, showing seasonal fluctuations and regional gradients
- results of geophysical surveys and back-hoe pits, showing thickness of surface deposits
- results of packer tests in the upper part of the bedrock, and resistivity traverses
- results from porosity and permeability measurements on drillcore samples.

Hydrochemistry

An extensive set of data on groundwater chemistry has been obtained from sampling in more than 70 boreholes. All recent data are from packed-off sections at different depths in the boreholes, both in the weathered and unweathered zone. Earlier data exist from pumping and sampling over the entire depth of the holes. Groundwater colloids and fine particles have been sampled and their physical nature and radionuclide content investigated.

The following hydrochemical data are available:

- pH, Eh, electrical conductivity and temperature in groundwaters
- groundwater concentration of
  - cations (Mg, Na Al, Si, S, K, Ca, Ti, Mn, Fe)
  - anions (F, HCO_3, SO_4, Cl, PO_4)
  - trace metals (Cd, Cr, Cu, Pb, Mn, Mo, Ni, Zn, etc.)
  - uranium series nuclide (U, Th, Ra, Rn, Pb)
  - isotopes (^3H, ^{14}C, $\delta^{13}C$, $^{36}Cl/Cl$, ^{129}I)
- elemental and radionuclide content in colloids and particles
- size distribution of colloids and particles
- mineralogy of colloids and particles.

Mineralogy and Radiochemistry

Mineralogic data are based on mineralogic and uranium assay logs of 140 percussion holes and 107 drillcores in the immediate vicinity of the uranium deposit. The distribution of uranium, thorium and radium isotopes has been determined in the different mineralisation zones at the site. Selective extraction procedures have been used on rock samples to determine the distribution of uranium, thorium and radium between the "amorphous" and "crystalline" phases of the rock. In addition, laboratory sorption experiments have been carried out using rock samples from the site, and distribution coefficients have been measured on natural particles extracted from the groundwater.

The following mineralogy and radiochemistry data are available:

- mineralogic composition of rock samples
- results from chemical analyses of core samples in terms of concentrations of Al, Si, Mg, K, Ca, Ti, Fe, Mn, etc., and U and rare earth elements
- uranium concentration distribution assay (247 drilling locations) in core pulp and soil samples
- uranium series radioisotope activity ratios for selected samples in the ore zone
- concentrations and activity ratios of uranium and thorium in crystals of secondary uranium mineral
- concentrations and activity ratios of uranium, thorium and radium in different mineral phases
- concentration of ^{129}I, ^{36}Cl, ^{99}Tc and ^{239}Pu in rock samples
- results from sorption studies on well-defined mineral phases conducted over a range of solution pH, ionic strength, carbonate content, adsorbent and adsorbate concentrations, in the presence of uranium complexants and potentially competing adsorbates, such as phosphate and fluoride.

MAIN SALES OUTLETS OF OECD PUBLICATIONS
PRINCIPAUX POINTS DE VENTE DES PUBLICATIONS DE L'OCDE

AUSTRALIA – AUSTRALIE
D.A. Information Services
648 Whitehorse Road, P.O.B 163
Mitcham, Victoria 3132 Tel. (03) 9210.7777
Fax: (03) 9210.7788

AUSTRIA – AUTRICHE
Gerold & Co.
Graben 31
Wien I Tel. (0222) 533.50.14
Fax: (0222) 512.47.31.29

BELGIUM – BELGIQUE
Jean De Lannoy
Avenue du Roi, Koningslaan 202
B-1060 Bruxelles Tel. (02) 538.51.69/538.08.41
Fax: (02) 538.08.41

CANADA
Renouf Publishing Company Ltd.
1294 Algoma Road
Ottawa, ON K1B 3W8 Tel. (613) 741.4333
Fax: (613) 741.5439

Stores:
61 Sparks Street
Ottawa, ON K1P 5R1 Tel. (613) 238.8985

12 Adelaide Street West
Toronto, ON M5H 1L6 Tel. (416) 363.3171
Fax: (416)363.59.63

Les Éditions La Liberté Inc.
3020 Chemin Sainte-Foy
Sainte-Foy, PQ G1X 3V6 Tel. (418) 658.3763
Fax: (418) 658.3763

Federal Publications Inc.
165 University Avenue, Suite 701
Toronto, ON M5H 3B8 Tel. (416) 860.1611
Fax: (416) 860.1608

Les Publications Fédérales
1185 Université
Montréal, QC H3B 3A7 Tel. (514) 954.1633
Fax: (514) 954.1635

CHINA – CHINE
China National Publications Import
Export Corporation (CNPIEC)
16 Gongti E. Road, Chaoyang District
P.O. Box 88 or 50
Beijing 100704 PR Tel. (01) 506.6688
Fax: (01) 506.3101

CHINESE TAIPEI – TAIPEI CHINOIS
Good Faith Worldwide Int'l. Co. Ltd.
9th Floor, No. 118, Sec. 2
Chung Hsiao E. Road
Taipei Tel. (02) 391.7396/391.7397
Fax: (02) 394.9176

CZECH REPUBLIC – RÉPUBLIQUE TCHÈQUE
National Information Centre
NIS – prodejna
Konviktská 5
Praha 1 – 113 57 Tel. (02) 24.23.09.07
Fax: (02) 24.22.94.33
(Contact Ms Jana Pospisilova, nkposp@dec.niz.cz)

DENMARK – DANEMARK
Munksgaard Book and Subscription Service
35, Nørre Søgade, P.O. Box 2148
DK-1016 København K Tel. (33) 12.85.70
Fax (33) 12.93.87

J. H. Schultz Information A/S.
Herstedvang 12,
DK – 2620 Albertslung Tel. 43 63 23 00
Fax 43 63 19 69
Internet: s-info@inet.uni-c.dk

EGYPT – ÉGYPTE
The Middle East Observer
41 Sherif Street
Cairo Tel. 392.6919
Fax: 360-6804

FINLAND – FINLANDE
Akateeminen Kirjakauppa
Keskuskatu 1, P.O. Box 128
00100 Helsinki

Subscription Services/Agence d'abonnements :
P.O. Box 23
00371 Helsinki Tel. (358 0) 121 4416
Fax: (358 0) 121.4450

FRANCE
OECD/OCDE
Mail Orders/Commandes par correspondance :
2, rue André-Pascal
75775 Paris Cedex 16 Tel. (33-1) 45.24.82.00
Fax: (33-1) 49.10.42.76
Telex: 640048 OCDE

Internet: Compte.PUBSINQ@oecd.org

Orders via Minitel, France only/
Commandes par Minitel, France exclusivement :
36 15 OCDE

OECD Bookshop/Librairie de l'OCDE :
33, rue Octave-Feuillet
75016 Paris Tel. (33-1) 45.24.81.81
(33-1) 45.24.81.67

Dawson
B.P. 40
91121 Palaiseau Cedex Tel. 69.10.47.00
Fax: 64.54.83.26

Documentation Française
29, quai Voltaire
75007 Paris Tel. 40.15.70.00

Economica
49, rue Héricart
75015 Paris Tel. 45.75.05.67
Fax: 40.58.15.70

Gibert Jeune (Droit-Économie)
6, place Saint-Michel
75006 Paris Tel. 43.25.91.19

Librairie du Commerce International
10, avenue d'Iéna
75016 Paris Tel. 40.73.34.60

Librairie Dunod
Université Paris-Dauphine
Place du Maréchal-de-Lattre-de-Tassigny
75016 Paris Tel. 44.05.40.13

Librairie Lavoisier
11, rue Lavoisier
75008 Paris Tel. 42.65.39.95

Librairie des Sciences Politiques
30, rue Saint-Guillaume
75007 Paris Tel. 45.48.36.02

P.U.F.
49, boulevard Saint-Michel
75005 Paris Tel. 43.25.83.40

Librairie de l'Université
12a, rue Nazareth
13100 Aix-en-Provence Tel. (16) 42.26.18.08

Documentation Française
165, rue Garibaldi
69003 Lyon Tel. (16) 78.63.32.23

Librairie Decitre
29, place Bellecour
69002 Lyon Tel. (16) 72.40.54.54

Librairie Sauramps
Le Triangle
34967 Montpellier Cedex 2 Tel. (16) 67.58.85.15
Fax: (16) 67.58.27.36

A la Sorbonne Actual
23, rue de l'Hôtel-des-Postes
06000 Nice Tel. (16) 93.13.77.75
Fax: (16) 93.80.75.69

GERMANY – ALLEMAGNE
OECD Bonn Centre
August-Bebel-Allee 6
D-53175 Bonn Tel. (0228) 959.120
Fax: (0228) 959.12.17

GREECE – GRÈCE
Librairie Kauffmann
Stadiou 28
10564 Athens Tel. (01) 32.55.321
Fax: (01) 32.30.320

HONG-KONG
Swindon Book Co. Ltd.
Astoria Bldg. 3F
34 Ashley Road, Tsimshatsui
Kowloon, Hong Kong Tel. 2376.2062
Fax: 2376.0685

HUNGARY – HONGRIE
Euro Info Service
Margitsziget, Európa Ház
1138 Budapest Tel. (1) 111.62.16
Fax: (1) 111.60.61

ICELAND – ISLANDE
Mál Mog Menning
Laugavegi 18, Pósthólf 392
121 Reykjavik Tel. (1) 552.4240
Fax: (1) 562.3523

INDIA – INDE
Oxford Book and Stationery Co.
Scindia House
New Delhi 110001 Tel. (11) 331.5896/5308
Fax: (11) 371.8275

17 Park Street
Calcutta 700016 Tel. 240832

INDONESIA – INDONÉSIE
Pdii-Lipi
P.O. Box 4298
Jakarta 12042 Tel. (21) 573.34.67
Fax: (21) 573.34.67

IRELAND – IRLANDE
Government Supplies Agency
Publications Section
4/5 Harcourt Road
Dublin 2 Tel. 661.31.11
Fax: 475.27.60

ISRAEL – ISRAËL
Praedicta
5 Shatner Street
P.O. Box 34030
Jerusalem 91430 Tel. (2) 52.84.90/1/2
Fax: (2) 52.84.93

R.O.Y. International
P.O. Box 13056
Tel Aviv 61130 Tel. (3) 546 1423
Fax: (3) 546 1442

Palestinian Authority/Middle East:
INDEX Information Services
P.O.B. 19502
Jerusalem Tel. (2) 27.12.19
Fax: (2) 27.16.34

ITALY – ITALIE
Libreria Commissionaria Sansoni
Via Duca di Calabria 1/1
50125 Firenze Tel. (055) 64.54.15
Fax: (055) 64.12.57

Via Bartolini 29
20155 Milano Tel. (02) 36.50.83

Editrice e Libreria Herder
Piazza Montecitorio 120
00186 Roma
Tel. 679.46.28
Fax: 678.47.51

Libreria Hoepli
Via Hoepli 5
20121 Milano
Tel. (02) 86.54.46
Fax: (02) 805.28.86

Libreria Scientifica
Dott. Lucio de Biasio 'Aeiou'
Via Coronelli, 6
20146 Milano
Tel. (02) 48.95.45.52
Fax: (02) 48.95.45.48

JAPAN – JAPON

OECD Tokyo Centre
Landic Akasaka Building
2-3-4 Akasaka, Minato-ku
Tokyo 107
Tel. (81.3) 3586.2016
Fax: (81.3) 3584.7929

KOREA – CORÉE

Kyobo Book Centre Co. Ltd.
P.O. Box 1658, Kwang Hwa Moon
Seoul
Tel. 730.78.91
Fax: 735.00.30

MALAYSIA – MALAISIE

University of Malaya Bookshop
University of Malaya
P.O. Box 1127, Jalan Pantai Baru
59700 Kuala Lumpur
Malaysia
Tel. 756.5000/756.5425
Fax: 756.3246

MEXICO – MEXIQUE

OECD Mexico Centre
Edificio INFOTEC
Av. San Fernando no. 37
Col. Toriello Guerra
Tlalpan C.P. 14050
Mexico D.F.
Tel. (525) 665 47 99
Fax: (525) 606 13 07

NETHERLANDS – PAYS-BAS

SDU Uitgeverij Plantijnstraat
Externe Fondsen
Postbus 20014
2500 EA's-Gravenhage
Tel. (070) 37.89.880
Voor bestellingen:
Fax: (070) 34.75.778

Subscription Agency/
Agence d'abonnements :
SWETS & ZEITLINGER BV
Heereweg 347B
P.O. Box 830
2160 SZ Lisse
Tel. 252.435.111
Fax: 252.415.888

NEW ZEALAND – NOUVELLE-ZÉLANDE

GPLegislation Services
P.O. Box 12418
Thorndon, Wellington
Tel. (04) 496.5655
Fax: (04) 496.5698

NORWAY – NORVÈGE

NIC INFO A/S
Ostensjoveien 18
P.O. Box 6512 Etterstad
0606 Oslo
Tel. (22) 97.45.00
Fax: (22) 97.45.45

PAKISTAN

Mirza Book Agency
65 Shahrah Quaid-E-Azam
Lahore 54000
Tel. (42) 735.36.01
Fax: (42) 576.37.14

PHILIPPINE – PHILIPPINES

International Booksource Center Inc.
Rm 179/920 Cityland 10 Condo Tower 2
HV dela Costa Ext cor Valero St.
Makati Metro Manila
Tel. (632) 817 9676
Fax: (632) 817 1741

POLAND – POLOGNE

Ars Polona
00-950 Warszawa
Krakowskie Przedmiescie 7
Tel. (22) 264760
Fax: (22) 265334

PORTUGAL

Livraria Portugal
Rua do Carmo 70-74
Apart. 2681
1200 Lisboa
Tel. (01) 347.49.82/5
Fax: (01) 347.02.64

SINGAPORE – SINGAPOUR

Ashgate Publishing
Asia Pacific Pte. Ltd
Golden Wheel Building, 04-03
41, Kallang Pudding Road
Singapore 349316
Tel. 741.5166
Fax: 742.9356

SPAIN – ESPAGNE

Mundi-Prensa Libros S.A.
Castelló 37, Apartado 1223
Madrid 28001
Tel. (91) 431.33.99
Fax: (91) 575.39.98

Mundi-Prensa Barcelona
Consell de Cent No. 391
08009 – Barcelona
Tel. (93) 488.34.92
Fax: (93) 487.76.59

Libreria de la Generalitat
Palau Moja
Rambla dels Estudis, 118
08002 – Barcelona
(Subscripcions) Tel. (93) 318.80.12
(Publicacions) Tel. (93) 302.67.23
Fax: (93) 412.18.54

SRI LANKA

Centre for Policy Research
c/o Colombo Agencies Ltd,
No. 300-304, Galle Road
Colombo 3
Tel. (1) 574240, 573551-2
Fax: (1) 575394, 510711

SWEDEN – SUÈDE

CE Fritzes AB
S-106 47 Stockholm
Tel. (08) 690.90.90
Fax: (08) 20.50.21

For electronic publications only/
Publications électroniques seulement
STATISTICS SWEDEN
Informationsservice
S-115 81 Stockholm
Tel. 8 783 5066
Fax: 8 783 4045

Subscription Agency/Agence d'abonnements :
Wennergren-Williams Info AB
P.O. Box 1305
171 25 Solna
Tel. (08) 705.97.50
Fax: (08) 27.00.71

SWITZERLAND – SUISSE

Maditec S.A. (Books and Periodicals/Livres et périodiques)
Chemin des Palettes 4
Case postale 266
1020 Renens VD 1
Tel. (021) 635.08.65
Fax: (021) 635.07.80

Librairie Payot S.A.
4, place Pépinet
CP 3212
1002 Lausanne
Tel. (021) 320.25.11
Fax: (021) 320.25.14

Librairie Unilivres
6, rue de Candolle
1205 Genève
Tel. (022) 320.26.23
Fax: (022) 329.73.18

Subscription Agency/Agence d'abonnements :
Dynapresse Marketing S.A.
38, avenue Vibert
1227 Carouge
Tel. (022) 308.08.70
Fax: (022) 308.07.99

See also – Voir aussi :
OECD Bonn Centre
August-Bebel-Allee 6
D-53175 Bonn (Germany)
Tel. (0228) 959.120
Fax: (0228) 959.12.17

THAILAND – THAÏLANDE

Suksit Siam Co. Ltd.
113, 115 Fuang Nakhon Rd.
Opp. Wat Rajbopith
Bangkok 10200
Tel. (662) 225.9531/2
Fax: (662) 222.5188

TRINIDAD & TOBAGO, CARIBBEAN TRINITÉ-ET-TOBAGO, CARAÏBES

SSL Systematics Studies Limited
9 Watts Street
Curepe
Trinidad & Tobago, W.I.
Tel. (1809) 645.3475
Fax: (1809) 662.5654

TUNISIA – TUNISIE

Grande Librairie Spécialisée
Fendri Ali
Avenue Haffouz Imm El-Intilaka
Bloc B 1 Sfax 3000
Tel. (216-4) 296 855
Fax: (216-4) 298.270

TURKEY – TURQUIE

Kültür Yayinlari Is-Türk Ltd. Sti.
Atatürk Bulvari No. 191/Kat 13
06684 Kavaklidere/Ankara
Tél. (312) 428.11.40 Ext. 2458
Fax : (312) 417.24.90
et 425.07.50-51-52-53

Dolmabahce Cad. No. 29
Besiktas/Istanbul
Tel. (212) 260 7188

UNITED KINGDOM – ROYAUME-UNI

HMSO
Gen. enquiries
Tel. (0171) 873 0011

Postal orders only:
P.O. Box 276, London SW8 5DT
Personal Callers HMSO Bookshop
49 High Holborn, London WC1V 6HB
Fax: (0171) 873 8463

Branches at: Belfast, Birmingham, Bristol, Edinburgh, Manchester

UNITED STATES – ÉTATS-UNIS

OECD Washington Center
2001 L Street N.W., Suite 650
Washington, D.C. 20036-4922
Tel. (202) 785.6323
Fax: (202) 785.0350
Internet: washcont@oecd.org

Subscriptions to OECD periodicals may also be placed through main subscription agencies.

Les abonnements aux publications périodiques de l'OCDE peuvent être souscrits auprès des principales agences d'abonnement.

Orders and inquiries from countries where Distributors have not yet been appointed should be sent to: OECD Publications, 2, rue André-Pascal, 75775 Paris Cedex 16, France.

Les commandes provenant de pays où l'OCDE n'a pas encore désigné de distributeur peuvent être adressées aux Éditions de l'OCDE, 2, rue André-Pascal, 75775 Paris Cedex 16, France.

8-1996

THE INTERNATIONAL INTRAVAL PROJECT

Phase 2, Working Group Reports

Intraval parties:
Agence Nationale pour la Gestion des Déchets Radioactifs (France), Atomic Energy of Canada Ltd. (Canada), Australian Nuclear Science and Technology Organisation (Australia), Bundesanstalt für Geowissenschaften und Rohstoffe/Bundesamt für Strahlenschutz (Germany), Commissariat à l'Énergie Atomique/Institut de Protection et de Sûreté Nucléaire (France), Empresa Nacional de Residuos Radioactivos S.A. (Spain), Gesellschaft für Reaktorsicherheit (Germany), Gesellschaft für Strahlen- und Umweltforschung (Germany), Her Majesty's Inspectorate of Pollution (United Kingdom), Industrial Power Company Ltd. (Finland), Japan Atomic Energy Research Institute (Japan), Nationale Genossenschaft für die Lagerung Radioaktiver Abfälle (Switzerland), National Institute of Public Health and Environmental Hygiene (the Netherlands), National Radiological Protection Board (United Kingdom), Nuclear Safety Inspectorate (Switzerland), Power Reactor and Nuclear Fuel Development Corporation (Japan), Swedish Nuclear Fuel and Waste Management Co. (Sweden), Swedish Nuclear Power Inspectorate (Sweden), U.K. Nirex Ltd. (United Kingdom), U.S. Department of Energy (United States), U.S. Environmental Protection Agency (United States), U.S. Nuclear Regulatory Commission (United States).

Observers:
International Atomic Energy Agency (IAEA), State of Nevada (United States).

Project Secretariat:
Swedish Nuclear Power Inspectorate, Her Majesty's Inspectorate of Pollution/Harwell Laboratories, Kemakta Consultants Co., Organisation for Economic Co-operation and Development/Nuclear Energy Agency.

Copies of this report are available from:

The Swedish Nuclear Power Inspectorate (SKi)
Box 27106
S-102 52 Stockholm (Sweden)